(1)

(6) THE EFFECT OF FILM COOLING ON THE HEAT TRANSFER BETWEEN A SHROUDED ROTATING DISK AND A RADIALLY INWARD FLOW

(10) BY

DARRYL E. METZGER

64-5

TECHNICAL REPORT NO. 58

PREPARED UNDER CONTRACT Nonr 225(23)
(NR-090-342)
FOR
OFFICE OF NAVAL RESEARCH

DEPARTMENT OF MECHANICAL ENGINEERING
STANFORD UNIVERSITY
STANFORD, CALIFORNIA

AUGUST 1963

THE EFFECT OF FILM COOLING ON THE HEAT TRANSFER BETWEEN A SHROUDED ROTATING DISK AND A RADIALLY INWARD FLOW

Technical Report No. 58

Prepared under Contract Nonr 225(23)
(NR-090-342)

For

Office of Naval Research

Department of Mechanical Engineering
Stanford University
Stanford, California

August, 1963

Report Prepared By:

Darryl E. Metzger

Approved By:

A. L. London

Project Supervisor

ABSTRACT

A study of the cooling effect of a film stream on the heat transfer between a shrouded rotating disk and radially inward main flow stream is presented. The investigation is intended as a model study of the film cooled radial flow gas turbine. Film heating and film cooling are shown to be similar problems described by the same set of equations when property variations can be neglected. Experimental results were obtained from a film heated, rotating disk facility. These results were obtained over the range of radial flow gas turbine operating conditions.

The heat transfer behavior of the main stream only was determined separately, and the film cooling results are presented as ratios of the heat transfer obtained with film cooling to the heat transfer obtained with only a single radial inflow.

An analysis of the heat transfer to a film cooled, uniform temperature flat plate is presented. This analysis predicts the form but not the magnitude of the results obtained on the rotating disk.

ACKNOWLEDGMENTS

The author wishes to express his indebtedness to the following persons and organizations: Professor A. L. London was the project supervisor and the author's adviser. Dr. J. W. Mitchell designed and supervised construction of the test facility. The Office of Naval Research and the AiResearch Manufacturing Division of the Garrett Corporation supported the project. The author's graduate study was made possible by the Office of Naval Research, the National Science Foundation, and the Ford Foundation.

TABLE OF CONTENTS

LIST OF TABLES

LIST OF FIGURES

Figures (cont'd) Page

REFERENCES

1. "Air Cooling of Small Gas Turbine Disks," by Ulrich Oprecht, International Developments in Heat Transfer, 1961, Part 1, pp. 183-189.

2. "Studying the Air Jet Cooling of Gas Turbine Disks," by L.A. Dorfman and J.S. Osherov, ЭНЕРГОМАШИНОСТРОЕИЕ, Vol. 7, 1961, pp. 23-26. (in Russian)

3. "Heat Transfer in a Cooled Radial Flow Turbine with an Aluminum Rotor," by R.D. Smith, Purdue University Gas Turbine Laboratory Interim Report 56 - 1, Contract N7 - onr - 39415, February, 1956.

4. "Comparison of Effectiveness of Convection-, Transpiration-, and Film-Cooling Methods with Air as Coolant," by E.R.G. Eckert and J.N.B. Livingood, NACA TN 3010, 1953.

5. "Investigation of Veil Cooling for Radial Flow Turbines," by W.U. Rossler and J.W. Mitchell, AiResearch Manufacturing Division, The Garrett Corporation, AiResearch Report No. K-451-R, Astia No. AD-260 085, May, 1961.

6. "Hot Air Discharge for De-Icing," ATI 24536, original in Deutsche Luftfahrtforsching, Forschungsbericht, 1900, 1943.

7. "Experimental Inverstigation of Air Film Cooling Applied to an Adiabatic Wall by Means of an Axially Discharging Slot," by S.S. Papell and A.M. Trout, NASA TN D-9, 1959.

8. "Heat Tranffer and Effectiveness for a Turbulent Boundary Layer with Tangential Fluid Injection," by R.A. Seban, Trans. ASME, Series C, Vol. 82, 1960, pp. 303-312.

9. "Velocity Distributions, Temperature Distributions, Effectiveness and Heat Transfer for Air Injected Through a Tangential Slot Into a Turbulent Boundary Layer." by J.P. Hartnett, R.C. Birkebak, and E.R.G. Eckert, Trans. ASME, Series C. Vol. 83, 1961, pp. 293-306.

10. "Velocity Distributions, Temperature Distributions, Effectiveness and Heat Transfer in Cooling of a Surface with a Pressure Gradient," by J.P. Hartnett, R.C. Birkebak, and E.R.G. Eckert, International Developments in Heat Transfer, 1961, Part IV, pp. 682-689.

11. "Effectiveness and Heat Transfer for a Turbulent Boundary Layer with Tangential Injection and Variable Free Stream Velocity," by R.A. Seban and L. H. Back, ASME Paper No. No. 61—WA-156, 1961.

12. "A Study of the Fluid Dynamics and Heat Transfer Behavior for Radially Inward Flow Over a Shrouded Rotating Disk," by J.W. Mitchell, TR No. 57, Contract Nonr 225(23), Stanford University, April, 1963. Also published as a Ph.D. Dissertation under the same title, Stanford University, 1963.

13. "A Summary of Experiments on Turbulent Heat Transfer from a Nonisothermal Flat Plate," by W.C. Reynolds, W.M. Kays, and S.J. Kline, Trans. ASME, Series C. Vol. 82, 1960, pp. 341-348.

14. "Boundary Layer Theory," by H. Schlichting, Pergamon Press, 1955.

15. "The Radial Turbine," by W.T. von der Nuell, Technical Data Digest, Vol. 12, 1947, pp. 5-31.

16. "A Contribution to the Problem of Designing Radial Turbomachines," by O.E. Balje, Trans. ASME, 1952, pp. 451-472.

17. "Current Technology of Radial Inflow Turbines for Compressible Fluids," by H.J. Wood, Trans. ASME, Series A. Vol. 85, 1963.

18. "Flow Measurement, Part 5, Measurement of Quantity of Materials," American Society of Mechanical Engineers, 1959.

19. "Fluid Meters, Their Theory and Application," American Society of Mechanical Engineers, 1959.

20. "Describing Uncertainties in Single-Sample Experiments," by S.J. Kline and F.A. McClintock, Mechanical Engineering, January, 1953.

21. "Heat and Mass Transfer," by E.R.G. Eckert and R.M. Drake, Jr., McGraw-Hill Book Company, Inc., 1959.

22. "Research on Application of Cooling to Gas Turbines, "by J.B. Esgar, J.N.B. Livingood, and R.O. Hickel, Trans. ASME, Vol. 79, 1957.

23. "Turbine Cooling," by Jack B. Esgar, Trans. ASME, Series A, Vol. 81, 1959.

24. "Design and Development of a Convective Air Cooled Turbine and Test Facility," by W.F. Weatherwax, Trans. ASME, Series A, Vol. 83, 1961.

NOMENCLATURE

English Letter symbols:

c_p	Specific heat, Btu/(lbm °F)
g_c	Proportionality factor in Newton's Second Law, 32.2 (lbm/lbf)(ft/sec^2)
G	Mass velocity, lbm/(hr ft^2)
h	Local heat transfer coefficient, Btu/(hr ft^2 °F)
h_{av}	Average heat transfer coefficient, Btu/(hr ft^2 °F)
k	Thermal conductivity, Btu/(hr ft °F)
ℓ	Plate length, ft
N	Rotative speed, rpm
p	Fluid pressure, lbf/ft^2
q"	Heat Flux, Btu/(hr ft^2)
r	Radial coordinate, ft
R	Disk radius, ft
s	Slot gap, ft
T	Temperature, °R
t	Temperature, °F
u	Fluid radial velocity component, ft/sec
v	Fluid tangential velocity component, ft/sec
W	Mass flow rate, lbm/hr
w	Fluid axial velocity component, ft/sec
x	Rectilinear coordinate, ft
y	Rectilinear coordinate, ft
z	Axial coordinate, ft
z_o	Disk - shroud spacing, ft

Greek Letter Symbols:

α Flow angle with respect to the radial direction, degrees

θ Temperature referred to the main stream temperature, see Eq. 1

μ Fluid dynamic viscosity, lbm/(hr ft)

ρ Fluid density, lbm/ft^3

ω Disk angular velocity, radians/sec

Nondimensional Quantities:

$N_{Pr} \triangleq \mu c_p/k$, Prandtl number

$N_{R,F} \triangleq 2\pi R u_m \rho_m/\mu$, Flow Reynolds number

$N_{R,M} \triangleq R^2 \omega \rho_m/\mu$, Machine Reynolds number

$N_{St} \triangleq h/G_m c_p$, Average Stanton number

$N_{St,av} \triangleq h_{av}/G_m c_p$, Average Stanton number

$\theta^* \triangleq \theta_f/\theta_w$, A temperature difference ratio, see Eq. 12

$G^* \triangleq G_f/G_m$, Mass velocity ratio

$\phi \triangleq N_{St,av}/(N_{St,av})_{\theta^* = 0}$, A Stanton number ratio

$p' \triangleq g_c p/(\rho u_m^2)$, Nondimensional pressure

$r' \triangleq r/R$, Nondimensional radial coordinate

$u' \triangleq u/u_m$, Nondimensional radial velocity component

$v' \triangleq v/u_m$, Nondimensional tangential velocity component

$w' \triangleq w/u_m$, Nondimensional axial velocity component

$z' \triangleq z/R$, Nondimensional axial coordinate

Subscripts:

a Denotes average

f Denotes film flow, indicates a quantity evaluated at the film flow inlet

m Denotes main flow, indicates a quantity evaluated at the main flow inlet

w	Denotes wall, indicates a quantity evaluated at the disk test surface
I	Denotes Case I in the analysis
II	Denotes Case II in the analysis

Miscellaneous:

lbf	Denotes pound force
lbm	Denotes pound mass

I INTRODUCTION

The desirability of operating gas turbines at the highest possible turbine inlet temperature is well known. All gas turbine designs with high efficiency as an objective embody a certain compromise between the turbine inlet temperature desired and the temperatures that can be tolerated by practical turbine materials. The practicality of the turbine material may be based on economic, or on strictly metallurgical considerations, or on both.

The necessary compromise can be lessened by using an auxiliary flow of cool air or some other coolant to lower the temperature of the highly stressed parts exposed to the working gas. This idea is not new; in fact, designers of axial flow turbines have been successful in applying blade and disk cooling to existing production engines. There are several ways in which such cooling can be accomplished, with the differences arising from the different means of application employed and the places of application of the coolant fluid.

The N.A.C.A. (now N.A.S.A.) has conducted an extensive turbine cooling research program, with an emphasis on investigation of the problems associated with the internal cooling of cooling of hollow axial flow turbine blades.[22,23*] The results of this research program are currently being applied to the design of operational axial flow machines.[24]

A comparatively simple, frequently used method of cooling axial flow turbines is to cool the turbine disk either by a flow of coolant air from the hub to the rim[1] or by jets of air impinging on the disk.[2] The blades, in direct contact with the working gas, are thus cooled by conduction to the cooler disk. A similar cooling method was employed by Smith[3] for cooling a radial flow turbine impeller.

---

* Raised numerals denote references.

In Smith's study, which was the first published attempt at cooling a radial flow turbine, a cool air flow was directed onto the rear face of the turbine disk.

These methods suffer from the fact that the total amount of heat transfer to the turbine disk and blading is not reduced, and relatively large amounts of coolant are required to induce the conduction cooling. Transpiration cooling and film cooling, on the other hand, reduce the heat transfer between the working gas and the turbine surface.

Transpiration cooling involves the injection of a coolant through the surface to be cooled into the boundary layer of the main flow. The method usually implies a more or less continuous injection through some type of porous surface as shown in Fig. 1a. Film cooling is accomplished by blowing the coolant through a slot upstream of the surface to be cooled so that the coolant will flow between the working gas and the surface (see Fig. 1b). Both transpiration cooling and film cooling in effect "insulate" the surface from the hot main stream. Of course turbulent mixing of the coolant and the main stream tends to destroy the identity of the coolant and thereby lessens its cooling effect. Eckert and Livingood[4] have discussed the relative merits of transpiration and film cooling. While transpiration cooling has some theoretical advantages over film cooling, the technical difficulties encountered in applying it to an actual cooling situation usually preclude its use.

Very little work has been done on the problem of cooling radial flow turbine wheels, but the film cooling method holds promise as a technique particularly applicable to this type of turbine. Fig. 1c shows a typical cross section of a raidal flow turbine wheel and indicates how the coolant flow may be introduced. In a typical radial turbine application of film cooling, a small percentage of the compressor output air would be bled off and used as the film coolant.

Rossler of the AiResearch Manufacturing Division of the Garrett Corporation, with Office of Naval Research sponsorship, experimentally investigated the effect of film cooling on an actual radial flow turbine, modified in a manner similar to that of Fig. 1c to admit the coolant flow. His results[5] indicate that significant cooling can be achieved with relatively small amounts of coolant air. With a coolant flow rate of 5 percent of the main gas flow, an increase in inlet temperature of 250 °F was achieved without raising the turbine wheel temperature.

The program at Stanford, the investigation of film cooling on a shrouded rotating disk, was undertaken in parallel with the AiResearch program with the objective of providing a better understanding of the mechanisms governing film cooling. The first results of the Stanford program have already been reported by Mitchell,[12] who investigated the fluid dynamics and heat transfer behavior for radial inflow without a film flow. The purposes of the present investigation were (1) to improve on the test facility to eliminate some of the deficiencies noted by Mitchell, and (2) to determine the heat transfer behavior with a film flow underlying the main flow.

FIGURE 1

(a) TRANSPIRATION COOLING

(b) FILM COOLING

(c) CROSS SECTION OF A FILM COOLED RADIAL TURBINE

FIG. 1

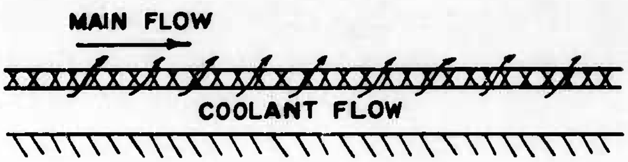

MAIN FLOW
COOLANT FLOW

(a)

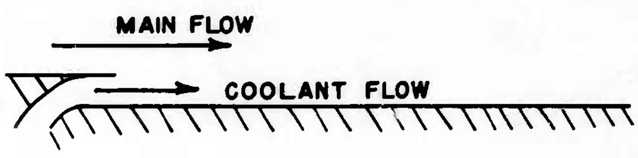

MAIN FLOW
COOLANT FLOW

(b)

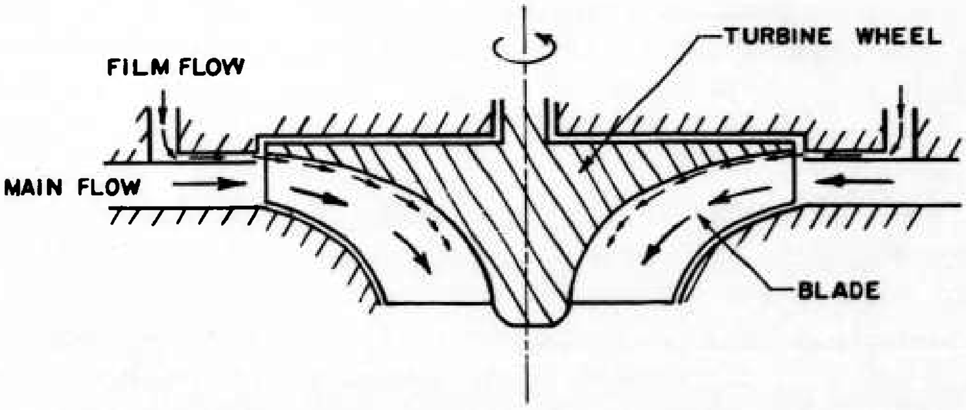

TURBINE WHEEL
FILM FLOW
MAIN FLOW
BLADE

(c)

II THE FILM COOLING METHOD

The injection of an air film into the turbulent boundary layer on a flat plate has been studied by numerous researchers.[6, 7,8,9,10,11] Papell and Trout[7] experimentally investigated an actual film cooling situation with high main stream and low coolant temperatures. It can be shown that for small temperature differences between the main and coolant streams, film cooling and film heating become similar problems governed by the same differential equations. (In section IV, this is shown to be the case for the film cooling of a rotating disk as well) Film heating is usually more convenient to investigate experimentally, since the smaller film stream can be electrically heated easily. For this reason, all other researchers have experimentally investigated the problem of a heated film injected into a cool stream. Seban[8], Seban and Back[11], and Hartnett, Birkebak, and Eckert[9,10] have experimentally studied the film heating problem on flat plates both with and without pressure gradients in the main stream.

These initial experiments have been carried out only for two specific boundary conditions: (1) an adiabatic plate, and (2) constant heat flux per unit area over the entire plate. It is informative to look at these two problems in terms of typical developing temperature profiles on the boundary surface. Fig. 2a shows the profile development on an adiabatic wall while Fig. 2b pictures the constant heat flux case. In both cases the free stream temperature is shown as the datum temperature. Virtually all the investigation in film cooling and heating thus far has been experimental: the lack of similarity evident in the profiles of Figs. 2a and 2b suggests some of the difficulties encountered in analysis of the problem.

While adiabatic wall and constant heat flux boundary conditions do model some physical situations of interest, they do not adequately describe the situation encountered in the film cooling of turbine wheels. This situation is better described by the constant wall temperature boundary condition pictured in Fig. 2c. Here the case of practical importance is a wall temperature somewhere between the temperature of the film and main flows. For example, inlet film and main flow temperatures of 100°F and 1200°F, respectively, with a fairly uniform rotor temperature of about 1000°F, are representative of a turbine wheel cooling situation.[5]

It can be seen in Fig. 2c that the situation with a constant wall temperature between that of the film and main flow temperatures (with film heating instead of film cooling) is quite different from the other boundary conditions studied to date, Figs. 2a and 2b, in that the heat flux is initially in one direction, then at some point downstream changes to the other direction. The constant wall temperature boundary condition, because of its applicability to turbine wheel cooling, is the boundary condition of interest in the present study. As mentioned previously, film heating and film cooling are similar problems.

FIGURE 2

TYPICAL TEMPERATURE PROFILE DEVELOPMENT
FOR FILM HEATING

(a) Adiabatic Wall Boundary Condition

(b) Constant Heat Flux Boundary Condition

(c) Constant Wall Temperature Boundary Condition

FIG. 2

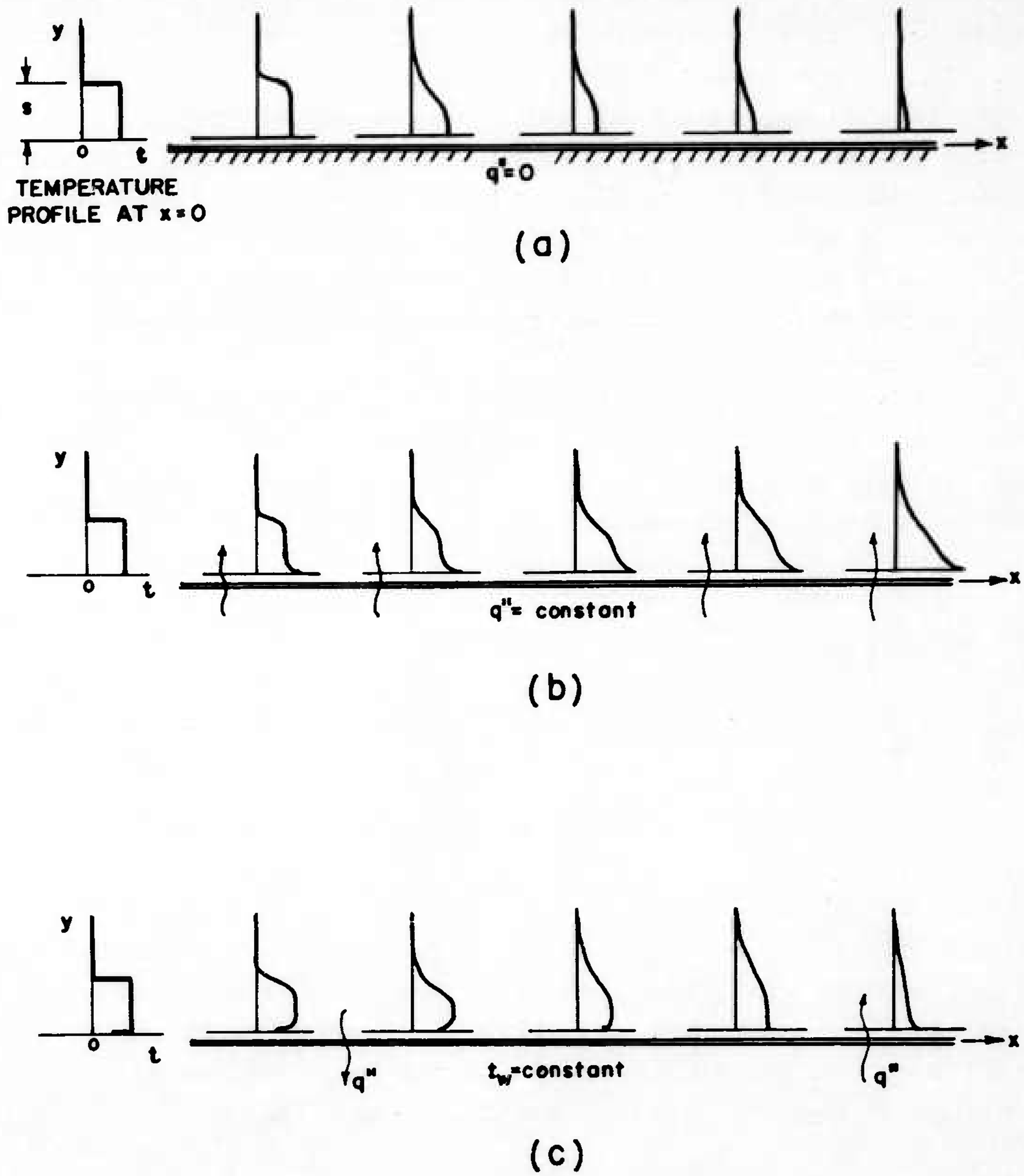
y
s
0
t
TEMPERATURE
PROFILE AT x = 0
q" = 0
x
(a)
q" = constant
(b)
q"
t_w = constant
(c)

III ANALYSIS

In view of the difficulties inherent in analysis of the film cooling problem and the lack of even an adequate analytical solution for heat transfer to a shrouded, rotating disk without film cooling,[12] the analytical efforts of the present study have been directed towards formulating a theory for the film cooling of a constant temperature flat plate. The approach used is semi-empirical and utilizes the results of the previous adiabatic wall and constant heat flux studies. A further stipulation is that the film and main flow mass velocities be equal. In addition to providing a prediction for flat plate film cooling, such an analysis should provide an understanding of the parameters governing the film cooling of a rotating disk as well.

If the fluid properties are assumed to be independent of temperature, then the energy differential equation which governs the heat transfer to the plate is linear, and superposition techniques are valid.

Consider the entering temperature profile (at x = 0) pictured in Fig. 2c and define the following:

$$\theta \triangleq t - t_m \tag{1}$$

and

$$\theta^* \triangleq \frac{\theta_f}{\theta_w} \triangleq \frac{t_f - t_m}{t_w - t_m} \tag{2}$$

where t_m, t_f, and t_w are the temperatures of the main flow, film flow, and the wall, respectively. The temperature profile may then be represented as in Fig. 3a; moreover, it may be considered as the superposition of the two profiles pictured in Fig. 3b and 3c, labeled Case I and Case II.

The superposition is a combined one: first, it is a superposition in the y-direction of the entering temperature profile, and second, it is a superposition of the wall boundary condition. The problem of film cooling a constant temperature plate is thus broken into two separate constant wall temperature problems.

In Case I the temperature potential for heat transfer is always $(\theta_w - \theta_f)$, since the wall temperature is maintained at $(\theta_w - \theta_f)$ and the effective free stream temperature is zero. In Case II the potential is initially zero since the wall temperature is maintained at θ_f and the effective free stream temperature is also θ_f. However, the turbulent mixing of the film and main streams acts to smooth out the initial step temperature profile and at a short distance downstream the temperature potential assumes a positive value which increases with distance. (Note: the heat flux is defined as positive in the positive y-direction; hence, positive out of the wall).

For the purposes of the present analysis the heat transfer coefficients for Case I and Case II, h_I and h_{II}, are assumed to be equal. Although this at first seems unlikely, there is both analytical and empirical justification for such a hypothosis. First, for small temperature differences between the two streams, the momentum and energy equations describing the situation will not be coupled. Thus the fluid mechanics for both cases will be identical. Secondly, it is well known that different wall boundary conditions do not affect the heat transfer coefficients very much in turbulent flow. For example, from Ref. 13 the turbulent heat transfer from an isothermal plate is given by:

$$N_{St} \, N_{Pr}^{0.4} = 0.0296 \quad N_{R,x}^{-0.2} \qquad (3)$$

if fluid property variations are neglected. For the quite different case of constant heat flux per unit area along the wall, the heat transfer is given by:

FIGURE 3

SUPERPOSITION PROFILES

(a) Superposition of Case I and Case II

(b) Case I

(c) Case II

FIG. 3

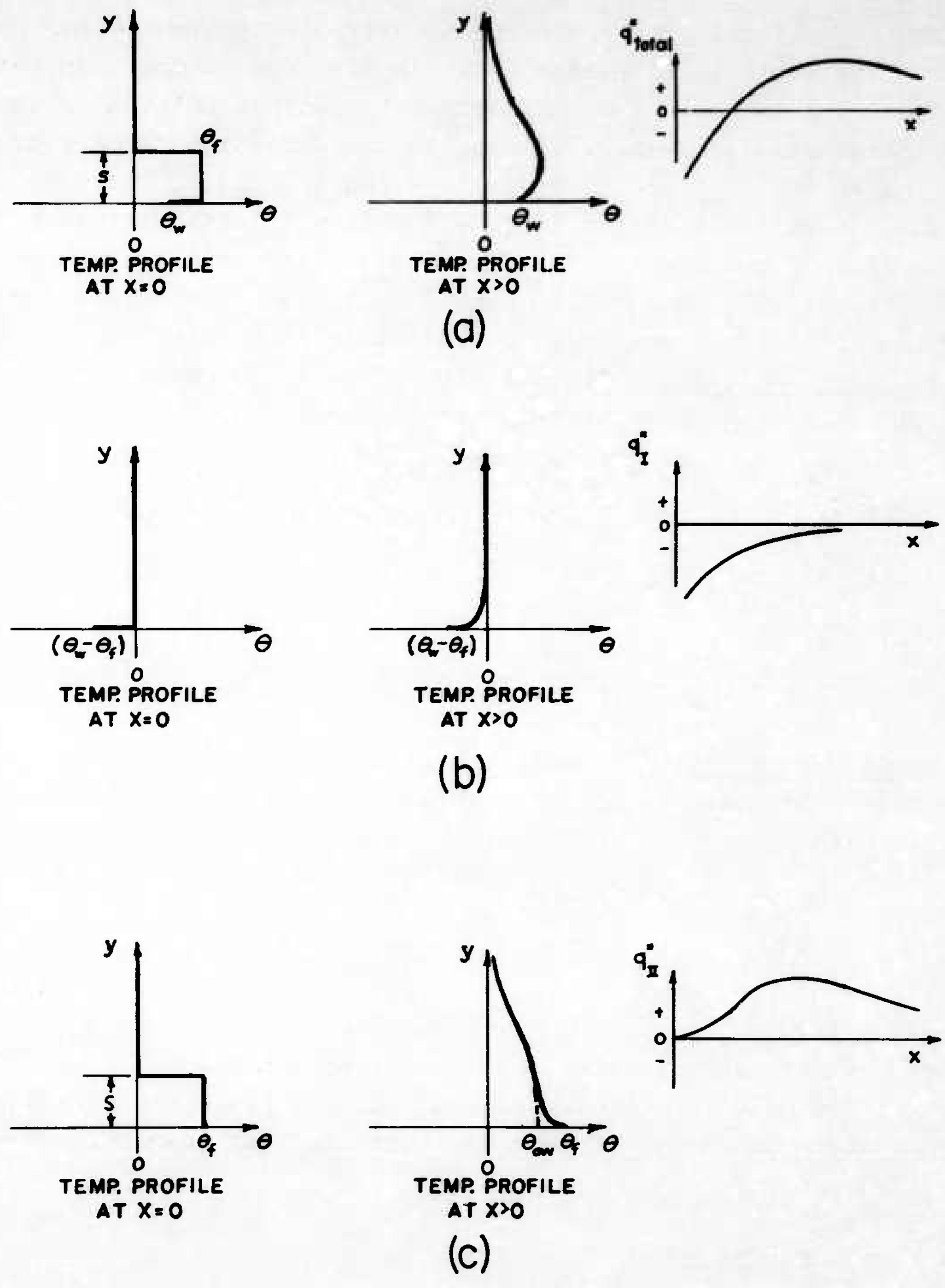

TEMP. PROFILE
AT X=0
TEMP. PROFILE
AT X>0
(a)
TEMP. PROFILE
AT X=0
TEMP. PROFILE
AT X>0
(b)
TEMP. PROFILE
AT X=0
TEMP. PROFILE
AT X>0
(c)

$$N_{St} N_{Pr}^{0.4} = 0.0309 \; N_{R,x}^{-0.2} \tag{4}$$

Thus the heat transfer coefficients differ only about 4 per cent for these entirely different wall boundary conditions. In both Cases I and II above the x-direction boundary condition is an isothermal wall; however, in Case II the effective temperature potential for heat transfer varies along the wall. The analysis assumes that the isothermal plate solution (3) is applicable to both Cases I and II; that is, $h_I = h_{II}$, and that the component heat fluxes, q''_I and q''_{II} can be evaluated from a consideration of the effective temperature potential in each case.

<u>Case I Solution</u> The solution given in (3), page 9 is directly applicable to this case. Therefore:

$$h_I = 0.0296 \; G \; c_p \; N_{Pr}^{-0.4} \; N_{R,x}^{-0.2}$$

where:

$$q''_I = h_I \; (\theta_w - \theta_f)$$

Therefore:

$$q''_I = (\theta_w - \theta_f)(0.0296) \; G \; c_p \; N_{Pr}^{-0.4} \; N_{R,x}^{-0.2} \tag{5}$$

<u>Case II Solution</u> Under the assumption that the heat transfer coefficients h_I and h_{II} are equal, h_{II} is also given by:

$$h_{II} = 0.0296 \; G \; c_p \; N_{Pr}^{-0.4} \; N_{R,x}^{-0.2}$$

and:

$$q''_{II} = h_{II} \; \theta_e \tag{6}$$

where θ_e is an effective temperature potential.

It is noted that near the start of the plate the effective temperature potential is zero and thus the heat transfer q''_{II} is also zero.

In this region the heat transfer coefficient, h_{II}, is indeterminate, and results in an apparent contradiction with the assumed heat transfer coefficient. However, this mathematical difficulty exists only in the region where θ_e is zero, and in this region $q''_{II} = h_{II}\theta_e$ is zero regardless of the value of h_{II}.

A plausible assumption regarding the effective temperature potential, θ_e, is that θ_e is approximately equal to the difference between the Case II wall temperature, θ_f (see Fig. 3c), and the Case II adiabatic wall temperature, θ_{aw}. θ_{aw} is the equilibrium wall temperature that would exist on an adiabatic plate exposed to the entering temperature profile of Case II (see Fig. 2a). This is precisely the situation studied in most of the previous work on film cooling. Thus the experimental work of others can be utilized to estimate θ_e. A summary of most of the available adiabatic wall temperature data is provided by Hartnett, et al (Fig. 26 of Ref. 9). There is considerable spread to the data which can be partially attributed to the differences in slot geometry used by the various researchers. If a best fit curve is drawn through this data, it can be represented approximately by the following pair of equations:

$$\theta_{aw}/\theta_f = 1 - 0.006\ (x/s) \qquad \text{for } 0 \leq x/s \leq 50 \tag{7}$$

$$\theta_{aw}/\theta_f = 16\ (x/s)^{-0.8} \qquad \text{for } x/s \geq 50 \tag{8}$$

Consequently, $\theta_e = \theta_f - \theta_{aw}$ can be represented as:

$$\theta_e = \left\{ \begin{array}{l} \theta_f - \theta_f \left[1 - 0.006\ (x/s)\right] \\ \qquad \text{for } 0 \leq x/s \leq 50 \\ \theta_f - \theta_f \left[16\ (x/s)^{-0.8}\right] \\ \qquad \text{for } x/s \geq 50 \end{array} \right\} \tag{9}$$

Therefore, for Case II:

$$q''_{II} = 0.0296\ G\ c_p\ N_{Pr}^{-0.4} N_{R,x}^{-0.2} \left\{ \begin{array}{l} \theta_f \left[0.006(x/s)\right] \\ \qquad \text{for } 0 \leq x/s \leq 50 \\ \theta_f \left[1 - 16\ (x/s)^{-0.8}\right] \\ \qquad \text{for} \qquad x/s \geq 50 \end{array} \right\} \tag{10}$$

Combining Cases I and II For the superposed or original boundary condition, the total heat flux, q'' total, is given as:

$$q''\ \text{total} = h\theta_w = q''_I + q''_{II} \tag{11}$$

Adding (5) and (10) in (11) and noting that $\theta_f / \theta_w \triangleq \theta^*$ results in:

$$N_{St} \triangleq \frac{h}{G\ c_p} = 0.0296\ N_{Pr}^{-0.4} N_{R,x}^{-0.2} \left\{ \begin{array}{l} 1 - \theta^* \left[1 - 0.006(x/s)\right] \\ \qquad \text{for } \ 0 \leq x/s \leq 50 \\ 1 - 16\ \theta^*\ (x/s)^{-0.8} \\ \qquad \text{for} \qquad x/s \geq 50 \end{array} \right\}$$

- - - (12)

Note that the quantity $(0.0296\ N_{Pr}^{-0.4}\ N_{R,x}^{-0.2})$ is just the local Stanton number obtained on a flat plate without any film cooling. It is convenient to normalize the above results with this quantity. Then:

$$N_{St}/(N_{St})_{\theta^*=0} = \begin{cases} 1 - \theta^* \left[1 - 0.006\,(x/s)\right] & \text{for } 0 \leq x/s \leq 50 \\ 1 - 16\,\theta^*\,(x/s)^{-0.8} & \text{for } x/s \geq 50 \end{cases} \tag{13}$$

This equation is presented in graphical form for some representative values of θ^* in Fig. 4a.

It should be noted that negative local Stanton numbers are obtained near the front edge of the plate for values of θ^* exceeding 1.0. The greater the value of θ^*, the greater the extent of the negative Stanton number region. From Fig. 3a it can be seen that when $\theta^* = \theta_f / \theta_w$ is greater than 1.0 that heat transfer will first be into the wall and will continue in this direction until the turbulent mixing between the film and main streams has reduced the temperature of the fluid adjacent to the wall to a value equal to or less than the wall temperature itself. Since the heat transfer coefficient contained in the Stanton number is based upon the overall temperature difference between the wall and the main stream, θ_w, the coefficient will have a negative value in the region where the heat flux is into the wall. This results in a negative local Stanton number in this region.

The average effect of the film on a flat plate of length ℓ may be expressed as the ratio of the average Stanton number with film cooling to the average Stanton number without film cooling. Defining:

$$\phi \triangleq N_{St,av} / (N_{St,av})_{\theta^*=0} \tag{14}$$

where:

$$N_{St,av} \triangleq (s/\ell) \int_{0}^{\ell/s} N_{St}\, d(x/s)$$

and:

$$(N_{St,av})_{\theta^* = 0} \triangleq (s/\ell) \int_{0}^{\ell/s} (N_{St})_{\theta^* = 0}\, d(x/s)$$

$(N_{St})_{\theta^* = 0}$ is given by (3) as:

$$(N_{St})_{\theta^* = 0} = 0.0296\, N_{R,x}^{-0.2}\, N_{Pr}^{-0.4}$$

Thus:

$$(N_{St,av})_{\theta^* = 0} = (s/\ell) \int_{0}^{\ell/s} 0.0296\, N_{R,x}^{-0.2}\, N_{Pr}^{-0.4}\, d(x/s)$$

N_{St} is given by (12); therefore:

$$N_{St,av} = (s/\ell) \int_{0}^{50} (N_{St})_{\theta^* = \theta} \left\{1 - \theta^* \left[1 - 0.006(x/s)\right]\right\} d(x/s)$$

$$+ (s/\ell) \int_{50}^{\ell/s} (N_{St})_{\theta^* = 0} \left\{1 - 16\, \theta^* (x/s)^{-0.8}\right\} d(x/s)$$

Where $(N_{St})_{\theta^* = 0}$ is given above.

Noting that $N_{R,x} \triangleq G\, x/\mu = (G\, s/\mu)(x/s)$ and performing the indicated integration yields the following result:

$$\phi = 1 - \theta^{*}\left[\frac{12.8 \ln (\ell/s) - 30.3}{(\ell/s)^{0.8}}\right] \qquad (15)$$

$$\text{for } \ell/s \geq 50$$

Equation 15 is presented in graphical form in Fig. 4b for various values of ℓ/s. Only the case of practical significance is shown; that is, $0 \leq \phi \leq 1.0$.

<u>Extension to film cooling of a rotating disk</u> The heat transfer solution for flow over a rotating disk (shrouded with no film flow), in analogy to the flat plate case, Eq. 3, may be represented as:

$$N_{St} = \text{Function}\,(N_{Pr},\ N_{R,F},\ N_{R,M}/N_{R,F},\ z_o/R)$$

where the additional parameters, $N_{R,M}/N_{R,F}$ and z_o/R are included to allow for effects of the rotating disk and flow passage size on the heat transfer behavior. (This functional relationship is obtained in a more formal manner in the next section)

If it is assumed that the adiabatic wall temperature variation with radius is the same as that obtained experimentally for the flat plate as a function of length, then the analysis may be carried out as before and a result similar to that of Eq. 13 for the ratio of the local Stanton numbers with and without film cooling will be obtained. A determination of the average effect of the film on the rotating disk cannot be made without more specific knowledge of the above indicated function. However, if Eq. 15 is modified by an empirically determined factor 0.36 and the disk radius, R, is substituted for the plate length, ℓ:

$$\phi = 1 - 0.36\ \theta^* \left[\frac{12.8\ \ln (R/s) - 30.3}{(R/s)^{0.8}}\right] \tag{16}$$

then the resulting equation (16) fits most of the experimental data of the present study to within $\pm$ ten percent. A discussion of the factor 0.36 in the above equation is contained in Section VII, DISCUSSION OF RESULTS.

FIGURE 4

RESULTS OF ANALYSIS - FLAT PLATE
FILM COOLING

(a) Local Heat transfer

$$N_{St}/(N_{St})_{\theta^*=0} = \left\{ \begin{array}{ll} 1 - \theta^* \left[1 - 0.006(x/s)\right] & \\ & 0 \leq x/s \leq 50 \\ 1 - 16\theta^* (x/s)^{-0.8} & \\ & x/s \geq 50 \end{array} \right\}$$

(b) Average Film Cooling Effect

$$\phi \triangleq N_{St,av} / (N_{St,av})_{\theta^*=0}$$

$$= 1 - \theta^* \left[\frac{12.8 \ln (\ell/s) - 30.3}{(\ell/s)^{0.8}}\right]$$

for $\ell/s \geq 50$

FIG. 4

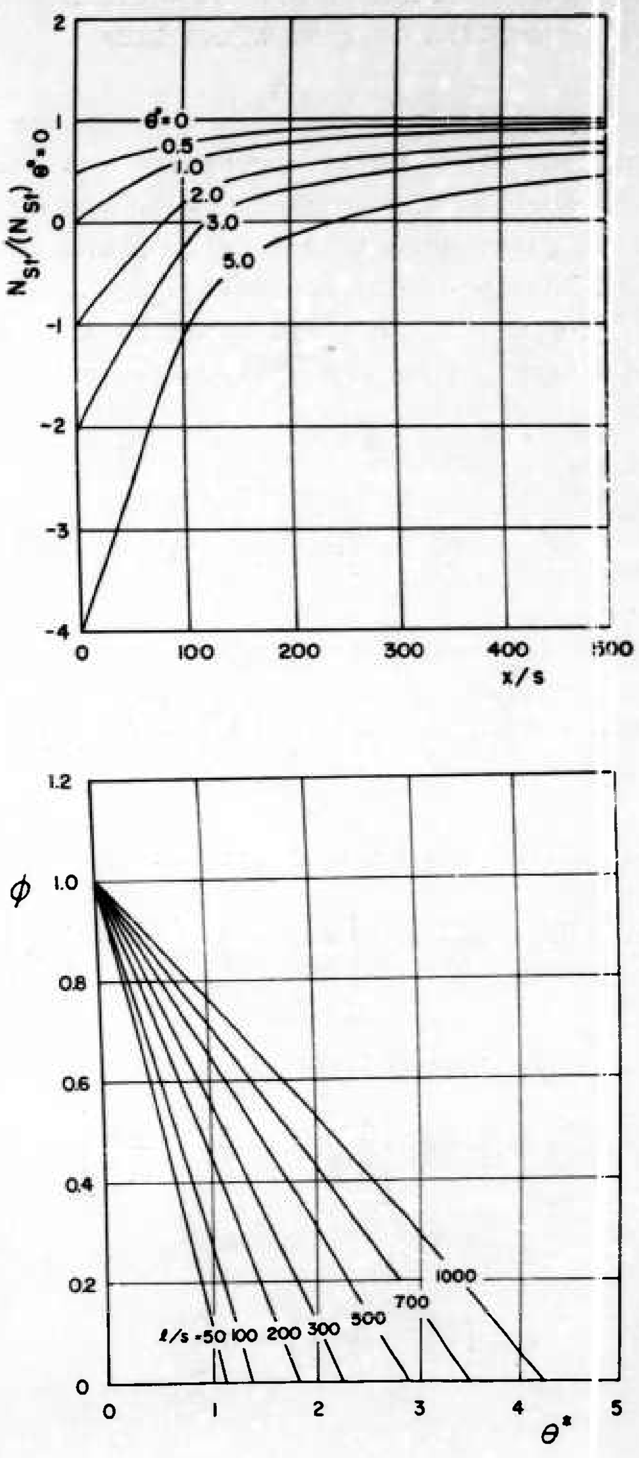

$N_{St}/(N_{St})_{\theta^*=0}$
$\theta^*=0$
0.5
1.0
2.0
3.0
5.0
x/s
ϕ
1000
700
500
300
200
100
$\ell/s = 50$
θ^*

(a)

(b)

IV. GOVERNING NONDIMENSIONAL PARAMETERS FOR FILM COOLING OF A ROTATING DISK

The governing nondimensional parameters are obtained from the pertinent differential equations and boundary conditions which describe the problem. With the nomenclature and coordinate system described in Fig. 5 and with rotational symmetry taken into account, the following equations from Schlichting[14] represent the fluid dynamics and heat transfer in the flow passage. They are written for uniform and constant density, ρ.

Continuity:

$$\frac{\partial w}{\partial z} + \frac{\partial u}{\partial r} + \frac{u}{r} = 0 \qquad (17)$$

Momentum in the radial direction:

$$u\frac{\partial u}{\partial r} - \frac{v^2}{r} + w\frac{\partial u}{\partial z} = -\frac{g_c}{\rho}\frac{\partial p}{\partial r} + \frac{\mu}{\rho}\left[\frac{\partial^2 u}{\partial r^2} + \frac{\partial}{\partial r}\left(\frac{u}{r}\right) + \frac{\partial^2 u}{\partial z^2}\right] \qquad (18)$$

Momentum in the tangetial direction:

$$u\frac{\partial v}{\partial r} + \frac{uv}{r} + w\frac{\partial v}{\partial z} = \frac{\mu}{\rho}\left[\frac{\partial^2 v}{\partial r^2} + \frac{\partial}{\partial r}\left(\frac{v}{r}\right) + \frac{\partial^2 v}{\partial z^2}\right] \qquad (19)$$

Momentum in the z-direction:

$$u\frac{\partial w}{\partial v} + w\frac{\partial w}{\partial z} = \frac{\mu}{\rho}\left[\frac{\partial^2 w}{\partial r^2} + \frac{1}{r}\frac{\partial w}{\partial r} + \frac{\partial^2 w}{\partial z^2}\right] \qquad (20)$$

Energy:

$$c_p\rho\left(u\frac{\partial t}{\partial r} + w\frac{\partial t}{\partial z}\right) = k\frac{\partial^2 t}{\partial z^2} \qquad (21)$$

The boundary conditions are:

Temperature:

$$\text{at } r = R; \quad t = t_f \quad 0 \leq z \leq s$$
$$t = t_m \quad s \leq z \leq z_o$$

$$\text{at } z = 0; \quad t = t_w = \text{constant}$$

Velocity:

$$\text{at } r = R; \quad u = u_f \quad 0 \leq z \leq s$$
$$u = u_m \quad s \leq z \leq z_o$$
$$v = R\omega$$
$$w = 0$$

$$\text{at } z = 0; \quad u = w = 0$$
$$v = r\omega$$

$$\text{at } z = z_o; \quad u = 0$$
$$v = 0$$
$$w = 0$$

These are the pertinent equations and boundary conditions in dimensional form based upon the idealization of a constant density fluid. They can be nondimensionalized to yield the governing parameters by defining the following quantities:

Coordinates:

$$r' \triangleq r/R \ , \ z' \triangleq z/R$$

Velocities:

$$u' \triangleq u/u_m \ , \ v' \triangleq v/u_m \ , \ w' \triangleq w/u_m$$

FIGURE 5

(a) ROTATING DISK COORDINATE SYSTEM

(b) FILM COOLING SYSTEM NOMENCLATURE

FIG. 5

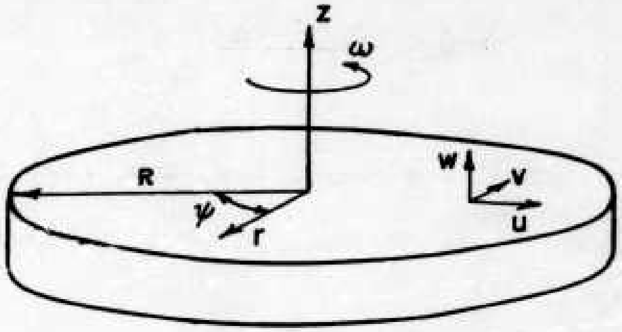

(a)

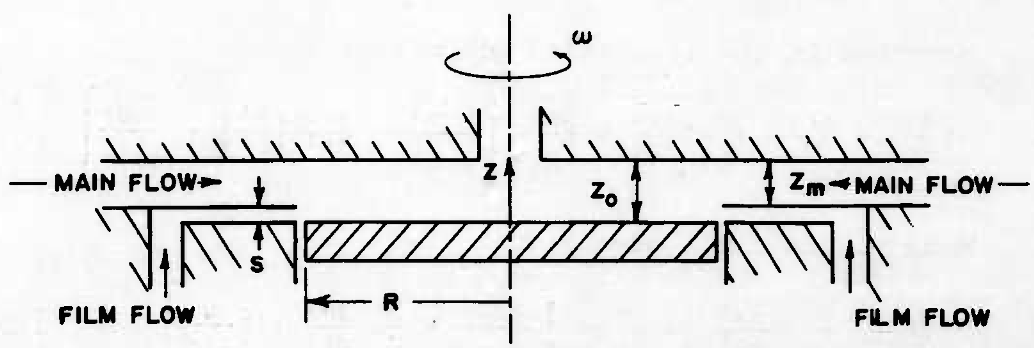

(b)

Pressure:

$$p' \triangleq g_c p \,/\, \rho\, u_m^2$$

Temperature:

$$\theta' \triangleq \frac{\theta}{\theta_w} \triangleq \frac{t - t_m}{t_w - t_m}$$

In terms of these normalized quantities, Eqs. (17) through (21) become:

Continuity:

$$\frac{\partial w'}{\partial z'} + \frac{\partial u'}{\partial r'} + \frac{u'}{r'} = 0 \qquad (22)$$

Momentum in the radial direction:

$$u'\frac{\partial u'}{dr'} - \frac{v'^2}{r'} + w'\frac{\partial u'}{\partial z'} = -\frac{\partial p'}{\partial r'} + \frac{2\pi}{N_{R,F}}\left[\frac{\partial^2 u'}{\partial r'^2} + \frac{\partial}{\partial r'}\left(\frac{u'}{r'}\right) + \frac{\partial^2 u'}{\partial z'^2}\right] \qquad (23)$$

Momentum in the tangential direction:

$$u'\frac{\partial v'}{\partial r'} + \frac{u'v'}{r'} + w'\frac{\partial v'}{\partial z'} = \frac{2\pi}{N_{R,F}}\left[\frac{\partial^2 v'}{\partial r'^2} + \frac{\partial}{\partial r'}\left(\frac{v'}{r'}\right) + \frac{\partial^2 v'}{\partial z'^2}\right] \qquad (24)$$

Momentum in the z-direction:

$$u'\frac{\partial w'}{\partial r'} + w'\frac{\partial w'}{\partial z'} = \frac{2\pi}{N_{R,F}}\left[\frac{\partial^2 w'}{\partial r'^2} + \frac{1}{r'}\frac{\partial w'}{\partial r'} + \frac{\partial^2 w}{\partial z'^2}\right] \qquad (25)$$

Energy:

$$N_{Pr}\ N_{R,F}\left[u'\frac{\partial\theta'}{\partial r'} + w'\frac{\partial\theta'}{\partial z'}\right] = 2\pi\frac{\partial^2\theta'}{\partial z'^2} \qquad (26)$$

where: $N_{R,F} \triangleq 2\pi R\ u_m\ \rho\ /\ \mu$

and: $N_{Pr} \triangleq \mu c_p\ /\ k$

The boundary conditions, in terms of the normalized quantities, are:

Temperature:

$$\text{at } r' = 1;\ \theta' = \frac{t_f - t_m}{t_w - t_m} = \frac{\theta_f}{\theta_w} \triangleq \theta^* \qquad 0 \le z \le s$$

$$\theta' = 0 \qquad s \le z \le z_o$$

$$\text{at } z' = 0;\ \theta' = 1$$

Velocity:

$$\begin{aligned}
\text{at } r' = 1;\quad & u' = u_f/u_m \quad 0 \le z \le s\\
& u' = 1 \qquad s \le z \le z_o\\
& v' = R\omega/u_m = 2\pi\ (N_{R,F}/N_{R,F})\\
& w' = 0\\
\text{at } z' = 0;\quad & u' = 0\\
& v' = r'\omega R/u_m\\
& w' = o\\
\text{at } z' = z_o/R;\quad & u' = 0\\
& v' = 0\\
& w' = 0
\end{aligned}$$

An inspection of the nondimensionalized equations and boundary conditions reveals the dependence of the heat transfer behavior on the following parameters:

$$N_{R,F} \; ; \; N_{Pr} \; ; \; N_{R,M}/N_{R,F} \; ; \; z_o/R \; ; \; u_f/u_m \; ; \; \theta^* \; ; \; R/s$$

$N_{R,F}$ and N_{Pr} are the parameters usually associated with the flat plate heat transfer case; $N_{R,M}/N_{R,F}$ and z_o/R are additional parameters introduced by the shrouded rotating disk; and u_f/u_m , θ^* , and R/s are additional parameters introduced by the film cooling. For the ranges of these parameters of interest in the turbine cooling problem, see Section VII, DISCUSSION OF RESULTS.

It is noted that for flows with uniform and constant density and viscosity, film heating and film cooling are similar processes described by the same set of differential equations.

V EXPERIMENTAL APPARATUS

The test facility at Stanford consists of an unvaned aluminum disk rotating about a vertical axis which is heated by infrared lamps on the upper surface and cooled by a main radial inflow of ambient temperature air on the lower, or test surface. An auxiliary flow of air, heated relative to the main flow, is injected adjacent to the test surface and also flows radially inward, forming the film layer. The effect of this film layer on the heat transfer to the disk has been investigated experimentally in the present study.

The bulk of the apparatus has been described in detail by Mitchell.[12] Thus only a rather brief description will be given here, with emphasis on revisions to the equipment not described previously. The facility is described by a schematic drawing in Fig. 6 and by a photograph in Fig. 7.

The complete rotating disk, 16 inches in diameter and 1.816 inches thick, consists of a sandwich construction of two thinner aluminum disks between which is bonded a 0.063 inch transite disk. The transite disk contains five National Instrument Laboratory heat meters, 0.40 inches in diameter and 0.060 inches thick, for measuring the heat flux through the disk. Separate thermocouples are located adjacent to each heat meter to measure its operating temperature. Five additional thermocouples are located on the test surface to measure the test surface temperatures. Both the heat meters and the thermocouples are located at the area-average radius of equal area annular sections. For a complete tabulation of the disk and heat meter specifications, refer to APPENDIX D.

FIGURE 6

(a) SCHEMATIC OF THE EXPERIMENTAL APPARATUS

(b) CROSS SECTION OF THE DISK

(c) DETAIL OF THE SEALING SECTION

FIG. 6

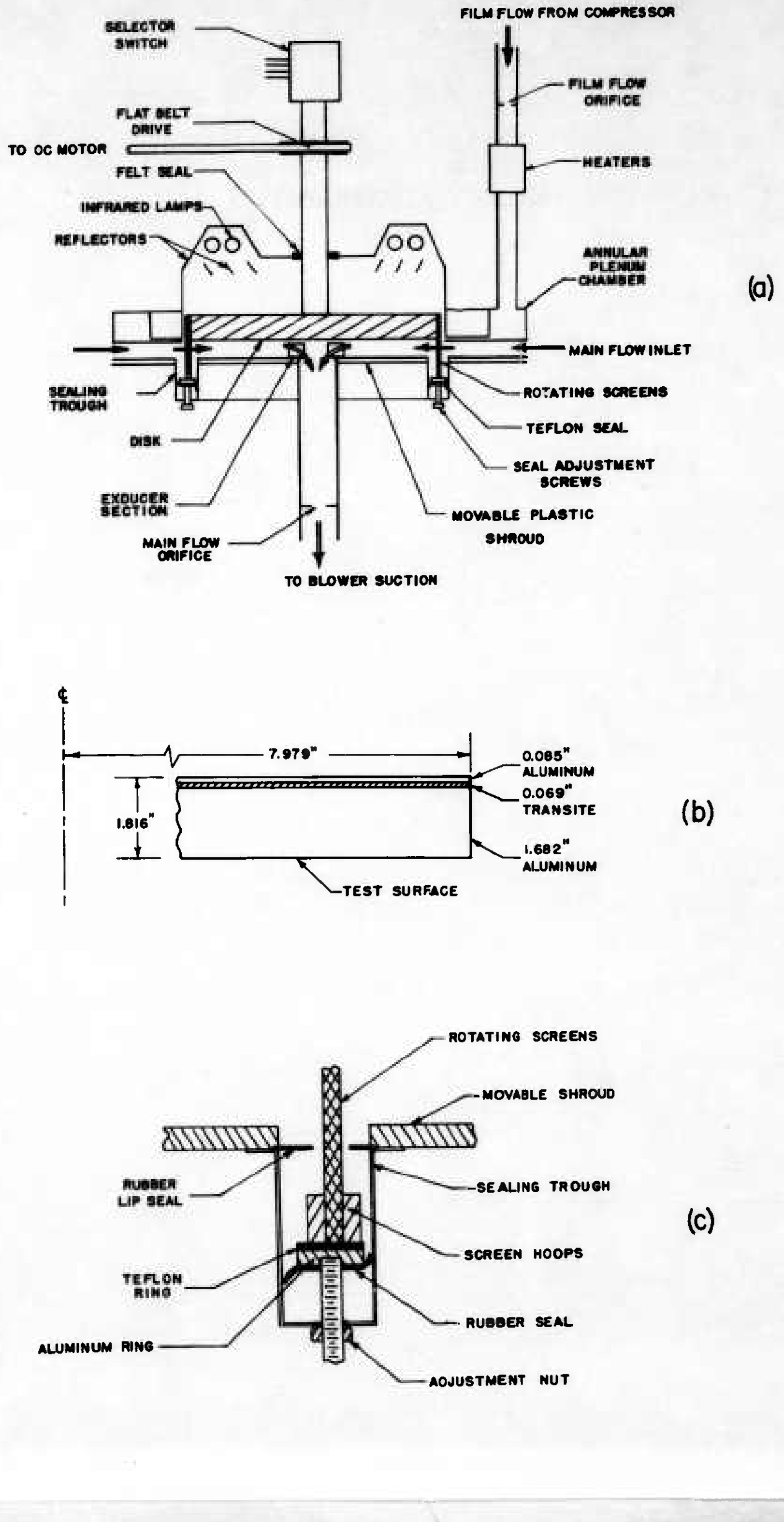

SELECTOR SWITCH
FILM FLOW FROM COMPRESSOR
FILM FLOW ORIFICE
FLAT BELT DRIVE
TO DC MOTOR
HEATERS
FELT SEAL
INFRARED LAMPS
REFLECTORS
ANNULAR PLENUM CHAMBER
(a)
MAIN FLOW INLET
SEALING TROUGH
ROTATING SCREENS
TEFLON SEAL
DISK
SEAL ADJUSTMENT SCREWS
EXDUCER SECTION
MOVABLE PLASTIC SHROUD
MAIN FLOW ORIFICE
TO BLOWER SUCTION
7.979"
0.065" ALUMINUM
0.069" TRANSITE
1.816"
(b)
1.682" ALUMINUM
TEST SURFACE
ROTATING SCREENS
MOVABLE SHROUD
RUBBER LIP SEAL
SEALING TROUGH
(c)
SCREEN HOOPS
TEFLON RING
RUBBER SEAL
ALUMINUM RING
ADJUSTMENT NUT

FIGURE 7

EXPERIMENTAL APPARATUS

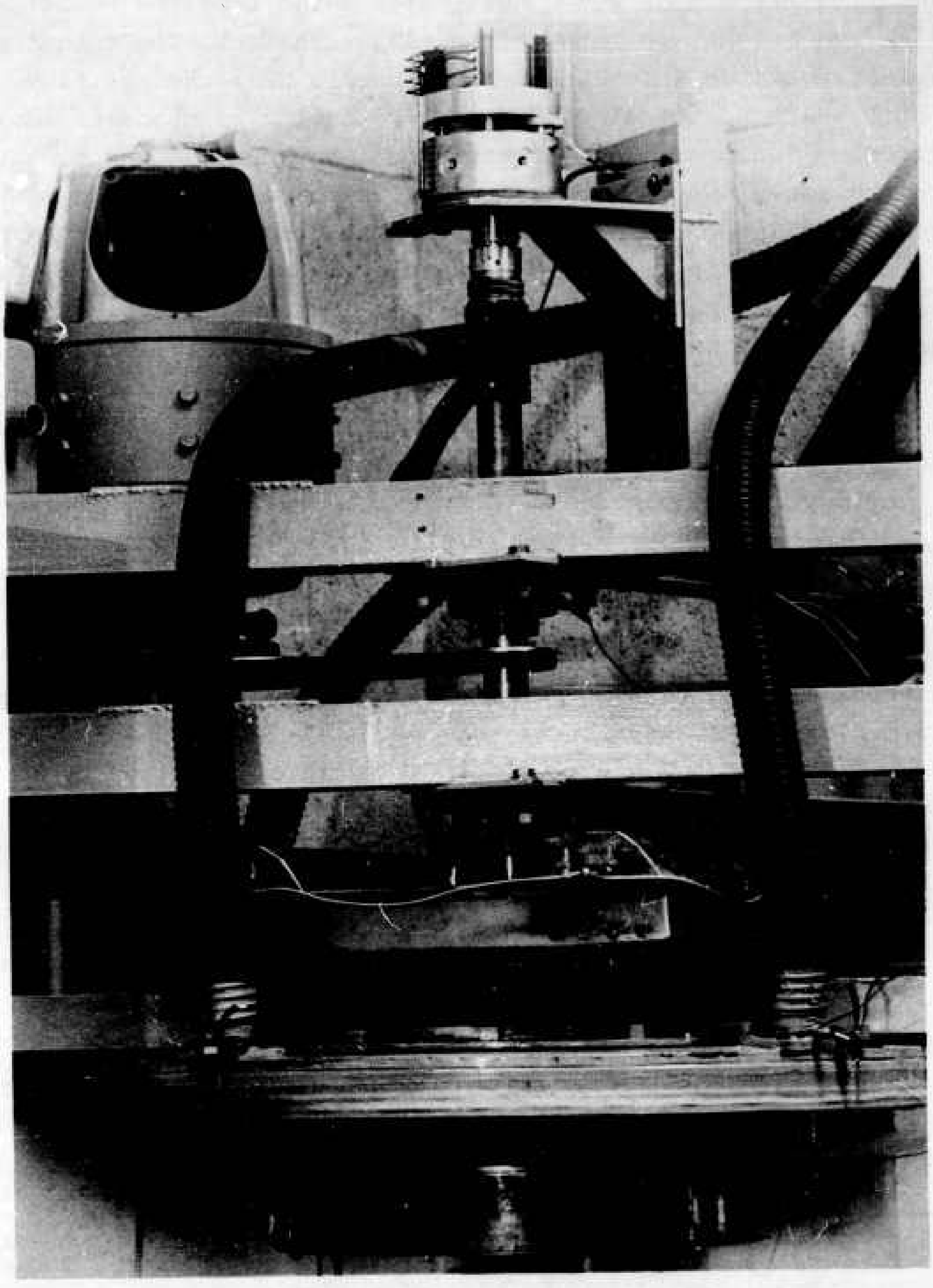

The thermocouple and heat meter leads from the rotating disk are brought up through the hollow shaft to the rotating selector switch which transmits the emfs from the rotating inner shaft to the stationary outer housing by means of small circular springs. These springs roll between grooved contacts in the inner hub and outer housing in the manner of planetary gears.† Since rolling, rather than sliding, contact is maintained, the extraneous emf production in the switch itself is held to a minimum ($\pm$ 5 microvolts). The thermocouple and heat meter temperatures are referenced against a distilled water-ice junction and measured with a precision potentiometer.

The flow passage under the disk is bounded by a transparent acrilic plastic shroud which can be moved in the vertical direction to vary the passage depth.

The main flow air (500 to 1800 lbm/hr) is induced by means of a centrifugal blower located downstream of the disk. The air flow passing through the blower, consisting of both the main and film flows, is measured by means of an A.S.M.E. standard orifice located between the disk system and the blower. The film flow air is separately metered.

The film flow air (40 to 150 lbm/hr) is provided by the laboratory air compressor system, and is heated relative to the main flow by electric resistance heaters installed in the line upstream of the disk system. The flow is metered with a standard A.S.M.E. orifice located upstream of the heating section. The heated film flow is supplied at four locations to an annular plenum chamber surrounding the disk. The air flows from the plenum into the film passage formed by the thin plastic divider between the film and main flows. The position of this plastic divider can be changed to vary the film passage spacing.

---

† Suggested by W. A. Casler of the Aero jet General Corporation. Patents on the contactor are pending. See Mitchell[12] for a detailed description of this quite simple and low noise non-slip contactor.

At design point operation, actual gas turbines operate with the rotor tip velocity approximately equal to the tangential velocity component of the entering gas. Fullfillment of this boundary condition is achieved on the model by the use of screens wound around the circumference of the disk. Ten layers of 50 mesh aluminum screening, 4.5 inches wide are wound around the disk and secured with steel hoops. As the screens rotate with the disk they accelerate both the main and film flows to the disk tangential velocity so that the relative velocity of the air leaving the screens with respect to the disk is purely radial at all test conditions.

The lower portion of the screens and the inner and outer lower steel hoops rotate in a copper sealing section attached to the shroud. Within the sealing section trough is an aluminum backed Teflon ring which bears against the lower surface of the steel hoops attached to the screens. (See Fig. 6c) This ring is free to move in the vertical direction within the trough, and in operation the small vacuum present in the flow passage results in a pressure differential across the seal which seats the ring against the hoops. Adjustable stops attached to the bottom of the ring limit its upward travel and permit adjustment of the bearing pressure.

The experimental work of Mitchell[12] was done without the Teflon ring seal. Velocity profiles of the flow revealed that about 30 to 40 percent of the flow bypassed the screens by traveling down and around the lower screen hoops. This situation resulted in a deficiency in the tangential velocity component for the bypass portion of the main flow, as well as stalled regions in the flow near the shroud. With the Teflon seal in place, much more satisfactory velocity profiles were obtained, as shown in APPENDIX A. The heat transfer results reported by Mitchell[12] were measurably affected by the bypass flow as will be shown in the next section.

VI EXPERIMENTAL RESULTS

The main objective of the experimental program was to determine the effect of the film air on the heat transfer rate at the disk surface. A necessary preliminary objective was the establishment of the heat transfer characteristics of the system with no film cooling; in particular, the effect of eliminating the bypass flow on the heat transfer behavior reported by Mitchell[12] was desired.

Heat Transfer to a Shrouded Rotating Disk Without Film Flow

The nondimensionalized governing equations (see Section IV) indicate that in the absence of a film cooling flow the data should correlate as:

$$N_{St,av} = \text{Function}\ (N_{Pr}\ ,\ N_{R,F}\ ,\ N_{R,M}/N_{R,F}\ ,\ z_o/R)$$

where $N_{St,av}$ is defined as the average Stanton number over the entire disk surface.

Fig. 8 shows some representative data plotted as $N_{St,av}$ vs. $N_{R,F}$ for a constant N_{Pr}, at four approximately constant values of $N_{R,M}/N_{R,F}$ and with z_o/R held constant. This family of curves will correlate onto a single line when plotted as $N_{St,av}N_{R,F}^{0.65}$ vs. $N_{R,M}/N_{R,F}$ as in Fig. 9.

Effect of z_o/R: Most of the data Fig. 9 was obtained at a value of $z_o/R \cong 0.11$. Moreover, it was felt that this parameter would probably have a minor effect on the heat transfer results. It has been previously shown by Mitchell[12] that the effect of the boundary layer growth on the disk and shroud and the associated increase in the fluid velocity in the flow passage should have at most a 3 percent effect on the heat transfer results in the range $0.1 < z_o/R < \infty$. The velocity profiles presented in APPENDIX A support the conclusion that the passage flow is virtually a potential flow and therefore changes in z_o/R should affect the flow only through the boundary layer effect predicted.

Some data at $z_o/R \cong 0.18$ was taken to check this effect. Fig. 9 shows that there may be a slight effect of z_o/R in this range, but that all of the data can be represented within the experimental uncertainty by:

$$N_{St,av} N_{R,F}^{0.65} = 66.0 + 30\ N_{R,M}/N_{R,F} \tag{27}$$

This equation is believed to be representative of radial inflow heat transfer over at least the range $0.1 \leq z_o/R \leq 0.2$ and probably for even higher magnitudes.

<u>Comparison with the results of Mitchell[12]:</u> Some representative data obtained by Mitchell[12] on the same test facility, but with inadequate sealing of the rotating screens, is plotted in Fig. 10 as $N_{St,av} N_{R,F}^{0.65}$ vs. $N_{R,M}/N_{R,F}$ and compared with the present results, Eq. 27. Mitchell's data is up to 20 percent higher than the present results at the lower range of $N_{R,M}/N_{R,F}$ and up to 10 percent lower at the highest values of $N_{R,M}/N_{R,F}$. Both sets of data are in essential agreement at $N_{R,M}/N_{R,F} = 0.9$. The differences can be rationalized on the basis of the effect of the bypass flow around the screens.

Higher heat transfer coefficients reflect larger relative velocities between the flow and the disk. It is reasonable to assume, therefore, that at low values of $N_{R,M}/N_{R,F}$ the previous flow conditions (with bypassing) produce higher relative velocities in the flow passage with respect to the disk. At values of $N_{R,M}/N_{R,F}$ greater than 0.9, the opposite situation appears to prevail.

The bypass flow creates several effects, some of which tend to increase the relative velocities while others act to decrease these velocities.

FIGURE 8

AVERAGE STANTON NUMBER vs. FLOW REYNOLDS NUMBER
WITHOUT FILM COOLING

FIGURE 9

CORRELATED HEAT TRANSFER RESULTS
WITHOUT FILM COOLING

The best fit line indicated is given by Eq. 27:

$$N_{St,av} N_{R,F}{}^{0.65} = 66.0 + 30 \; N_{R,M}/N_{R,F}$$

Figure	Symbol	Nominal $N_{R,M}/N_{R,F}$	Nominal z_o/R
8 & 9	⊙	0.3	0.11
8 & 9	◇ (with dot)	0.6	0.11
8 & 9	⊡	0.9	0.11
8 & 9	◺	1.25	0.11
9	△	---	0.18

FIG. 8

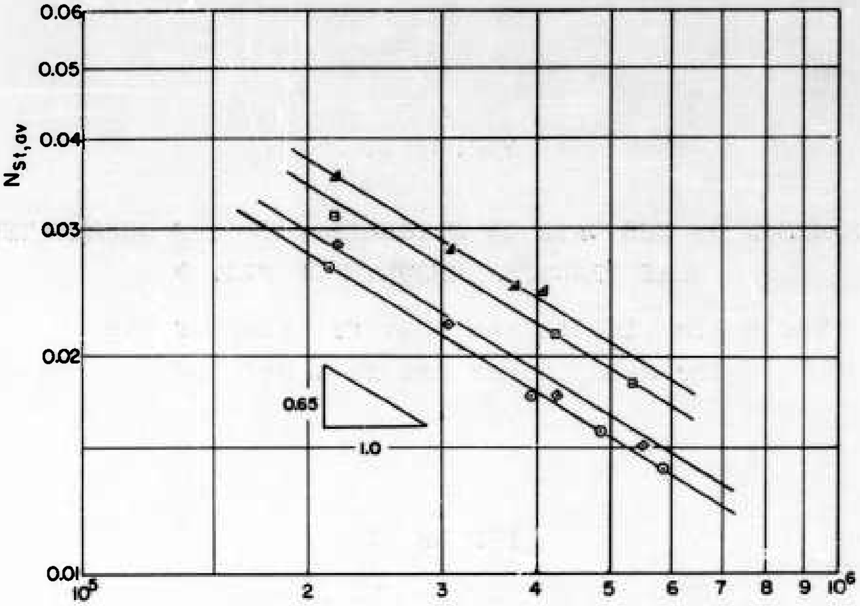
0.06
0.05
0.04
0.03
0.02
0.01
$N_{St,av}$
0.65
1.0
10^5
2
3
4
5
6
7
8
9
10^6
$N_{R,F}$

FIG. 9

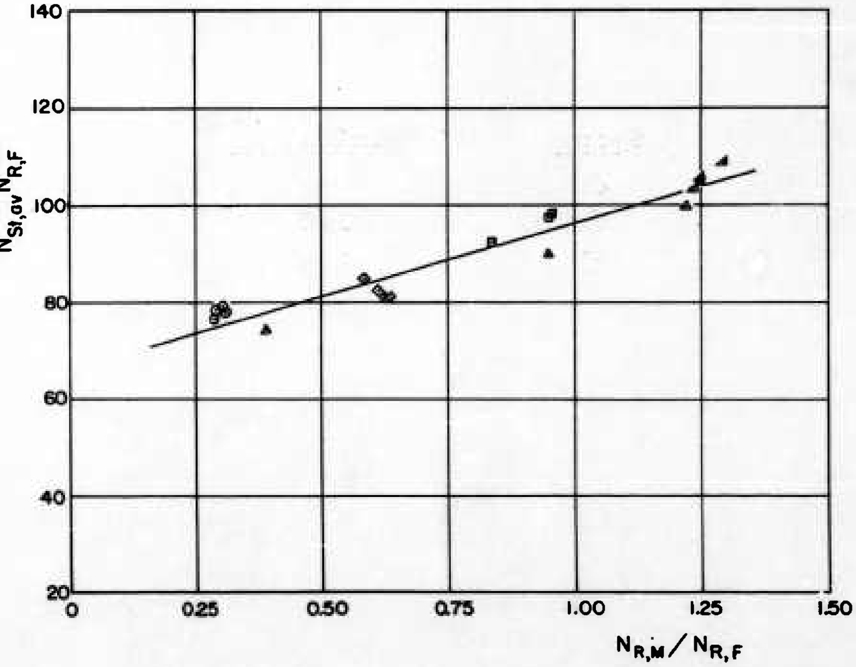
140
120
100
80
60
40
20
$N_{St,av}N_{R,F}^{0.65}$
0
0.25
0.50
0.75
1.00
1.25
1.50
$N_{R,M}/N_{R,F}$

FIGURE 10

COMPARISON OF THE DATA OF MITCHELL WITH THE CORRELATED HEAT TRANSFER RESULTS OF FIG. 9

The solid line is the best fit line of Fig. 9
The data points are from Ref. 12

FIGURE 11

EFFECT OF THE MASS VELOCITY RATIO, G^*, ON THE CORRELATED HEAT TRANSFER AT $\theta^* = 0$

$R/s = 200 \quad z_o/R = 0.11$

The solid line is the best fit line of Fig. 9

Symbol	Nominal G^*
△	0.5
⊙	1.0
⊡	1.5

FIG.10

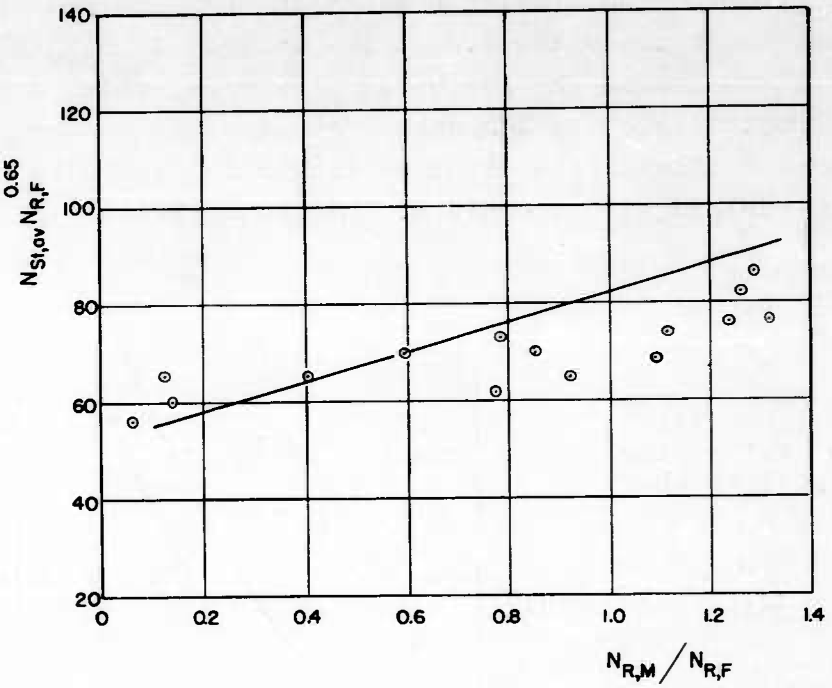

140
120
100
80
60
40
20
0
0.2
0.4
0.6
0.8
1.0
1.2
1.4
$N_{St,av} N_{R,F}^{0.65}$
$N_{R,M} / N_{R,F}$

FIG.11

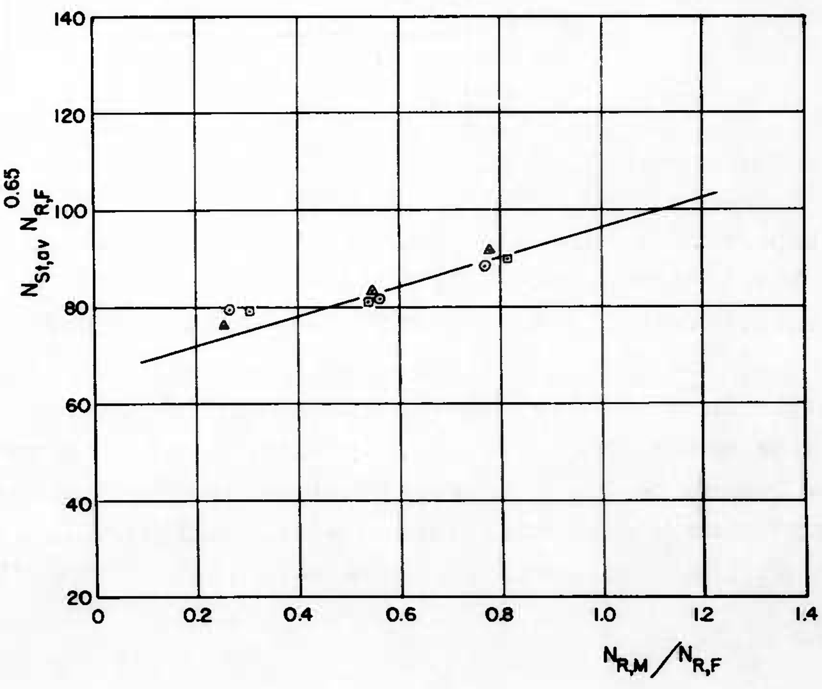

140
120
100
80
60
40
20
0
0.2
0.4
0.6
0.8
1.0
1.2
1.4
$N_{St,av} N_{R,F}^{0.65}$
$N_{R,M} / N_{R,F}$

Mitchell has reported stalled regions in the flow passage near the shroud which are extensive at low values of $N_{R,M}/N_{R,F}$. These stalls decrease the available flow area, which increases the flow radial velocity component near the disk. The effect of the bypass flow on the relative tangential velocity component is best described with the aid of the sketch below:

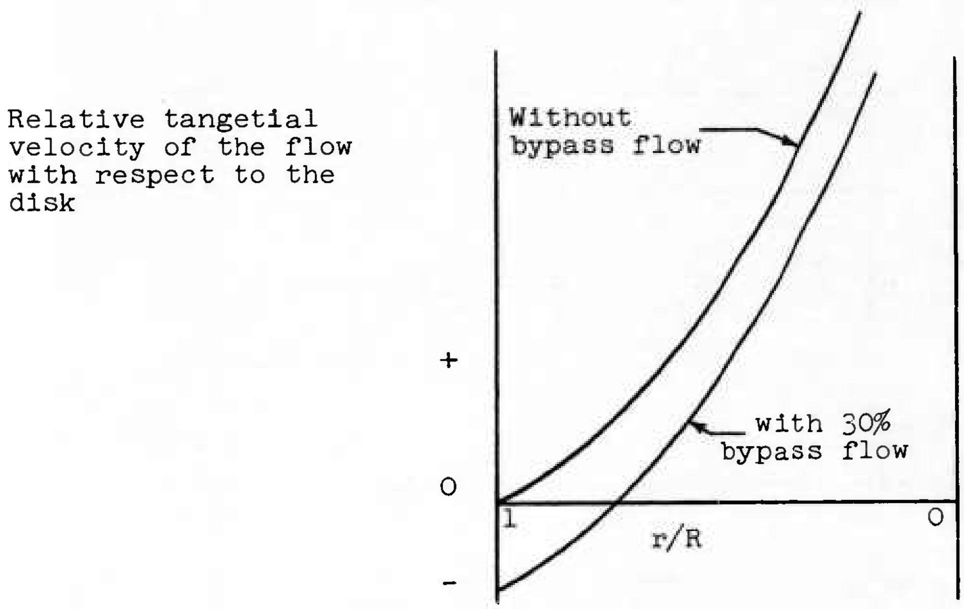

With no bypass flow, the flow leaves the screens without a tangential velocity component relative to the disk. However, the tangential velocity of the flow increases as it flows toward the center of the disk, in the manner of a potential vortex. This results in a relative tangential velocity between the flow and the disk which increases rapidly with decreasing radii. With flow bypassing the screens, the flow in the passage behaves approximately as a potential vortex with a tangential velocity component at the disk periphery less than that of the disk itself.

Although this results in a relative tangential velocity at the disk periphery, the overall effect for the amount of bypassing under consideration (30 to 40 percent) is a reduction in the average magnitude of the relative tangential velocity.

It appears that this reduction in relative tangential velocity is more than compensated for at low values of $N_{R,M}/N_{R,F}$ by the increase in relative radial velocity caused by the stalled regions. At higher values of $N_{R,M}/N_{R,F}$, however, the deficiency in the tangential velocity component seems to be relatively more important since the present (no bypass flow) heat transfer results are higher in this range.

Heat Transfer With Film Cooling

Effect of the film flow for $\theta^* = 0$: Heat transfer measurements were first obtained for one limiting case of the film flow, $\theta^* = 0$, $G^* = 1$; that is, a film flow with velocity and temperature identical to that of the main flow. The heat transfer behavior, as expected, is in agreement with the previous results where no film flow was used. These results are shown in Fig. 11 for $R/s = 200$ and $z_o/R \cong 0.11$.

In addition, results were obtained for the case where $\theta^* = 0$ but u_m and u_f were different. These results are also shown in Fig. 11. It should be noted that the results of Fig. 11 are given in the caption not in terms of a velocity ratio, but rather in terms of the mass velocity ratio, G^*, where:

$$G^* = (\rho u)_f \,/\, (\rho u)_m$$

For the temperature levels of the present study, the density differences between the main and film flows are at most 10 percent so that the mass velocity ratio is indicative of the velocity ratio, u_f/u_m. However, work of other researchers indicates that G^* is the significant correlating parameter, rather than u_f/u_m. Futher discussion of this point is included in Section VII, DISCUSSION OF RESULTS.

The results of Fig. 11 indicate that the effect of the unheated film on the average heat transfer from the disk is minor for $R/s = 200$. These results are in accord with the results of flat plate film cooling studies. Hartnett, et al[10] show that the unheated film affects the local heat transfer coefficients on a flat plate only for a relatively short distance downstream of the injection slot for $0.34 \leq G^* \leq 1.23$. It is expected, however, that for very large mass velocity ratios a wall jet condition is approached where the film flow completely governs the heat transfer.

Effect of θ^* and G^*: The effect of θ^* and G^* was investigated at various values of $N_{R,M}/N_{R,F}$ at a single value of $R/s = 200$. The results of this investigation are shown in Fig. (a) of Figs. 12 through 15. The effect of the film cooling is presented in terms of the ordinate ϕ defined as:

$$\phi = N_{St,av} N_{R,F}^{0.65} / (N_{St,av} N_{R,F}^{0.65})_{\theta^* = 0} \tag{28}$$

It should be noted that this definition is simply another representation of ϕ, as previously defined in Eq. (14). Equation (28) is the more convenient formulation for treating the experimental results.

An inspection of the data indicates that they will correlate reasonably well as ϕ vs. $\theta^* G^{*0.6}$. Fig. (b) of Figs. 12 through 15 and Fig. 16 show the development of this correlation. As θ^* approaches zero, the influence of G^* vanishes in agreement with the results of Fig. 11.

Effect of $N_{R,M}/N_{R,F}$: The effect of $N_{R,M}/N_{R,F}$ is quite small, as can be seen in Fig. 17 where the combined data of Figs. 12 through 16 is plotted. This data correlates within a band width which is approximately equal to the estimated uncertainty interval. Eq. 16, the modified analysis result, evaluated at $R/s = 200$ provides a good fit to this data.

<u>Effect of R/s</u>: Investigation of the effect of θ^* was carried out at various G^* and $N_{R,M}/N_{R,F}$ values at two additional R/s values, 500 and 143. The results of these tests are shown in Figs. 18 and 19. Again the data is seen to correlate reasonably well on a ϕ vs. $\theta^* G^{*0.6}$ basis for both values of R/s. The modified analysis result, Eq. 16, evaluated at the corresponding values of R/s is also plotted in Figs. 18b and 19b. This equation slightly overestimates the film cooling effect at $R/s = 500$ and slightly underestimates the effect at $R/s = 143$.

Finally, the results for all three R/s values can be correlated as ϕ vs. $\theta^* G^{*0.6}/ (R/s)^{0.7}$, and these results are shown in this form in Fig. 20. A best fit straight line, passing through the (1,0) point is represented by the equation:

$$\phi = 1.0 - 7.7\ \theta^* G^{*0.6}/ (R/s)^{0.7} \qquad (29)$$

FIGURE 12

FILM COOLING EFFECT AT A NOMINAL $N_{R,M}/N_{R,F}$ OF 1.25

$R/s = 200$

$z_o/R = 0.11$

(a) Effect of θ^* at various G^* values

(b) Correlated results

Symbol	Nominal G^*
⊙	1.0
△	1.75
⊡	2.85

FIG. 12

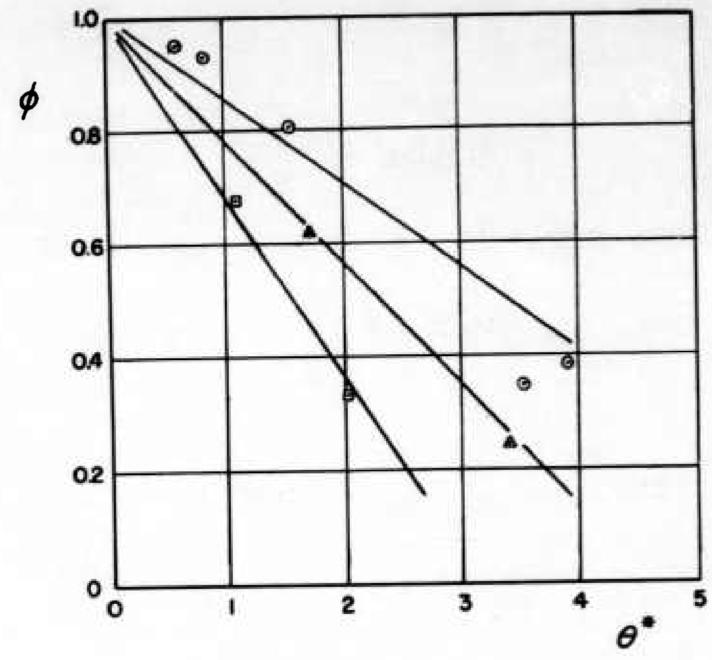

1.0
0.8
0.6
0.4
0.2
0
ϕ
0
1
2
3
4
5
θ^*

(a)

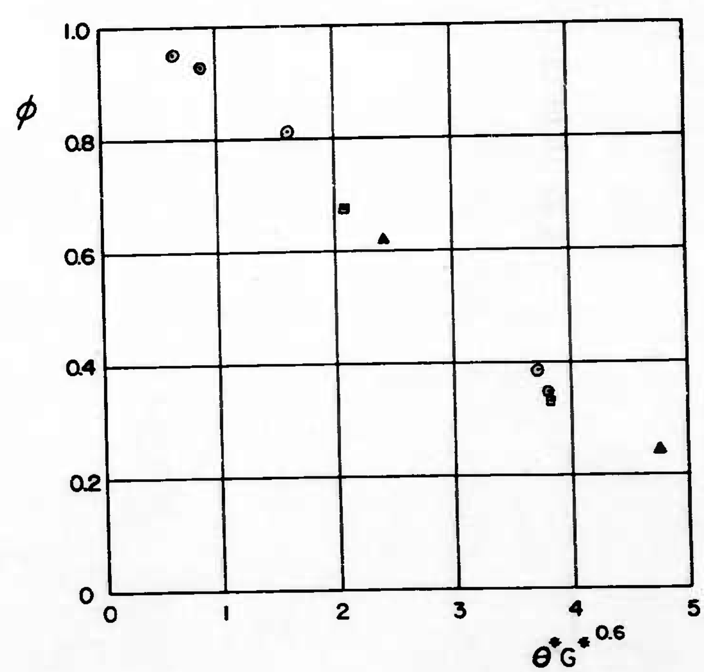

1.0
0.8
0.6
0.4
0.2
0
ϕ
0
1
2
3
4
5
$\theta^* G^{*0.6}$

(b)

FIGURE 13

FILM COOLING EFFECT AT A NOMINAL $N_{R,M}/N_{R,F}$ OF 1.0

$R/s = 200$

$z_o/R = 0.11$

(a) Effect of θ^* at various G^* values

(b) Correlated results

Symbol	Nominal G^*
◇ (dotted)	0.70
△ (dotted)	0.90
θ	0.92
⊡	1.30
▽ (dotted)	1.90

FIG. 13

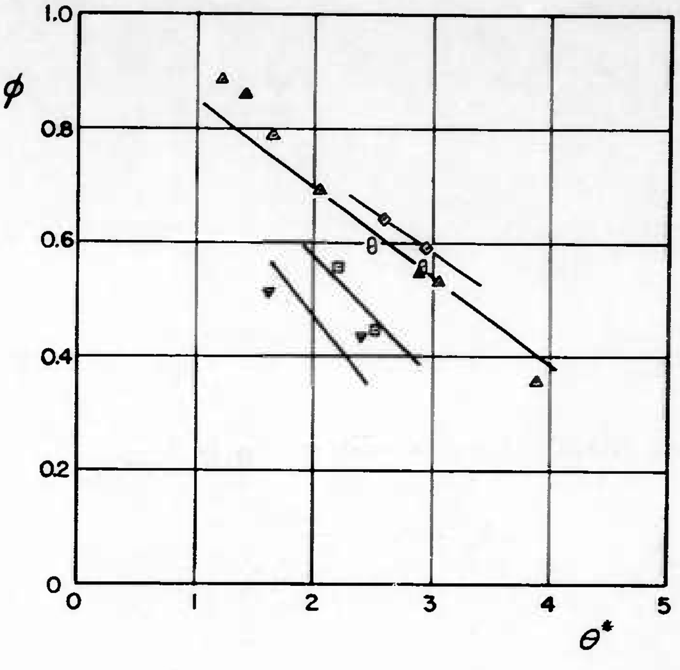

1.0
0.8
0.6
0.4
0.2
0
ϕ
0
1
2
3
4
5
θ^*

(a)

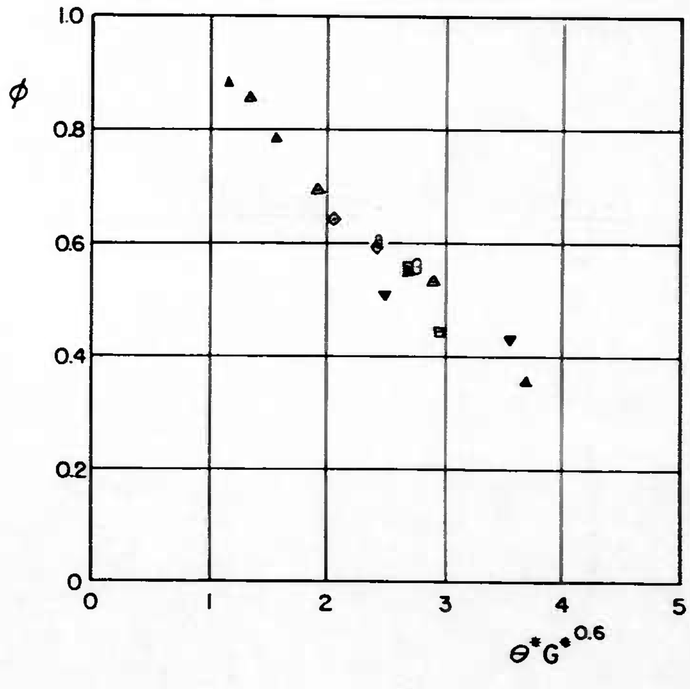

1.0
0.8
0.6
0.4
0.2
0
ϕ
0
1
2
3
4
5
$\theta^* G^{*0.6}$

(b)

FIGURE 14

FILM COOLING EFFECT AT A NOMINAL $N_{R,M}/N_{R,F}$ OF 0.85

$R/s = 200$

$z_o/R = 0.11$

(a) Effect of θ^* at various G^* values

(b) Correlated results

Symbol	Nominal G^*
⊙	1.4
▽	2.6

FIG. 14

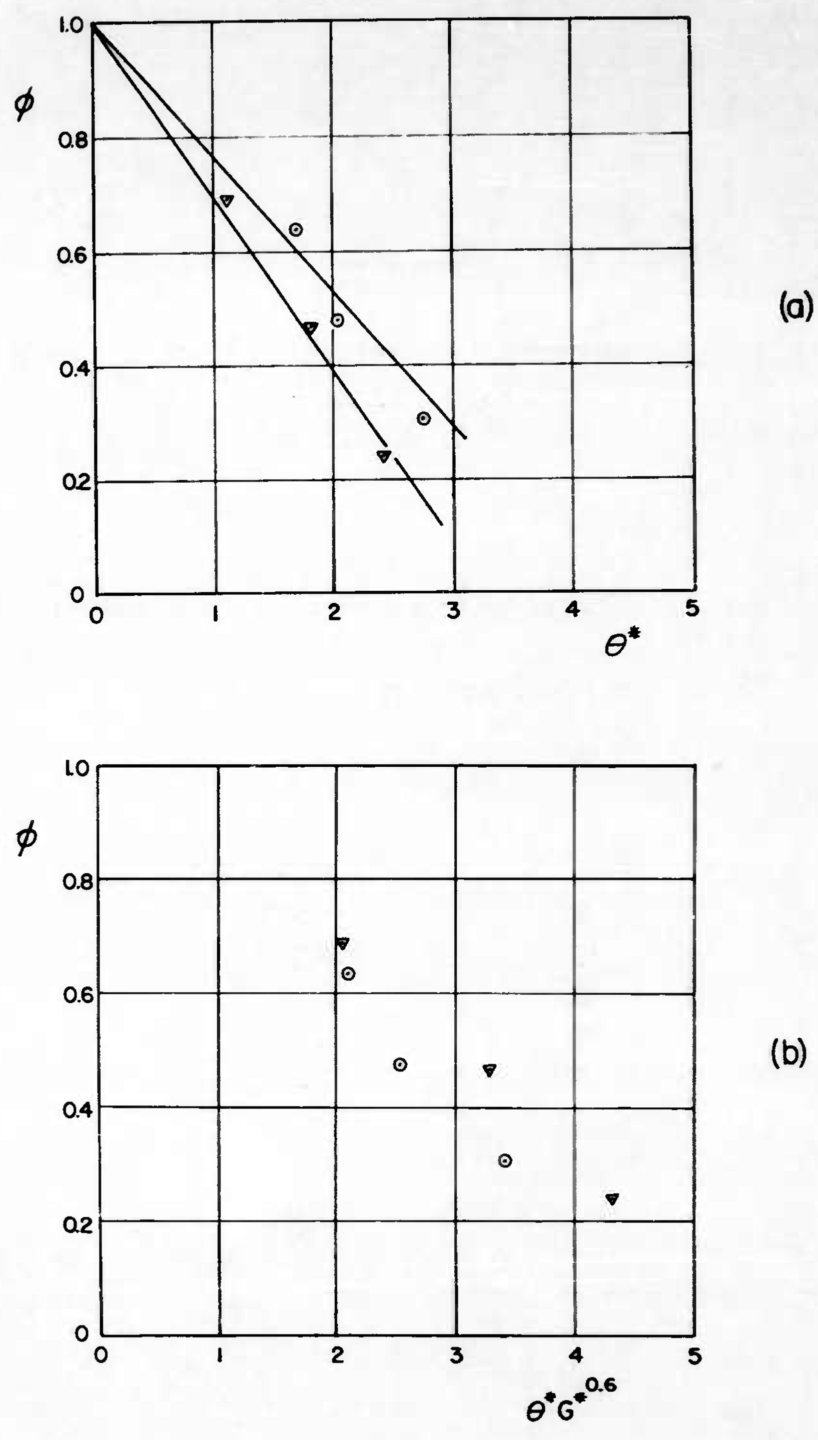

FIGURE 15

FILM COOLING EFFECT AT A NOMINAL $N_{R,M}/N_{R,F}$ OF 0.5

$R/s = 200$

$z_o/R = 0.11$

(a) Effect of θ^* at various G^* values

(b) Correlated results

Symbol	Nominal G^*
⊙	0.935
⊡	0.910
△	1.94
◇	2.28
▽	4.0

FIG. 15

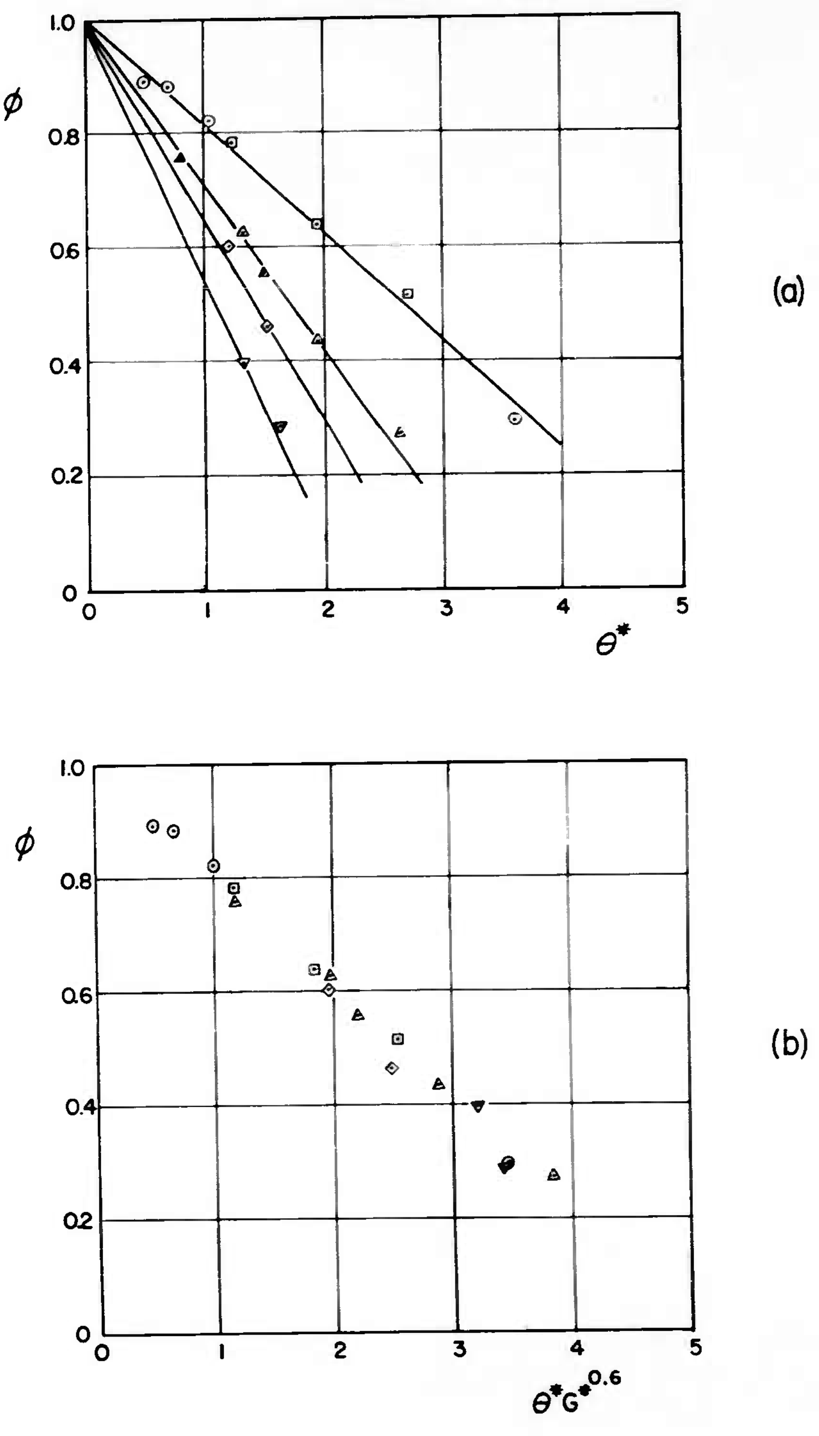

(a)
1.0
0.8
0.6
0.4
0.2
0
ϕ
0
1
2
3
4
5
θ^*
(b)
1.0
0.8
0.6
0.4
0.2
0
ϕ
0
1
2
3
4
5
$\theta^* G^{*0.6}$

FIGURE 16

FILM COOLING EFFECT AT A NOMINAL $N_{R,M}/N_{R,F}$ OF 0.3

$R/s = 200$ Nominal $G^* = 0.94$

$z_o/R = 0.11$

FIGURE 17

CORRELATED FILM COOLING EFFECT AT $R/s = 200$

$z_o/R = 0.11$

The solid line is the modified analysis result, Eq. 16, evaluated at $R/s = 200$

Symbol	Nominal $N_{R,M}/N_{R,F}$
⊙	0.3 (Data of Fig. 16)
⊡	0.5 (Data of Fig. 15)
▷	0.8 (Data of Fig. 14)
◇	1.0 (Data of Fig. 13)
△	1.25 (Data of Fig. 12)

FIG. 16

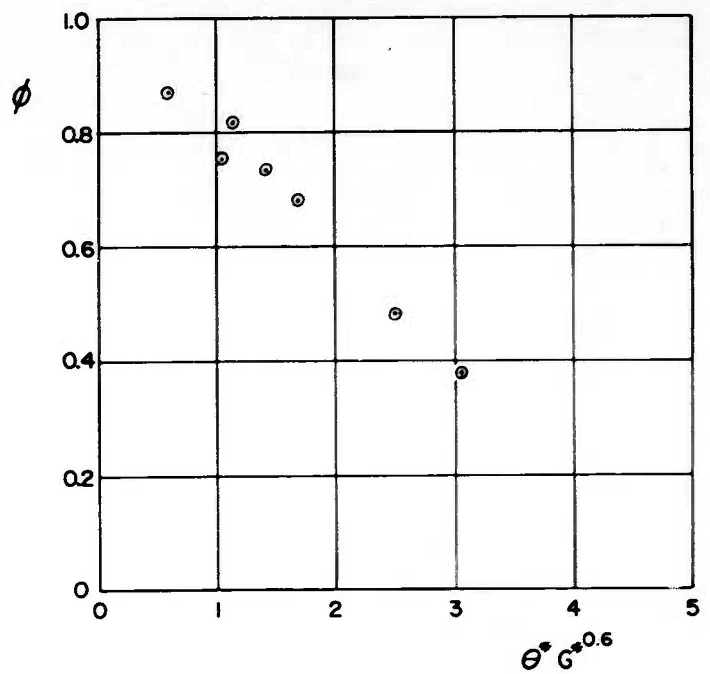

1.0
0.8
0.6
0.4
0.2
0
ϕ
0
1
2
3
4
5
$\theta^* G^{*0.6}$

FIG. 17

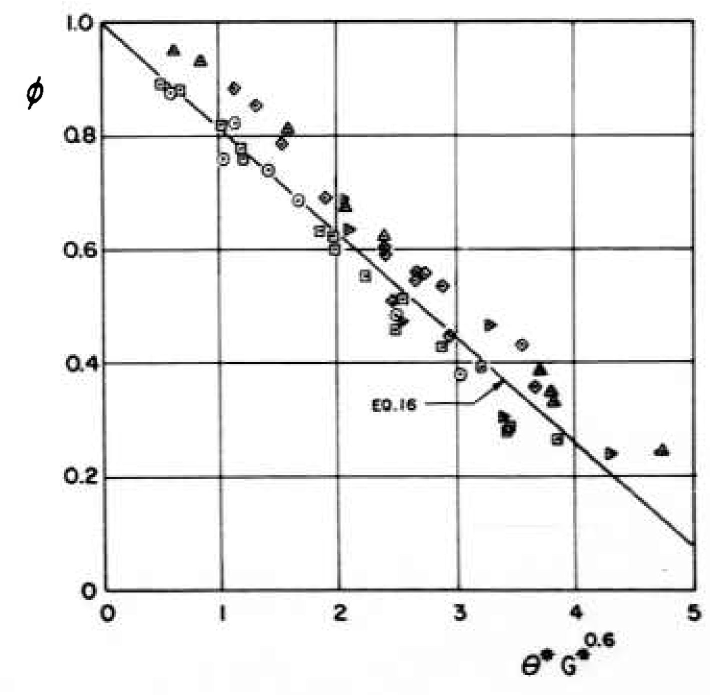

1.0
0.8
0.6
0.4
0.2
0
ϕ
EQ. 16
0
1
2
3
4
5
$\theta^* G^{*0.6}$

FIGURE 18

FILM COOLING EFFECT AT $R/s = 500$, $z_o/R = 0.11$

(a) Effect of θ^* at various G^* and $N_{R,M}/N_{R,F}$ values

(b) Correlated results
The solid line is the modified analysis result, Eq. 16, evaluated at $R/s = 500$

Symbol	Nominal $N_{R,M} / N_{R,F}$	Nominal G^*
⊙	0.3	1.0
△ (dotted)	0.3	2.3
⊡	0.5	1.9
▽ (dotted)	0.5	2.4
◇ (dotted)	0.75	1.75

FIG. 18

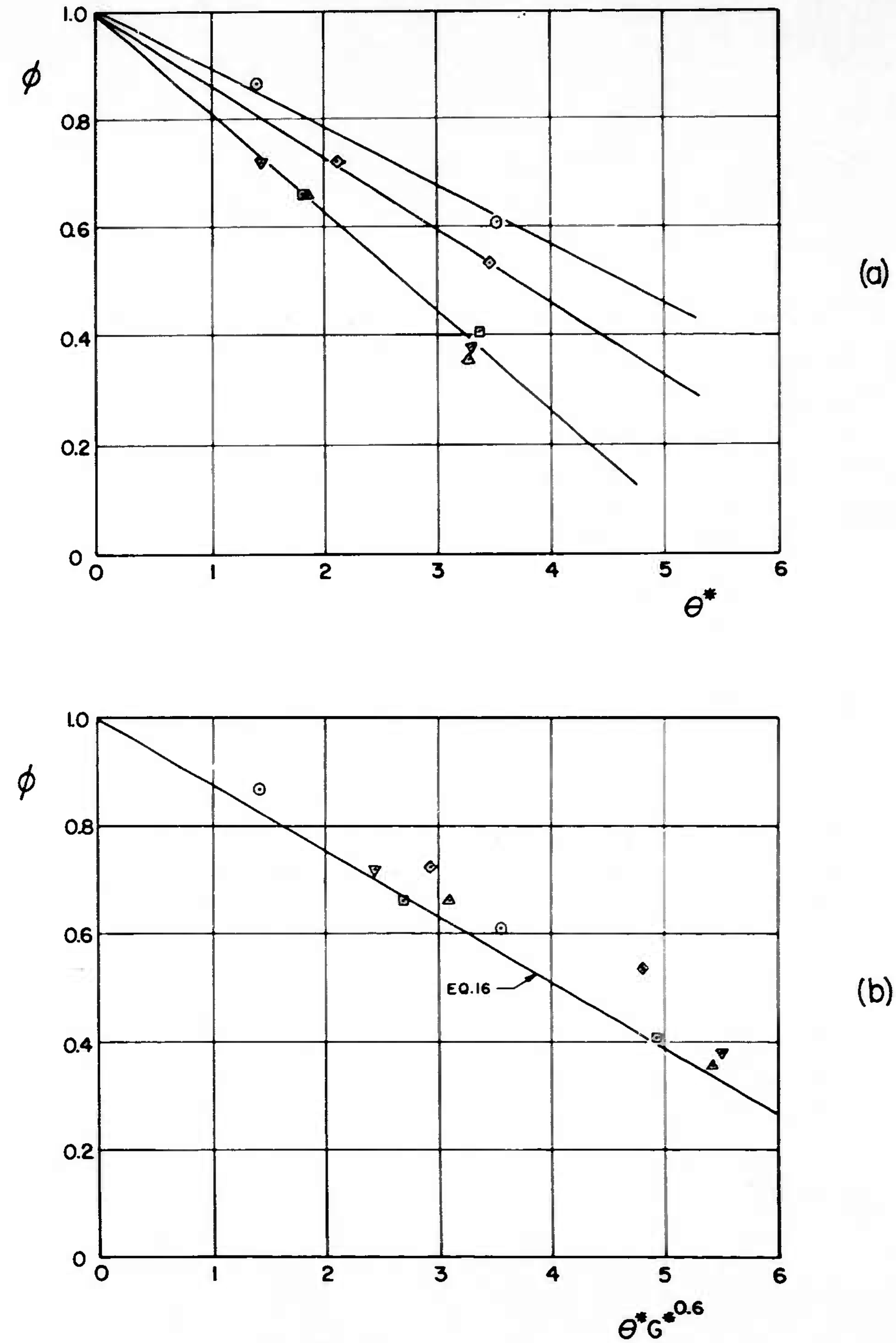

FIGURE 19

FILM COOLING EFFECT AT $R/s = 143$, $z_o/R = 0.11$

(a) Effect of θ^* at various G^* and $N_{R,M} / N_{R,F}$ values

(b) Correlated results
The solid line is the modified analysis result, Eq. 16, evaluated at $R/s = 143$

Symbol	Nominal $N_{R,M} / N_{R,F}$	Nominal G^*
⊙	0.3	1.0
⊡	0.3	2.0
▽	0.5	2.0
△	0.5	3.2
◇	0.75	3.2
◺	1.15	2.5

FIG. 19

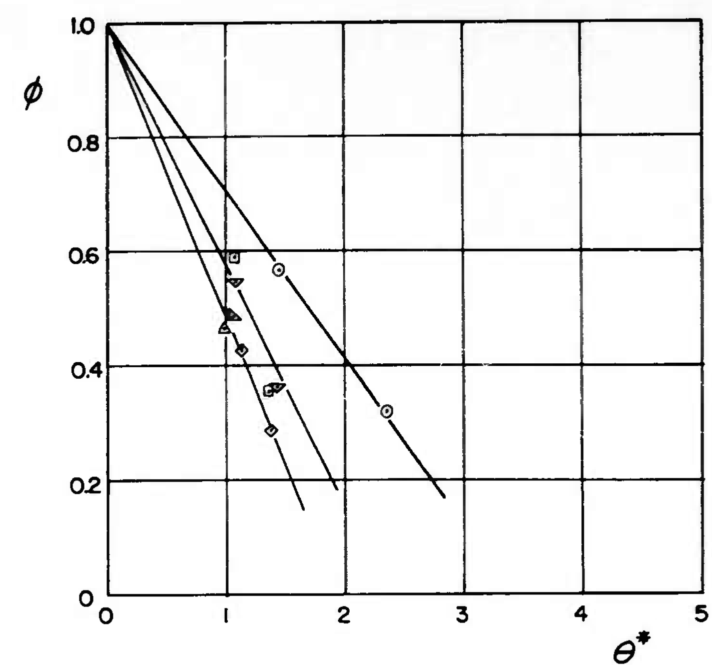
1.0
0.8
0.6
0.4
0.2
0
ϕ
0
1
2
3
4
5
θ^*

(a)

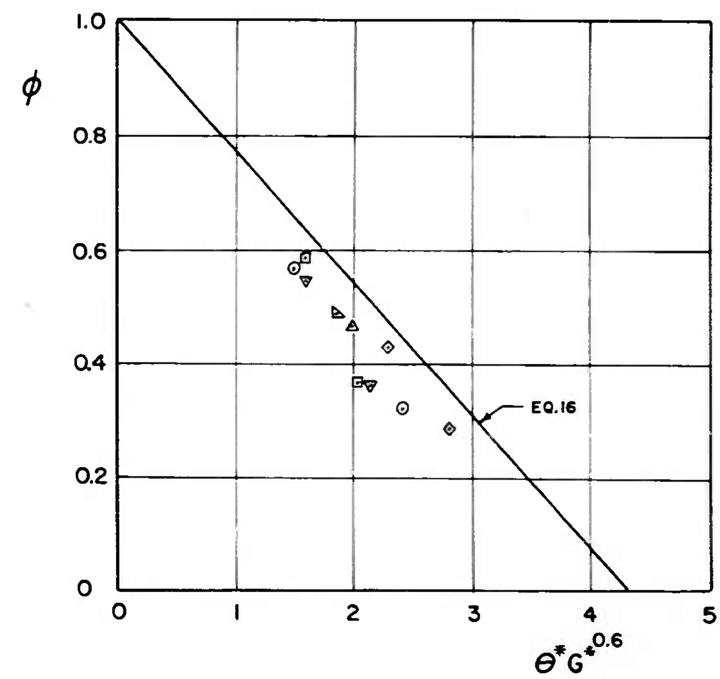
1.0
0.8
0.6
0.4
0.2
0
ϕ
0
1
2
3
4
5
EQ.16
$\theta^* G^{*0.6}$

(b)

FIGURE 20

CORRELATED FILM COOLING EFFECT IN THE RANGE $143 \leq R/s \leq 500$

$z_o/R = 0.11$

The solid line is the best fit line to the data through the point $\phi = 0$, $\theta^* G^{*0.6}/(R/s)^{0.7} = 0$

Symbol	R/s
◇ (dotted)	143
⊙	200
△	500

FIG. 20

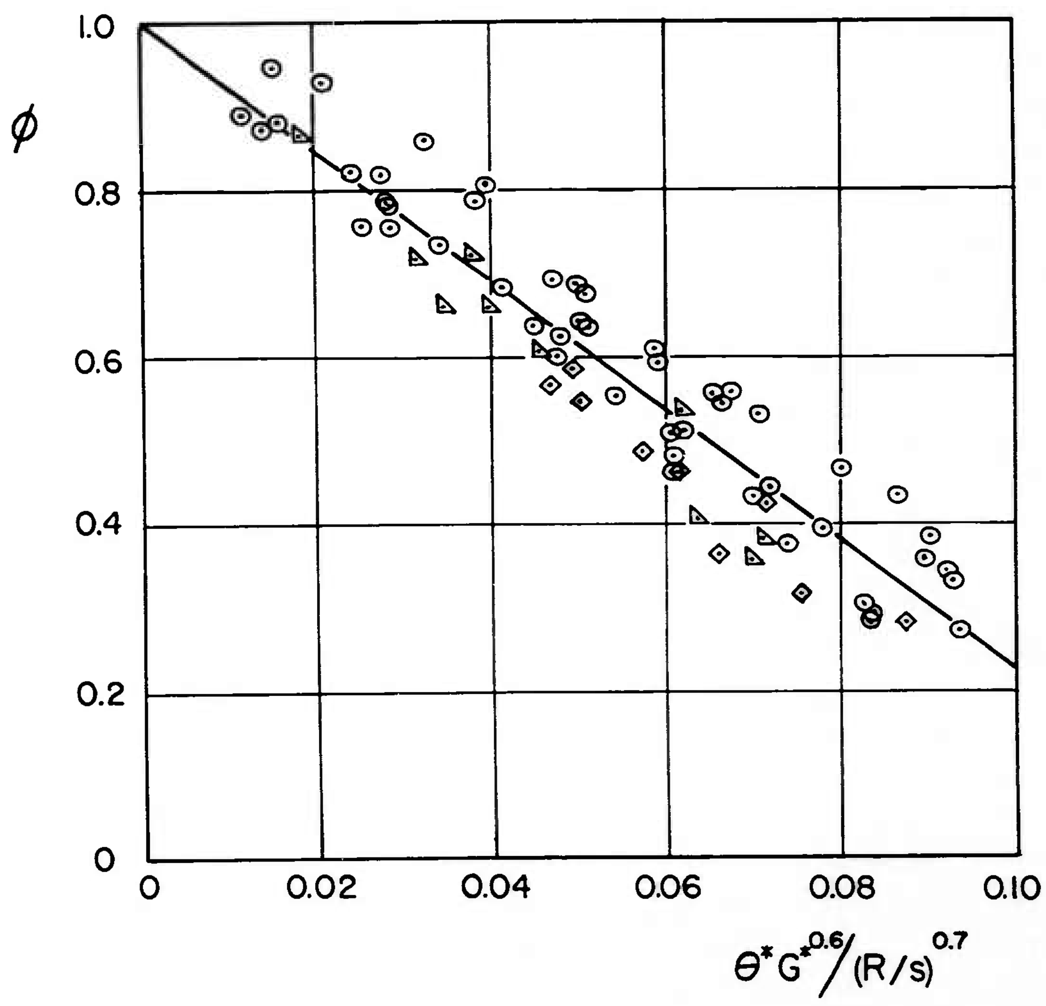

VII DISCUSSION OF RESULTS

<u>Test Range of the Model Parameters</u> A survey of the literature available on radial turbine design practice[12,15,16,17] indicates the following ranges as representative of current radial flow gas turbine operation:

$$10^5 \leq N_{R,F} \leq 10^6$$
$$10^5 \leq N_{R,M} \leq 10^6$$
$$0.2 \leq N_{R,M}/N_{R,F} \leq 0.8$$
$$0.1 \leq z_o/R \leq 0.3$$
$$N_{Pr} \cong 0.7$$

The test facility was designed to match these prototype ranges, so that the test data does cover the operating range of most radial flow gas turbine disks. Since the present study is an initial investigation into radial turbine film cooling, the ranges for the parameters governing the film cooling, θ^*, G^*, and R/s are not well established, as are the more conventional parameters above. However, some simple considerations yield information about these film cooling parameters as follows.

The probable source of the film cooling air in an actual application will be the main flow compressor of the gas turbine cycle. A small percentage of air will be bled off of the compressor outlet and injected as the film flow at the turbine disk periphery. With such an arrangement, the pressure ratios will be approximately the same for both the film and main flows. For a compressor pressure ratio of 3 and a compressor inlet temperature of 70°F, the film temperature level will be of the order of 300°F, depending on the isentropic efficiency of the compressor and the temperature drop in the film flow ducting.

θ^* ratios will probably be in the range:

$$2 \leq \theta^* \leq 5$$

For example, with a main gas temperature, t_m, of 1200°F, a film temperature t_f, of 300°F, and a disk temperature of 900°F:

$$\theta^* = \frac{300 - 1200}{900 - 1200} = 3$$

The range of the mass velocity ratio, G^*, will be largely governed by the ratio of the film and main flow temperatures. A reasonable assumption for modern radial gas turbines is that a critical flow condition is approximated across the nozzles. For critical flow,

$$G \propto P/\sqrt{T}$$

where P and T are conditions upstream of the nozzle ring. Since the pressure ratios for both the film and main flows are equal, the mass velocity ratio will be given as:

$$G^* \triangleq \frac{G_f}{G_m} \cong \sqrt{T_m/T_f}$$

For the representative temperatures mentioned above:

$$G^* \cong \sqrt{1660/760} \cong 1.5$$

In the model, changes in the mass velocity ratio, $G^* = (u_f/u_m)/(\rho_f/\rho_m)$, are brought about by changing the velocity ratio, (u_f/u_m). Since the densities of the main and film flows on the model are approximately equal for the temperature levels used, the G^* correlation of the present results is a generalization which is not completely verified by the present results. Justification for this generalization of the model test results to a G^* basis is based on the work of the previous investigators in the film cooling field. Papell and Trout[7] obtained results for film cooling effectiveness with an actual film cooling situation with high (up to 1500°F) main flow temperatures. When correlated on a G^* basis, their results show essential agreement[9] with the data of other researchers who used film heating with relatively small temperature differences between the two flows. This lends support to the use of G^* as a correlating parameter although the correlation could not be completely verified in the present study.

The range of R/s tested was chosen to cover the range tested in the prototype study conducted by Rossler[5] in parallel with this investigation. The prototype range was:

$$187 \leq R/s \leq 545$$

that of the model is:

$$143 \leq R/s \leq 500$$

In addition, the size of the slot gap, s, in relation to the main flow passage depth, z_o is of interest. For both the model and the prototype:

$$0.02 \leq s/z_o \leq 0.06$$

<u>Effect of Large Differences Between the Film and Main Flow Temperatures</u> The effect of fluid property variations and buoyancy forces resulting from large temperature gradients

in the flow has not been investigated in the present study. Papell and Trout[7] found that in order to correlate effectiveness data obtained with small temperature differences with that obtained with large temperature differences, it was necessary to introduce a temperature ratio parameter, T_f/T_m. Some temperature ratio parameter is undoubtedly pertinent in the present study, and more knowledge of its effect is needed before the present results can be reliably extrapolated to the prototype case.

Comparison of Analytical and Experimental Results

The test results show a film cooling effect of the same form as that predicted by the flat plate analysis, but the magnitude of the effect is only approximately 36% of that predicted. Some of this difference can be attributed to the fact that the measured film flow temperature is greater than the actual film inlet temperature as seen by the disk.

The film temperature is measured at the film flow annular plenum chamber; subsequently the flow travels three and one-half inches through a passage whose depth is equal to the film spacing, s. This passage is separated from the main flow by a thin plastic divider, and heat transfer between the streams occurs. Some rough measurements of the film temperature at the exit of the passage, immediately upstream of the screens, have been made. These measurements indicate that the heat transfer across the plastic divider reduces $\theta_f = \left(t_f - t_m\right)$ by perhaps 10 to 20%.

The film flow, as well as the main flow, passes through the ten layers of 50 mesh aluminum screening, and an additional temperature drop undoubtedly occurs through the screens. The film flow temperature drop through the screens possibly is quite high, and until data is available to determine the magnitude of this effect, the present results should be considered as a conservative estimate of the film cooling effect obtainable on a rotating disk.

The results of Figs. 17, 18, and 19 show that the modified analysis result, Eq. 16, underpredicts the film effect at the largest slot gap and overpredicts the effect at the smallest slot gap. Since the heat transfer between the two flows in the entrance passages and screens would have a smaller effect for large slot gaps, the test data supports the conclusion that the test results indicate a film cooling effect less than that actually achieved.

Comparison of the Model Results with the Prototype Study of Ref. 5 In the prototype investigation, turbine wheel temperatures and temperature distributions were measured, but not heat fluxes. In these tests, the main stream temperature was held constant and the drop in turbine wheel temperature due to the film cooling was observed. The results are presented in terms of an effectiveness, where:

$$\text{Effectiveness} \triangleq \frac{(t_w)_{\text{without cooling}} - (t_w)_{\text{with cooling}}}{t_m - t_f}$$

Since the heat flux into the turbine wheel was not obtained for each value of t_w, no predictions regarding the ratio of heat transfer coefficients with and without film cooling can be made from the effectiveness values. For the same reason, no predictions of the effectiveness can be made from the ratios of heat transfer coefficients presented in the present study.

Rossler (Fig. 60 of Ref. 5) does, however, present some wheel temperature distributions normalized with respect to the main gas temperature. These results are indicated by shaded bands in Fig. 21. Also plotted in Fig. 21 are T_w/T_m ratios evaluated from Eq. 29 at conditions similar to these prototype tests ($R/s = 187$; $G^* = 0.8, 1.6$; $t_f = 100\,°F$). (The evaluation of T_w/T_m from Eq. 29 is a useful design application of the results of the present study and will be described in the next section) Eq. 29 is based upon a uniform disk test surface temperature, so the present results appear as constant values in Fig. 21. It can be seen from the prototype results that a uniform wheel temperature is a good approximation for the film cooled turbine. The agreement in magnitude between the prototype and model results is quite good.

A further comparison between the present results and those of the prototype is obtained by considering the results of some thermocolor tests presented in Ref. 5. These results are as follows: Operating without film cooling, a maximum wheel temperature of 850°F was recorded with a turbine inlet temperature of 1000°F. With a film mass flow rate of 5% that of the main flow rate, and with a slot configuration $R/s = 350$, the maximum wheel temperature of 850°F was recorded with a turbine inlet temperature of 1250°F and a film inlet temperature of 100°F, all other conditions identical. Assuming that the mean heat flux to the wheel was the same in both cases (sufficient to raise the wheel to 850°F) then the fact that this heat flux was produced by temperature potentials of 150°F and 400°F leads to the conclusion that the mean heat transfer coefficient was reduced some 60% by the presence of the film. This effect was obtained at:

$$\theta^* \triangleq \theta_f / \theta_w = \frac{100 - 1250}{850 - 1250} = \frac{-1150}{-400} = 2.9$$

with an approximate $G^* = 2.0$. For these values:

$$\theta^* \, G^{*\,0.6} / (R/s)^{0.7} = 0.0725$$

and Eq. 29 yields $\phi = 0.44$, a 56% reduction in heat transfer compared to the 60% for the prototype. This, together with the agreement evidenced in Fig. 21, provides some measure of confidence in the application of the model results for design predictions.

FIGURE 21

COMPARISON OF THE MODEL RESULTS WITH THOSE OF ROSSLER (Ref. 5)

The shaded areas are the results of the prototype study from Fig. 60 of Ref. 5.
($R/s = 187$, $t_f \cong 100°F$)

The solid lines are results obtained by evaluating Eq. 29 at:

$$R/s = 187$$
$$t_f = 100°F$$
$$t_w = 850°F$$
$$(t_m)_{uncooled} = 1080°F$$

FIG. 21

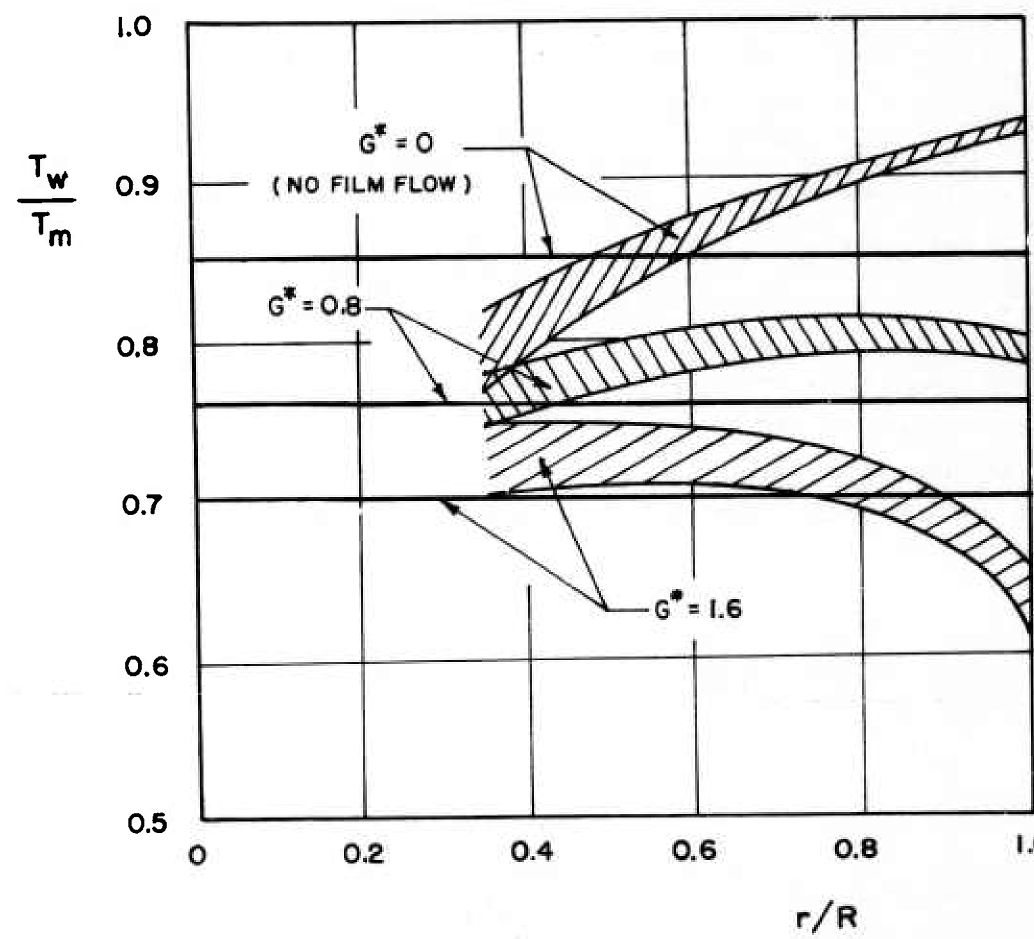

1.0
0.9
0.8
0.7
0.6
0.5
$\frac{T_w}{T_m}$
$G^* = 0$
(NO FILM FLOW)
$G^* = 0.8$
$G^* = 1.6$
0
0.2
0.4
0.6
0.8
1.0
r/R

Application to Design An important result from the point of view of the designer is the effect of film cooling on the maximum allowable main flow temperature for a given maximum wheel temperature. This result may be given in terms of T_w/T_m as in Fig. 21. As an example of how T_w/T_m may be predicted from the data of the present study, the model results that are compared with the prototype results in Fig. 21 will be obtained.

The model results are summarized by Eq. 29:

$$\phi = \frac{N_{St,av} N_{R,F}^{0.65}}{(N_{St,av} N_{R,F}^{0.65})_{\theta^* = 0}} = 1.0 - 7.7\ \theta^*\ G^{*0.6} / (R/s)^{0.7}$$

It is assumed, as in the treatment in the preceeding section of the prototype thermocolor results, that a given heat flux to the disk will elevate the disk temperature to a given level. If, in addition, the main flow mass velocity and fluid properties are the same for both the cooled and uncooled cases, then Eq. 29 reduces to:

$$\phi = \frac{(\theta_w)_{uncooled}}{(\theta_w)_{cooled}} = 1.0 - 7.7\ \theta^*\ G^{*0.6} / (R/s)^{0.7}$$

But: $$\theta^* \triangleq \frac{t_f - (t_m)_{cooled}}{t_w - (t_m)_{cooled}}$$

Therefore:

$$\left[\frac{(t_m)_{uncooled} - t_w}{(t_m)_{cooled} - t_w}\right] = 1.0 -$$

$$7.7\ G^{*0.6} / (R/s)^{0.7} \left[\frac{t_f - (t_m)_{cooled}}{t_w - (t_m)_{cooled}}\right]$$

For a given film cooling situation, with t_w, t_f, G^*, R/s, and $(t_m)_{uncooled}$ specified, $(t_m)_{cooled}$ can be determined from the above expression.

For example, with $t_w = 850°F$, $t_f = 100°F$, $G^* = 0.8$, $R/s = 187$, and $(t_m)_{uncooled} = 1080°F$, the main flow temperature with cooling, $(t_m)_{cooled}$, is equal to 1280°F. This is a rise of 200°F and results in a T_w/T_m of 0.76. For the same conditions, but with $G^* = 1.6$:

$$(t_m)_{cooled} = 1430°F \quad \text{and} \quad T_w/T_m = 0.70$$

These are the results that are presented with the prototype results in Fig. 21. A main flow temperature without cooling, $(t_m)_{uncooled}$, of 1080°F was selected so that T_w/T_m without cooling was equal to 0.85, in agreement with the prototype results.

A further result of the model study of importance to the turbine wheel designer is that with film cooling in the range of interest $(\theta^* > 1)$ the heat transfer is in a direction out of the disk near the disk edge and into the disk away from the disk edge. This characteristic of the local heat transfer coefficient means that consideration of longitudinal conduction will be important in determining the temperature distribution throughout the film cooled disk. Film cooling can not only reduce the high temperatures at the disk rim but can also even out the temperature distribution across the disk, resulting in lower overall stress levels. These effects are clearly evident in the results of the prototype study presented in Fig. 21.

VII SUMMARY OF RESULTS AND CONCLUSIONS

The principal results of the present study may be summarized as follows:

1. The heat transfer behavior for a shrouded, constant wall temperature rotating disk with radial inflow, but no separate film flow, has been determined (Fig. 9) as:

$$N_{St,av} N_{R,F}^{0.65} = 66.0 - 30\ N_{R,M}/N_{R,F} \qquad \text{(Eq. 27)}$$

   for:

$$10^5 \leq N_{R,F} \leq 10^6$$

$$0.25 \leq N_{R,M}/N_{R,M} \leq 1.25$$

$$0.1 \leq z_o/R \leq 0.2$$

2. An analytical prediction of the film cooling effect on a constant temperature flat plate has been obtained (Eq. 15). The analysis overpredicts the magnitude of the effect obtained for the rotating disk, but the equation, when empirically modified (Eq. 16), represents most of the data to within 10%.

3. The effect of film cooling a shrouded, constant wall temperature rotating disk (Fig. 20) can be represented by:

$$\phi = 1.0 - 7.7\ \theta^{*}\ G^{*0.6} / (R/s)^{0.7} \qquad \text{(Eq. 29)}$$

in the range:

$$0 \leq \theta^* \leq 5$$
$$1 \leq G^* \leq 4$$
$$143 \leq R/s \leq 500$$

This emperically determined equation should be considered as a somewhat conservative estimate of the film cooling effect on the disk. Heat transfer in the film flow passage and screens probably lowers the film temperature below its measured value.

4. A comparison of the results of the present study with some of the results obtained by Rossler[5] in the parallel prototype study has been made. The magnitude of the film cooling effect obtained on the model is in good agreement with that obtained on the prototype turbine wheel.

IX RECOMMENDATIONS FOR FURTHER WORK

The following recommendations are made for future modification and use of the test facility:

1. A modification of the film inlet thermocouple location to allow a more accurate determination of the actual value of this temperature.
2. A more complete fluid dynamics investigation of the single radial inflow in the presence of the rotating disk including velocity profiles during heat transfer tests. Such an investigation would hopefully lead to a better understanding of the physics of the problem and to a more successful analytical attack.
3. An investigation of the effect of T_f/T_m on the film flow heat transfer results.
4. An investigation of the heat transfer behavior of a single radial inflow on a vaned disk.
5. An investigation of the effect of a film flow on the vaned disk.

Apart from the above future use of the rotating disk test facility, it is felt that a more complete study of the film cooling problem on flat plates would be very worthwhile.

APPENDIX A FLOW PASSAGE VELOCITY PROFILES

For the fluid external to the shroud and disk boundary layers, Eqs. (17) and (19) become:

$$\frac{\partial u}{\partial r} - \frac{u}{r} = 0 \qquad (30)$$

and

$$u\frac{\partial v}{\partial r} - \frac{uv}{r} = 0 \qquad (31)$$

These equations can be integrated directly to yield the solutions:

$$ru = C_1 \qquad (32)$$

and

$$rv = C_2 \qquad (33)$$

where C_1 and C_2 are constants depending upon the tangential and radial velocity components at the disk periphery. The behavior described by (32) and (33) is termed free vortex flow. It can be seen that the angle of the resultant velocity with respect to the radial direction, α, should be uniform throughout the passage since:

$$\tan \alpha = \frac{v}{u} = \text{constant}$$

The velocity profiles and flow angles were measured at two values of $r' = r/R$ (0.642 and 0.893) for four different values of $N_{R,M}/N_{R,F}$ (0.75, 0.84, 0.93, and 1.18). Figures 22 through 25 show the results of these surveys.

The measured values generally agree with the predicted values within the experimental uncertainty, and are fairly uniform across the flow passage. In particular, the agreement between the predicted and measured tangential velocity indicates that the flow is satisfying the assumed initial condition $v = R\omega$ at $r = R$. That is, the flow is passing through the screens.

FIGURE 22

VELOCITY PROFILES AND FLOW ANGLES
FOR $N_{R,M}/N_{R,F} = 0.75$

(a) Velocity Profiles

⊡ — v at r' = 0.642

◁ — -u at r' = 0.642

▽ — v at r' = 0.893

⊙ — -u at r' = 0.893

(b) Flow Angle Profiles

⊙ — r' = 0.893

△ — r' = 0.642

The solid symbols indicate the predicted results.

FIG. 22

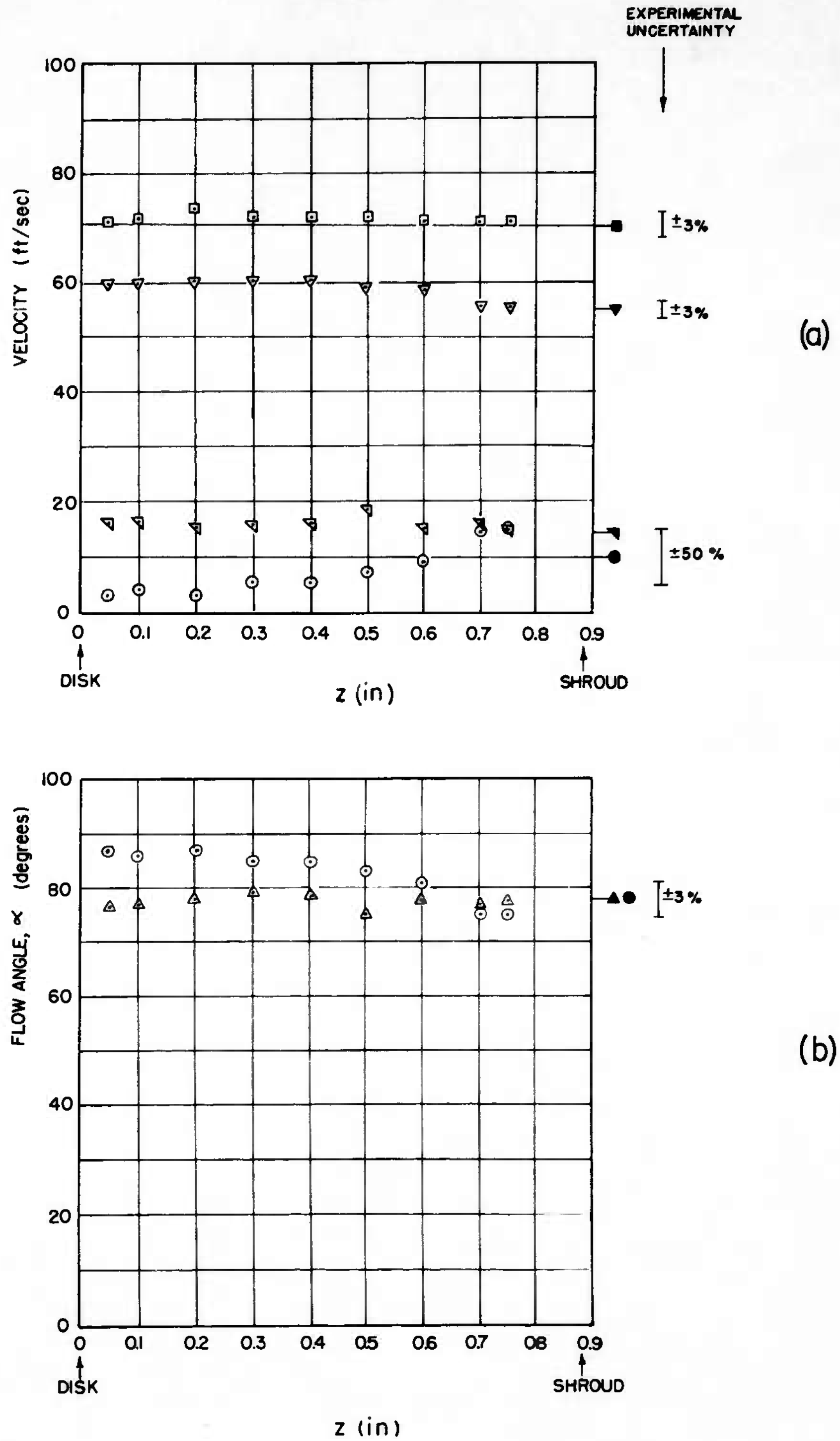
EXPERIMENTAL UNCERTAINTY
VELOCITY (ft/sec)
100
80
60
40
20
0
±3%
±3%
±50 %
(a)
0
0.1
0.2
0.3
0.4
0.5
0.6
0.7
0.8
0.9
DISK
SHROUD
z (in)
FLOW ANGLE, ∝ (degrees)
±3%
(b)
DISK
SHROUD
z (in)

FIGURE 23

VELOCITY PROFILES AND FLOW ANGLES
FOR $N_{R,M}/N_{R,F} = 0.84$

(a) Velocity Profiles

⊡ —— v at r' = 0.642

◹ —— -u at r' = 0.642

▽ —— v at r' = 0.893

⊙ —— -u at r' = 0.893

(b) Flow Angle Profiles

⊙ —— r' = 0.893

△ —— r' = 0.642

The solid symbols indicate the predicted results.

FIG. 23

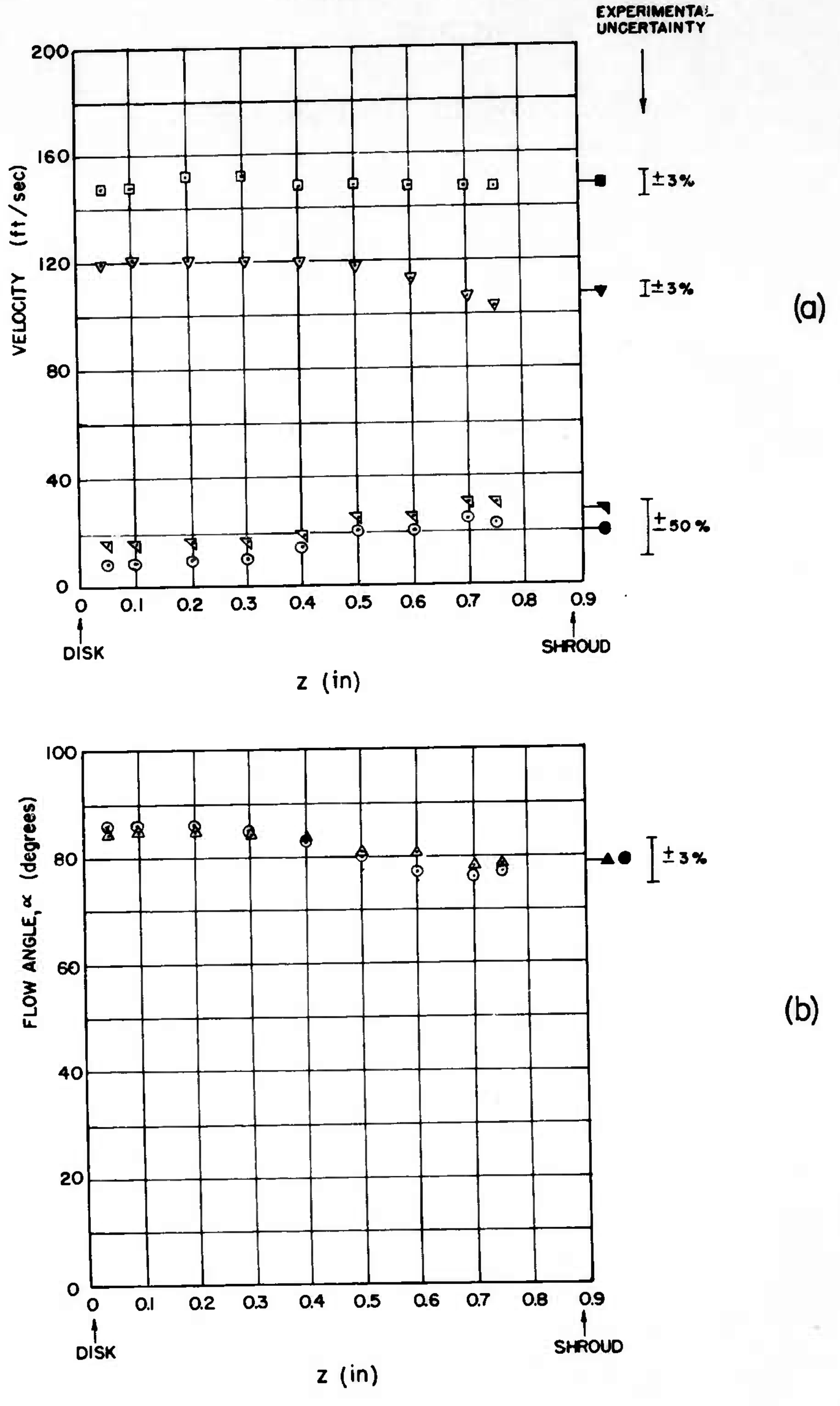
EXPERIMENTAL UNCERTAINTY
VELOCITY (ft/sec)
200
160
120
80
40
0
±3%
±3%
±50%
(a)
0
0.1
0.2
0.3
0.4
0.5
0.6
0.7
0.8
0.9
DISK
SHROUD
z (in)
FLOW ANGLE, α (degrees)
100
80
60
40
20
0
±3%
(b)
0
0.1
0.2
0.3
0.4
0.5
0.6
0.7
0.8
0.9
DISK
SHROUD
z (in)

FIGURE 24

VELOCITY PROFILES AND FLOW ANGLES
FOR $N_{R,M}/N_{R,F} = 0.93$

(a) Velocity Profiles

⊡ —— v at r' = 0.642

◸ —— -u at r' = 0.642

▽ —— v at r' = 0.893

⊙ —— -u at r' = 0.893

(b) Flow Angle Profiles

⊙ —— r' = 0.893

△ —— r' = 0.642

The solid symbols indicate the predicted results.

FIG. 24

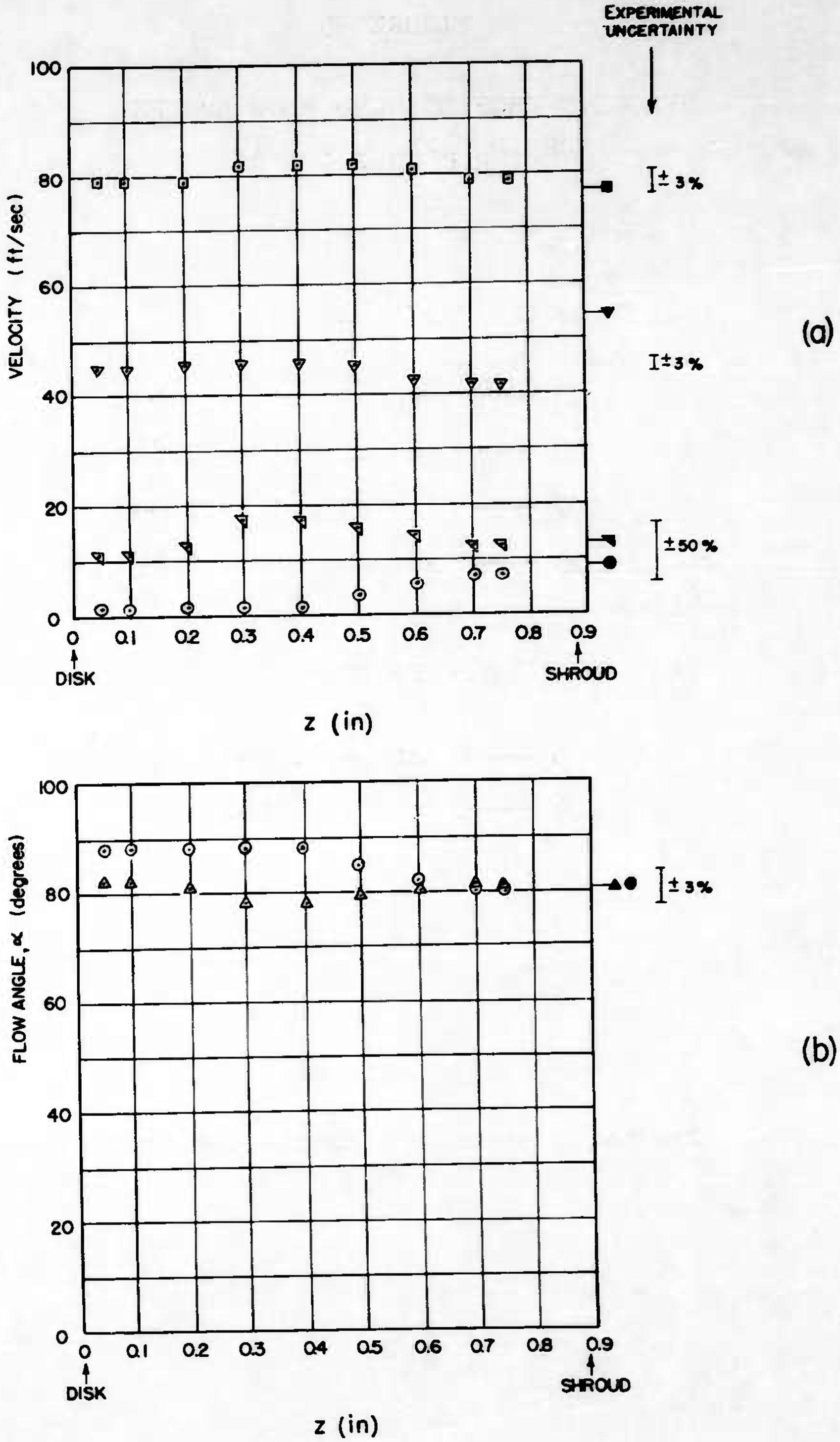

EXPERIMENTAL UNCERTAINTY
100
80
60
40
20
0
VELOCITY (ft/sec)
0
0.1
0.2
0.3
0.4
0.5
0.6
0.7
0.8
0.9
DISK
SHROUD
z (in)
±3%
±3%
±50%
(a)
100
80
60
40
20
0
FLOW ANGLE, α (degrees)
0
0.1
0.2
0.3
0.4
0.5
0.6
0.7
0.8
0.9
DISK
SHROUD
z (in)
±3%
(b)

FIGURE 25

VELOCITY PROFILES AND FLOW ANGLES
FOR $N_{R,M}/N_{R,F} = 1.18$

(a) Velocity Profiles

⊡ —— v at r' = 0.642

◁ —— -u at r' = 0.642

▽ —— v at r' = 0.893

⊙ —— -u at r' = 0.893

(b) Flow Angle Profiles

⊙ —— r' = 0.893

△ —— r' = 0.642

The solid symbols indicate the predicted results

FIG. 25

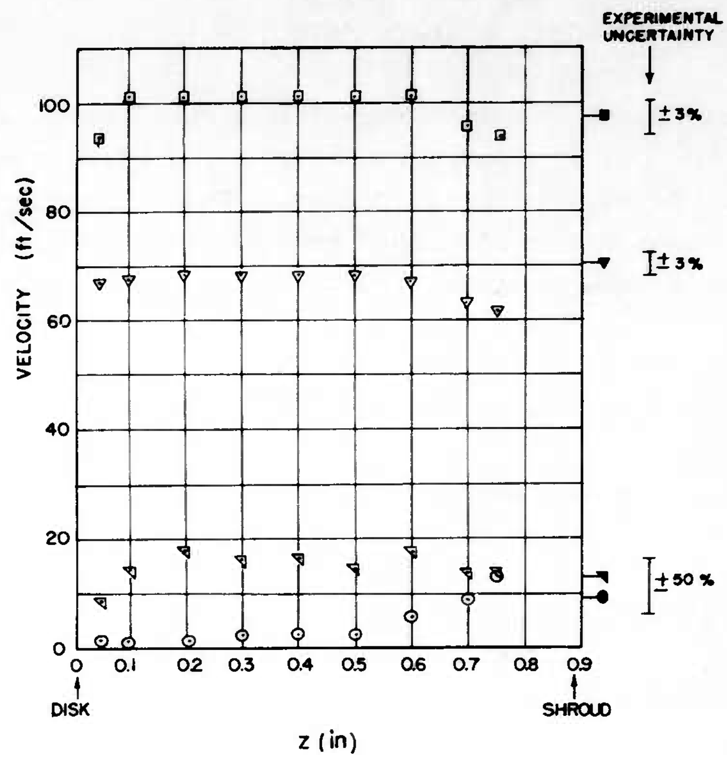
EXPERIMENTAL UNCERTAINTY
± 3%
± 3%
± 50 %
VELOCITY (ft/sec)
100
80
60
40
20
0
0 0.1 0.2 0.3 0.4 0.5 0.6 0.7 0.8 0.9
DISK
SHROUD
z (in)

(a)

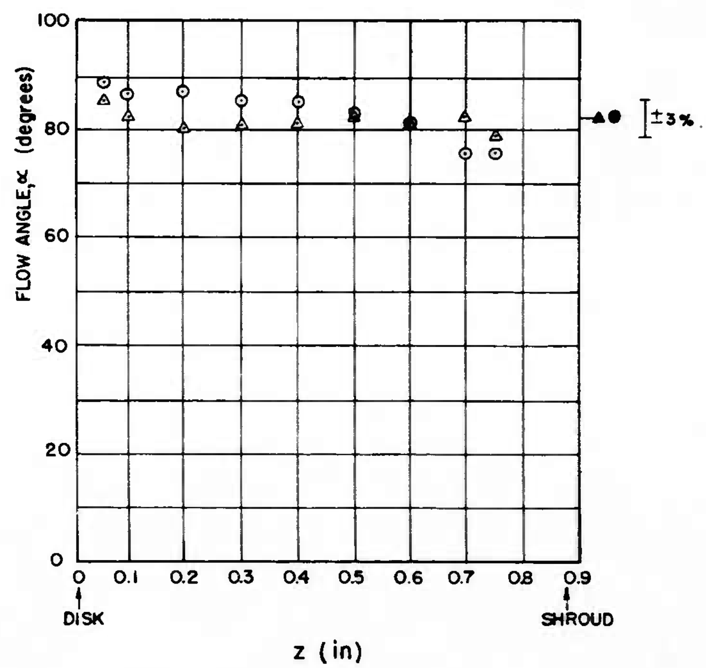
± 3%
FLOW ANGLE, α (degrees)
100
80
60
40
20
0
0 0.1 0.2 0.3 0.4 0.5 0.6 0.7 0.8 0.9
DISK
SHROUD
z (in)

(b)

APPENDIX B DATA REDUCTION

As an example of the data reduction method used to obtain the heat transfer coefficients, run number 163 (see Appendix E, TABULATED RESULTS) will be reduced here. This is a film cooling test at a film slot width of 0.040" and a main flow spacing of 0.847". The test data is given below.

Inlet Conditions:	
Barometric pressure, P_a	29.99 in Hg abs. at 32°F
Inlet pressure, P_i	-0.2 in Hg gage at 75°F
Main flow inlet temperature, t_m	70.6°F
Film flow inlet temperature, t_f	137°F
Main Flow Orifice Conditions:	
Orifice diameter, D_1	3.351 in.
Upstream pressure, P_1	-2.0 in. Hg gage at 75°F
Pressure differential, ΔP_1	4.35 in. H_2O at 75°F
Temperature, t_1	77.2°F
Film Flow Orifice Conditions:	
Orifice Diameter, D_2	0.2008 in.
Upstream pressure, P_2	19.0 psig
Pressure differential, ΔP_2	25.0 in. Hg gage at 75°F
Temperature, t_2	79.2°F
Speed, N	1620 rpm
Dimensions:	
Disk radius, R	7.979 in.
Main flow spacing, z_m	0.847 in.
Film flow spacing, s	0.040 in.

Temperature Data:

Test Surface Temperatures:

TC 1	$(r/R = 0.95)$	93.0°F
TC 2	$(r/R = 0.84)$	93.7°F
TC 3	$(r/R = 0.71)$	92.3°F
TC 4	$(r/R = 0.55)$	91.5°F
TC 5	$(r/R = 0.317)$	91.5°F

Heat Meter Temperatures and Outputs:

HM 1	97.7°F,	0.338 mv
HM 2	96.7°F,	0.355 mv
HM 3	97.9°F,	0.355 mv
HM 4	97.9°F,	0.320 mv
HM 5	99.3°F,	0.595 mv

The flows through the main and film flow orifices are given by:

$$W_t \text{ (lbm/hr)} = 4033\ K_1 Y_1 \left[\frac{1.3207\ (\Delta P_1)(P_a + P_1)}{(t_1 + 459.7)}\right]^{1/2}$$

and

$$W_f \text{ (lbm/hr)} = 53.3\ K_2\ Y_2 \left[\frac{1.3207\ (\Delta P_2)(P_a + 2.04\ P_2)}{(t_2 + 459.7)}\right]^{1/2}$$

where K_1, K_2, Y_1, and Y_2 are obtained from Ref. 18.

The mass flow, W_t, passing through the main flow orifice contains the film flow; consequently, the actual main flow rate is the difference in these two orifice flows:

$$W_m = W_t - W_f$$

For this particular test:

$$W_m = 1349.8 \text{ lbm/hr}$$

$$W_f = 59.0 \text{ lbm/hr}$$

From these results $N_{R,F}$, G_f , and G_m can be computed.

$$N_{R,F} \triangleq 2\pi R u_m \rho_m/\mu = 12.0\ W_m/(z_m \mu_m) = 4.37 \times 10^5$$

$$G_m \triangleq \rho_m u_m = 22.9\ W_m/(R z_m) = 4570 \text{ lbm/(hr ft}^2)$$

$$G_f \triangleq \rho_f u_f = 22.9\ W_f/(Rs) = 4200 \text{ lbm/(hr ft}^2)$$

Also, $N_{R,M} \triangleq R^2\ \omega\rho/\mu = 166.7\ N\rho_m/\mu_m = 4.61 \times 10^5$

Thus:

$$N_{R,M}/N_{R,F} = 1.06 \quad \text{and} \quad G^* \triangleq G_f/G_m = 0.918$$

The heat meter calibration factors are obtained from APPENDIX D, Figure 25. For these particular heat meter temperatures, the calibration factors are:

$$K_{HM\ 1} = 706.0$$

$$K_{HM\ 2} = 653.0$$

$$K_{HM\ 3} = 658.5$$

$$K_{HM\ 4} = 724.0$$

$$K_{HM\ 5} = 681.0$$

The heat flux through each meter is given as the product of the heat meter calibration factor and the heat meter output, in millivolts. For this run:

$$q''_1 = 238 \text{ Btu/(hr ft}^2) \quad (r/R = 0.95)$$
$$q''_2 = 232 \text{ Btu/(hr ft}^2) \quad (r/R = 0.84)$$
$$q''_3 = 243 \text{ Btu/(hr ft}^2) \quad (r/R = 0.71)$$
$$q''_4 = 232 \text{ Btu/(hr ft}^2) \quad (r/R = 0.55)$$
$$q''_5 = 404 \text{ Btu/(hr ft}^2) \quad (r/R = 0.317)$$

Notice the relatively high level of heat flux near the center of the disk (q''_5). This is probably the result of the high relative velocities between the disk and the flow in this region (see APPENDIX A). In addition, the effect of the film is relatively small at this large $(R-r)/s$ value. Since the heat meters are located at the area-average radius of equal area annular sections, the numerical average of the heat meter fluxes is interpreted as the mean heat flux, q''_{av}, through the disk. For Run No. 163:

$$q''_{av} = 269.8 \text{ Btu/(hr ft}^2)$$

A balance of the energies entering and leaving the disk system is used as a check on the test data. For Run No. 163, the energies balance to within 3%. This is representative of the results for the rest of the tests.

The average test surface temperature, t_w, is 92.4°F. Thus the difference between the main flow inlet temperature and the average test surface temperature, θ_w, is 21.8°F. The average heat transfer coefficient is given as:

$$h_{av} = q''_{av}/\theta_w = 12.35 \text{ Btu/(hr ft}^2 \text{ °F)}$$

Thus:

$$N_{St,av} \triangleq h_{av}/G_m\, c_p = 1.115 \times 10^{-2}$$

Also:

$$\theta^{*} \triangleq (t_f - t_m)/(t_w - t_m) = 3.05$$

The flow data was reduced on the Burroughs 220 digital computer facility at Stanford. The Balgol language program used for the computations follows.

```
COMMENT  VEIL FLOW DATA REDUCTIONS
INTEGER RPM, RUNS
WRITE ($$FMT)$
   FORMAT FMT(B1,*RUN*,B3,*MFLOM*,B2,*RPM*,B3,*RIM*,B8,*NRF*,B10,*NRM*,
      B5,*NRM/NRF*,B3,*MFLOF*,B3,*RIF*,B4,*GEF/GEM*,B8,*VIM*,B11,*VIF*,
      W4)$
START..READ ($$DATA)$
   INPUT  DATA(RUN,PATM,PI,MVIM,POM,DPOM,MVOM,POF,DPOF,MVOF,MVIF,DOM,
             ZM,ZF,RPM)$
VEIL.. COMMENT 0.2008 VEIL FLOW ORIFICES
      TOF = (SQRT(MVOF + 9.081) - 2.899)/0.003567$
      RHOF = 1.3207(PATM + 2.04POF)/(TOF + 459.7)$
      MUF = 0.0399 + 0.0000605TOF$
      NRDF = 239(SQRT(DPOF.RHOF))/MUF$
      LNRDF = LOG(NRDF)$
      KOF = 0.6841 - 0.0152LNRDF + 0.00071LNRDF.LNRDF$
      YOF = 1.0 - 0.294DPOF/(PATM + 2.04POF)$
      MFLOF = 53.3KOF.YOF.SQRT(DPOF.RHOF)$
TOM - (SQRT(MVOM + 9.081) - 2.899)/0.003567$
RHO = 1.3207(PATM + POM)/(TOM + 459.7)$
MU = 0.0399 + 0.0000605TOM$
EITHER IF DOM GEQ 3.0$  GO BIG$
OTHERWISE$  GO LITL$
BIG.. COMMENT 3.351 MAIN FLOW ORIFICES
      NRD = 6620(SQRT(DPOM.RHO))/MU$
```

```
        LNRD = LOG(NRD)$
        KO = 0.757254 - 0.0175707LNRD + 0.000645328LNRD.LNRD$
        YO = 1.0 - 0.0234DPOM/(PATM + POM)$
        MFLOT= 4033KO.YO.SQRT(DPOM.RHO)$  MFLOM = MFLOT - MFLOF$
        GO OUT$
LITL.. COMMENT 1.919 MAIN FLOW ORIFICE$
        NRD = 2034(SQRT(DPOM.RHO))/MU$
        LNRD = LOG(NRD)$
        KO = 0.692822 - 0.0152481LNRD + 0.000622632LNRD.LNRD$
        YO = 1.0 - 0.0218DPOM/(PATM + POM)$
        MFLOT= 1321KO.YO.SQRT(DPOM.RHO)$  MFLOM = MFLOT - MFLOF$
OUT..TIM = (SQRT(MVIM + 9.081) - 2.899)/0.003567$
MUIM = 0.0399 + 0.0000605TIM$
NRF =12.0MFLOM/(ZM.MUIM)$
RIM = 1.3207(PATM + PI)/(TIM + 459.7)$
NRM = 166.7RPM.RIM/MUIM$
TIF = (SQRT(MVIF + 9.081) - 2.899)/0.003567$
RIF = 1.3207(PATM + PI)/(TIF + 459.7)$
GEM = 2.87MFLOM/ZM$
GEF = 2.87MFLOF/ZF$
WRITE ($$ANS,HDG)$
    OUTPUT ANS(RUN,MFLOM,RPM,RIM,NRF,NRM,NRM/NRF,MFLOF,RIF,GEF/GEM,
               GEM/RIM,GEF/RIF)$
    FORMAT HDG(I4,X8.1,I5,X8.5,F13.5,F13.5,X8.4,X8.2,X8.5,3F13.5,W4)$
GO START$   FINISH$
```

APPENDIX C EXPERIMENTAL UNCERTAINTY

The following experimental uncertainties, based on 20:1 odds[21] were estimated for the results of this study.

Quantity		Uncertainty	% Uncertainty
Inlet Conditions:			
	$(P_1 + P_a)$, in. Hg	30.0 ± 0.05	± 1.5%
	t_m , °F	70.0 ± 0.2	
	θ_m , °F	50.0 ± 0.02	± 0.4%
Main Flow Orifice Conditions:			
	$(P_1 + P_a)$, in. Hg	28.0 ± 0.1	± 0.4%
	ΔP_1, in. H_2O	6.0 ± 0.03	± 0.5%
	t_1, °F	70.0 ± 0.1	
Film Flow Orifice Conditions:			
	$(P_2 + P_a)$, psig	35.0 ± 0.2	± 0.6%
	ΔP_2, in. Hg	20.0 ± 0.1	± 0.5%
	t_2, °F	70.0 ± 0.1	
Speed:	N , rpm	1500 ± 20	± 1.5%
Dimensions:			
	R, in.	7.979 ± 0.001	± 0.01%
	z_m, in.	0.8 ± 0.010	± 1%
	s, in.	0.040 ± 0.001	± 2%

Temperatures:

θ_w, °F	30.0	$\pm$ 1	$\pm$ 3%
heat meter temperature, °F	100	$\pm$ 1	

Heat Fluxes:

calibration factor	630	$\pm$ 2	= 0.3%
output	0.5	$\pm$ 0.01	= 2%

Based on these component uncertainties, the following uncertainties were estimated.

TABLE 1 SUMMARY OF UNCERTAINTIES

Quantity	% Uncertainty
Main Flow Rate, W_m	$\pm$ 1%
Film Flow Rate, W_f	$\pm$ 1%
Flow Reynolds number, $N_{R,F}$	$\pm$ 1.5%
Machine Reynolds number, $N_{R,M}$	$\pm$ 1%
Main Flow mass velocity, G_m	$\pm$ 1.5%
Film Flow mass velocity, G_f	$\pm$ 5%
Heat Transfer Coefficient, h_{av}	$\pm$ 3.5%
Stanton number, $N_{St,av}$	$\pm$ 4%
Normalized Stanton number, $N_{St,av}/(N_{St,av})_{\theta^*=0}$	$\pm$ 6%

APPENDIX D TEST FACILITY SPECIFICATIONS

Disk Specifications:

Material:	Aluminum Alloy 2024 - T4
Yield stress:	47,000 psi
Diameter:	15.958 in.
Thickness:	
Upper aluminum disk:	0.065 in.
Heat meter disk:	0.063 in.
Epoxy resin:	0.006 in.
Lower aluminum disk:	1.682 in.
Total	1.816 in.
Thermal conductivity:	
Disk:	72 Btu/(hr ft^2 °F/ft)
Heat meter section	0.37 Btu/(hr ft^2 °F/ft)

Heat Meter Specifications:

Material:	Silver-tellerium, copper
Diameter:	0.4 in.
Thickness:	0.06 in. (nominal)

The calibration factors as functions of temperature are presented in Fig. 26. For a discussion of their calibration, the reader is referred to Ref. 12.

FIGURE 26

HEAT METER CALIBRATION FACTORS

(a) Heat meters 1, 3, 4, and 5

(b) Heat meter 2

FIG. 26

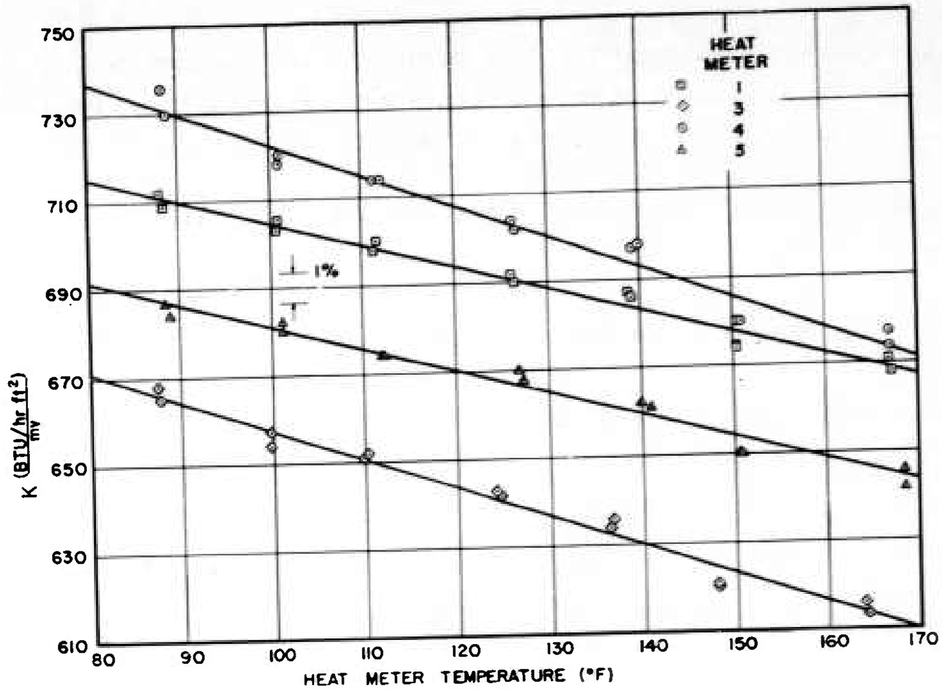
HEAT METER
1
3
4
5
1%
K (BTU/hr ft²)/mv
HEAT METER TEMPERATURE (°F)

(a)

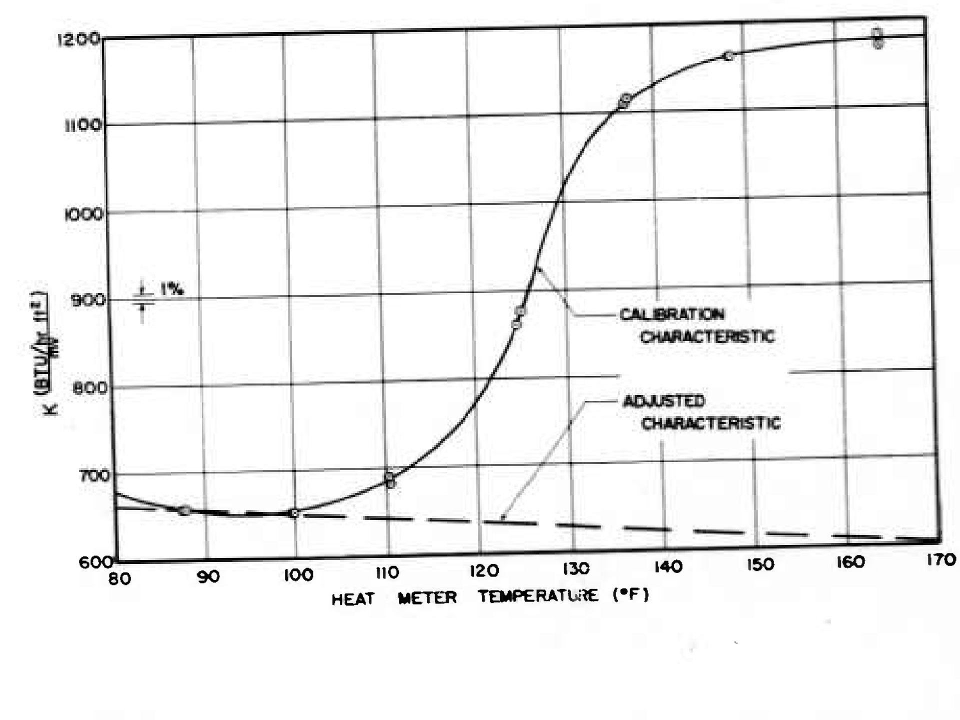
1%
CALIBRATION CHARACTERISTIC
ADJUSTED CHARACTERISTIC
K (BTU/hr ft²)/mv
HEAT METER TEMPERATURE (°F)

(b)

APPENDIX E TABULATED RESULTS

Tables 2 to 10 summarize the data of the present study. All the pertinent quantities can either be found directly in the table or calculated from the values therein.

Table 2 presents the heat transfer results without film cooling.

Table 3 presents the effect of G^* at $\theta^* \doteq 0$, with R/s = 200.

Table 4 presents the film cooling effect at a nominal $N_{R,M}/N_{R,F}$ of 1.25, with R/s = 200.

Table 5 presents the film cooling effect at a nominal $N_{R,M}/N_{R,F}$ of 1.0, with R/s = 200.

Table 6 presents the film cooling effect at a nominal $N_{R,M}/N_{R,F}$ of 0.85, with R/s = 200.

Table 7 presents the film cooling effect at a nominal $N_{R,M}/N_{R,F}$ of 0.5, with R/s = 200.

Table 8 presents the film cooling effect at a nominal $N_{R,M}/N_{R,F}$ of 0.3, with R/s = 200.

Table 9 presents the film cooling effect at R/s = 500.

Table 10 presents the film cooling effect at R/s = 143.

TABLE 2 HEAT TRANSFER RESULTS WITHOUT FILM COOLING

(See Figs. 8 and 9)

RUN	N	W_m	Z_o	ρ_m	h_{av}
111	235	690	0.0737	0.0754	14.3
112	400	1270	0.0737	0.0750	17.5
113	500	1568	0.0737	0.0746	19.3
114	650	1901	0.0736	0.0742	20.8
115	950	690	0.0725	0.0755	19.4
116	1315	973	0.0725	0.0756	21.5
117	1810	1271	0.0725	0.0754	24.9
1171	1700	1218	0.0728	0.0739	24.0
118	460	712	0.0737	0.0739	15.9
119	670	998	0.0737	0.0741	17.25
120	945	1377	0.0736	0.0740	19.0
121	1250	1784	0.0737	0.0737	20.9
122	650	718	0.0741	0.0748	17.4
123	1435	1365	0.0728	0.0743	23.0
124	1840	1719	0.0722	0.0741	25.2
130	360	1338	0.1190	0.0735	14.6
131	860	1308	0.1183	0.0733	17.6
132	1160	1360	0.1180	0.0730	19.8

RUN	$N_{St,av}$	$N_{R,M}$	$N_{R,F}$	$N_{R,M}/N_{R,F}$	$N_{St,av}N_{R,F}^{0.65}$
	$\times 10^2$	$\times 10^{-5}$	$\times 10^{-5}$		
111	2.65	0.67	2.14	0.32	77.4
112	1.77	1.14	3.93	0.29	76.3
113	1.58	1.41	4.83	0.29	77.8
114	1.40	1.82	5.85	0.31	78.7
115	3.54	2.74	2.18	1.26	104.2
116	2.80	3.80	3.08	1.23	103.2
117	2.47	5.23	4.08	1.30	108.5
1171	2.50	4.71	3.75	1.25	105.0
118	2.85	1.28	2.18	0.59	84.4
119	2.22	1.88	3.07	0.61	81.8
120	1.77	2.65	4.25	0.62	80.5
121	1.50	3.49	5.50	0.63	80.5
122	3.10	1.83	2.18	0.84	92.0
123	2.14	4.01	4.22	0.95	97.0
124	1.84	5.13	5.33	0.95	97.5
130	2.26	0.99	2.53	0.39	73.3
131	2.78	2.36	2.48	0.95	89.0
132	3.00	3.17	2.58	1.23	98.8

TABLE 3 EFFECT OF G^* AT $\theta^* = 0$, $R/s = 200$

(See Figure 11)

RUN	N	W_m	W_f	ρ_m	ρ_f	z_m
150	520	1710.4	42.4	0.0726	0.0725	0.0706
151	1110	1699.5	42.3	0.0725	0.0724	0.0700
152	1500	1599.3	42.3	0.0724	0.0723	0.0692
153	285	927.9	42.5	0.0737	0.0737	0.0717
154	600	920.9	42.4	0.0734	0.0733	0.0708
155	840	932.8	42.4	0.0733	0.0732	0.0708
156	310	892.5	58.5	0.0743	0.0742	0.0717
157	548	889.5	59.3	0.0741	0.0741	0.0715
158	850	905.4	59.2	0.0739	0.0739	0.0708

RUN	G^*	h_{av}	$N_{St,av}$ X10^2	$N_{R,M}/N_{R,F}$	$N_{St,av}N_{R,F}^{0.65}$
150	0.52	19.8	1.42	0.26	76.0
151	0.52	21.4	1.54	0.55	82.3
152	0.55	23.2	1.75	0.78	91.2
153	0.98	16.5	2.21	0.27	78.0
154	0.98	16.9	2.26	0.56	80.5
155	0.97	18.5	2.44	0.78	87.7
156	1.41	16.1	2.25	0.31	78.7
157	1.43	16.5	2.31	0.54	80.0
158	1.39	18.5	2.52	0.82	89.2

TABLE 4 FILM COOLING EFFECT AT A NOMINAL

$N_{R,M}/N_{R,F}$ OF 1.25, R/s = 200

(See Fig. 12)

RUN	N	W_m	W_f	ρ_m	ρ_f	z_m
160	1200	881.0	44.3	0.0735	0.0714	0.0706
161	1200	881.7	44.3	0.0735	0.0705	0.0706
162	1200	880.6	44.3	0.0727	0.0674	0.0706
167	2020	1270.2	56.3	0.0734	0.0655	0.0690
168	2010	1259.0	68.2	0.0737	0.0651	0.0690
214	1300	1030.8	82.4	0.0744	0.0657	0.0726
215	1300	1029.0	82.5	0.0745	0.0658	0.0726
216	1300	970.7	127.2	0.0733	0.0659	0.0726
217	1300	969.0	127.0	0.0731	0.0672	0.0726

RUN	G^*	h_{av}	$N_{St,av}$	$N_{R,M}/N_{R,F}$	$N_{St,av}N_{R,F}^{0.65}$	θ^*
			$x10^2$			
160	1.07	19.9	2.77	1.18	96.0	0.61
161	1.06	19.0	2.64	1.18	91.3	0.84
162	1.07	17.1	2.38	1.17	81.0	1.56
167	0.92	9.7	0.92	1.34	40.8	3.91
168	1.12	8.1	0.77	1.35	34.5	3.54
214	1.74	5.2	0.64	1.14	24.3	3.40
215	1.75	13.3	1.64	1.14	62.0	1.72
216	2.85	7.1	0.93	1.19	33.6	2.03
217	2.85	14.6	1.90	1.19	68.9	1.11

TABLE 5 FILM COOLING EFFECT AT A NOMINAL

$N_{R,M}/N_{R,F}$ OF 1.0, R/s = 200

(See Fig. 13)

RUN	N	W_m	W_f	ρ_m	ρ_f	z_m
163	1650	1349.8	59.0	0.0741	0.0658	0.0700
164	1640	1352.1	59.0	0.0743	0.0660	0.0700
165	1640	1350.2	59.0	0.0745	0.0660	0.0700
166	1640	1348.9	59.1	0.0747	0.0661	0.0700
175	780	632.9	56.5	0.0750	0.0663	0.0722
176	1140	927.9	56.5	0.0747	0.0662	0.0717
177	1520	1297.2	56.4	0.0743	0.0662	0.0707
178	1970	1619.7	56.4	0.0741	0.0660	0.0696
179	560	489.9	42.5	0.0753	0.0686	0.0735
180	750	681.7	42.5	0.0748	0.0674	0.0733
181	1160	962.2	42.4	0.0749	0.0673	0.0728
182	1580	1337.0	42.4	0.0744	0.0672	0.0717
183	1780	1503.0	63.9	0.0746	0.0660	0.0713
184	1760	1500.4	63.9	0.0745	0.0658	0.0713
185	1760	1495.6	63.9	0.0743	0.0658	0.0713

RUN	G^*	h_{av}	$N_{St,av}$ x10^2	$N_{R,M}/N_{R,F}$	$N_{St,av}N_{R,F}^{0.65}$	θ^*
163	0.92	12.4	1.12	1.06	51.7	3.05
164	0.92	8.4	0.76	1.05	35.0	3.88
165	0.92	18.9	1.70	1.06	77.0	1.65
166	0.92	20.6	1.86	1.06	86.3	1.21
175	1.93	7.7	1.54	1.11	42.8	2.40
176	1.31	9.1	1.23	1.10	44.0	2.51
177	0.92	12.7	1.21	1.03	54.0	2.90
178	0.73	14.6	1.10	1.05	57.6	2.95
179	1.91	8.2	2.12	1.05	49.4	1.64
180	1.37	9.9	1.86	1.00	53.7	2.21
181	0.96	12.2	1.61	1.09	58.7	2.48
182	0.68	14.7	1.38	1.05	62.3	2.59
183	0.91	13.1	1.08	1.05	53.2	2.87
184	0.91	16.5	1.37	1.04	67.3	2.04
185	0.92	20.5	1.71	1.04	83.5	1.42

TABLE 6 FILM COOLING EFFECT AT A NOMINAL

$N_{R,M}/N_{R,F}$ OF 0.85, R/s = 200

(See Fig. 14)

RUN	N	W_m	W_f	ρ_m	ρ_f	z_m
208	1180	1264.8	82.3	0.0738	0.0657	0.0727
209	1140	1260.7	82.2	0.0734	0.0653	0.0727
210	1120	1256.4	82.0	0.0730	0.0651	0.0727
211	850	876.7	104.9	0.0746	0.0663	0.0732
212	850	872.5	104.7	0.0741	0.0659	0.0732
213	850	869.7	104.5	0.0736	0.0672	0.0732

RUN	G^*	h_{av}	$N_{St,av}$	$N_{R,M}/N_{R,F}$	$N_{St,av}N_{R,F}^{0.65}$	θ^*
			$\times 10^2$			
208	1.42	6.4	0.64	0.83	27.6	2.75
209	1.42	9.9	1.00	0.80	43.0	2.05
210	1.42	13.1	1.32	0.79	56.7	1.70
211	2.63	4.5	0.65	0.88	22.1	2.42
212	2.63	8.7	1.27	0.88	42.9	1.84
213	2.63	12.9	1.89	0.88	63.3	1.14

TABLE 7 FILM COOLING EFFECT AT A NOMINAL

$N_{R,M}/N_{R,F}$ OF 0.5, R/s = 200

(See Fig. 15)

RUN	N	W_m	W_f	ρ_m	ρ_f	z_m
170	770	1327.9	57.4	0.0756	0.0753	0.0720
171	770	1320.3	57.2	0.0748	0.0730	0.0720
172	750	1319.7	57.1	0.0748	0.0721	0.0720
173	750	1318.6	57.1	0.0749	0.0692	0.0720
174	740	1318.5	57.1	0.0747	0.0663	0.0720
186	860	1521.5	62.9	0.0749	0.0664	0.0732
187	900	1519.6	62.8	0.0749	0.0662	0.0732
1881	830	1514.3	62.8	0.0755	0.0666	0.0732
197	450	735.2	64.3	0.0751	0.0664	0.0737
198	450	732.9	64.3	0.0748	0.0660	0.0737
199	450	732.9	64.1	0.0745	0.0658	0.0737
200	450	731.8	64.1	0.0743	0.0678	0.0737
202	450	736.8	64.1	0.0749	0.0717	0.0737
204	750	1220.8	127.5	0.0731	0.0655	0.0728
205	750	1218.0	127.4	0.0729	0.0653	0.0728
206	750	1162.5	182.8	0.0729	0.0660	0.0728
207	750	1121.5	223.9	0.0731	0.0664	0.0728

RUN	G^*	h_{av}	$N_{St,av}$ x10^2	$N_{R,M}/N_{R,F}$	$N_{St,av}N_{R,F}^{0.65}$	θ^*
170	0.93	18.2	1.75	0.53	80.0	0.00
171	0.94	17.0	1.61	0.52	72.5	0.50
172	0.94	16.8	1.60	0.51	71.5	0.69
173	0.94	15.6	1.48	0.51	66.5	1.05
174	0.94	5.6	0.53	0.50	24.0	3.58
186	0.91	10.2	0.85	0.52	41.8	2.70
187	0.91	12.7	1.07	0.54	52.3	1.95
1881	0.91	15.4	1.30	0.50	63.4	1.23
197	1.94	6.8	1.19	0.56	36.0	1.93
198	1.94	8.7	1.52	0.56	45.8	1.49
199	1.93	4.2	0.74	0.56	22.4	2.62
200	1.94	9.9	1.73	0.56	52.0	1.32
202	1.93	11.9	2.07	0.56	62.7	0.79
204	2.28	8.7	0.90	0.55	37.8	1.51
205	2.28	11.2	1.17	0.55	49.2	1.19
206	3.44	5.3	0.58	0.57	23.6	1.63
207	4.37	7.4	0.83	0.59	33.2	1.32

TABLE 8 FILM COOLING EFFECT AT A NOMINAL

$N_{R,M}/N_{R,F}$ OF 0.3, R/s = 200

(See Fig. 16)

RUN	N	W_m	W_f	ρ_m	ρ_f	z_m
189	495	1511.5	64.3	0.0748	0.0663	0.0735
190	500	1509.9	64.3	0.0748	0.0663	0.0735
191	480	1505.4	64.2	0.0747	0.0662	0.0735
193	500	1507.0	64.2	0.0743	0.0712	0.0735
194	495	1504.8	64.1	0.0743	0.0682	0.0735
195	505	1502.9	64.1	0.0743	0.0660	0.0735
196	500	1511.5	64.1	0.0748	0.0662	0.0735

RUN	G^*	h_{av}	$N_{St,av}$ x10^2	$N_{R,M}/N_{R,F}$	$N_{St,av}N_{R,F}^{0.65}$	θ^*
189	0.94	8.8	0.74	0.30	36.1	2.59
190	0.94	12.5	1.06	0.30	51.3	1.75
191	0.94	14.9	1.27	0.29	61.3	1.18
193	0.94	16.0	1.36	0.30	65.3	0.61
194	0.94	13.8	1.18	0.30	56.8	1.08
195	0.94	13.5	1.15	0.31	55.2	1.46
196	0.94	6.9	0.58	0.30	28.3	3.15

TABLE 9 FILM COOLING EFFECT AT R/s = 500

(See Fig. 18)

RUN	N	W_m	W_f	ρ_m	ρ_f	z_m
300	515	1574.9	28.8	0.0748	0.0695	0.0742
301	505	1574.7	28.8	0.0750	0.0696	0.0742
302	460	1512.8	63.9	0.0738	0.0660	0.0733
303	495	1501.8	63.8	0.0730	0.0657	0.0733
304	890	1505.2	52.5	0.0729	0.0661	0.0728
305	880	1500.8	52.6	0.0728	0.0657	0.0728
306	815	1480.7	63.7	0.0732	0.0657	0.0732
307	750	1464.2	63.4	0.0725	0.0661	0.0732
310	1080	1308.4	41.2	0.0738	0.0672	0.0733
311	1140	1291.9	41.1	0.0736	0.0626	0.0732

RUN	G^*	h_{av}	$N_{St,av}$	$N_{R,M}/N_{R,F}$	$N_{St,av}N_{R,F}^{0.65}$	θ^*
			$\times 10^2$			
300	1.02	11.2	0.92	0.30	45.8	3.51
301	1.02	16.0	1.31	0.30	65.2	1.41
302	2.33	6.5	0.55	0.27	26.4	3.26
303	2.34	12.2	1.04	0.29	49.5	1.86
304	1.90	8.2	0.69	0.52	33.2	3.35
305	1.91	13.2	1.12	0.52	53.7	1.83
306	2.36	7.4	0.64	0.49	30.6	3.29
307	2.38	14.1	1.22	0.45	57.2	1.45
310	1.73	11.0	1.08	0.74	47.3	3.45
311	1.75	15.4	1.50	0.79	65.0	2.11

TABLE 10 FILM COOLING EFFECT AT R/s = 143

(See Fig. 19)

RUN	N	W_m	W_f	ρ_m	ρ_f	z_m
400	485	1445.3	96.5	0.0743	0.0660	0.0730
401	470	1439.9	96.4	0.0743	0.0659	0.0730
402	450	1380.4	171.5	0.0741	0.0673	0.0733
403	420	1376.4	171.1	0.0738	0.0670	0.0733
404	820	1368.2	171.0	0.0737	0.0670	0.0726
405	820	1372.0	170.8	0.0740	0.0670	0.0726
407	830	1315.6	270.1	0.0742	0.0695	0.0728
408	1100	1270.3	269.8	0.0739	0.0677	0.0722
409	1060	1267.1	269.5	0.0736	0.0676	0.0722
410	1720	1292.4	216.1	0.0736	0.0670	0.0710

RUN	G^*	h_{av}	$N_{St,av}$ x10^2	$N_{R,M}/N_{R,F}$	$N_{St,av}N_{R,F}^{0.65}$	θ^*
400	1.03	5.7	0.50	0.30	23.9	2.36
401	1.03	10.2	0.90	0.30	42.3	1.47
402	1.49	6.3	0.58	0.30	26.5	1.37
403	1.50	10.3	0.96	0.28	43.4	1.07
404	1.49	10.7	0.98	0.53	44.8	1.09
405	1.49	7.1	0.65	0.54	29.6	1.43
407	2.01	9.0	0.87	0.57	38.6	0.99
408	2.04	5.8	0.58	0.77	25.3	1.38
409	2.04	8.8	0.87	0.74	37.8	1.13
410	1.75	11.5	1.10	1.16	48.8	1.06

TECHNICAL REPORTS DISTRIBUTION LIST, CONTRACT Nonr 225(23)

Aerojet-General Corp.
Liquid Engine Division
Azusa, California
(1) Attn: Mr. C.C. Ross

Aerojet-General Nucleonics
Fostoria Way
San Ramon, California
(1) Attn: Library
(1) Dr. D. L. Cochran
(1) Mr. A. V. Liain

The Air Preheater Corp.
Wellsville, New York
(1) Attn: Mr. Hilmer Karlsson
Technical Manager

Airesearch Mfg. Company
9851 9951 Sepulveda Blvd.
Los Angeles, 45, California
(2) Attn: Mr. S. K. Andersan
(1) Dr. J. E. Coppage
(1) Mr. A. L. Johnson, Jr.
(1) Dr. John Mason

Fairchild Engine and
Airplane Corporation
Fairchild Astrionics Div.
Wyandanch, Long Island, N.Y.
(1) Attn: Alex London, Sr.,
Engineer, Aero
Mechanics Div.

Fairchild Engine and
Airplane Corp.
Stratos Division
Bay Shore, Long Island, N.Y.
(1) Attn: Mr. V.L. Whitney, Jr.
Res. Engineer

Ferrotherm Company
1861 E 65th Street
Cleveland, 3, Ohio
(2) Attn: Mr. Sven Holm

Ford Motor Company
Dearborne, Michigan
(1) Attn: Mr Paul Klotcsh
Res. Div
(1) Dr. D. N. Frey
Scientific Lab.
(1) Mrs. Rachel MacDonald
Eng. Staff Library
(1) Mrs. L. B. Phillips
Superintendent
Tech. Info. Sec.,
Scientific Lab.

Foster-Wheeler Corp.
666 Fifth Avenue
New York, 6, N.Y.
(1) Attn: Mr. John Blizard,
Res. Consultant

The Franklin Institute
Laboratories for Research
and Development
Philadelphia, 3, Pa.
(1) Attn: Mr. F. L. Jackson

General Dynamics Corp.
General Atomic Division
P.O. Box 608
San Diego, 12, Calif.
(1) Attn: P. W. Simpson, Document
Custodian

General Electric Company
Atomic Power Equipment Div.
San Jose, California
(1) Attn: W. A. Sutherland
(1) P. E. Tippets

Jack and Heintz, Inc.
Engineering Dept., Plant 4
Cleveland, 1, Ohio
(1) Attn: Mrs. Harriet B. Trikilis
Librarian

M. W. Kellogg Company
711 Third Avenue
New York, 17, New York
(1) Attn: Mr. F. W. Peterson
(1) Mr. G. P. Eschenbrenner
(1) Mr. Ronald B. Smith,
Vice President

The Kraissl Co., Inc.
229 Williams Avenue
Hackensack, New Jersey
(1) Attn: Mr. F. Kraissl, Jr.

Lockheed Aircraft Co.
Technical Library
Burbank, California
(1) Attn: B. L. Messinger
Engrg. No. 7225

Stewart-Warner Corp.
1514 Drover Street
Indianapolis 7, Indiana
(2) Attn: Mr. R. D. Randall
Mgr. Research

Sulzer Bros. Ltd.
50 Church Street
New York 7, New York
(1) Attn: Mr. Richard Herold

(1) Sverdrup and Parcel, Inc.
Syndicate Trust Bldg.
St. Louis, 1, Missouri

Sylvania Electric Products, Inc.
Electronics Defense Lab.
P. O. Box 205
Mountain View, California
(1) Attn: Library

Texas Eastern Transmission
Corp.
P.O. Box 1612
Shreveport, Louisiana
(1) Attn: Mr. C. W. Narvin

Argonne National Labs.
9700 S. Cass Ave.
Argonne, Illinois
(1) Attn: Tech. Library
(1) Dr. B. I. Spinrad, Dir. Res. Engrg.
(1) Dr. David Miller, ISNE School
(1) Mr. M. Petrick

Arnold Equipment Corp.
3080 Main Street
Buffalo, New York
(1) Attn: Mr. R. G. Teasmer

Aro, Inc.
Technical Information Branch
Tullahoma, Tennessee
(1) Attn: Mr. G. E. Randall

Atlantic Research Corporation
Alexandria, Virginia
(1) Attn: Dr. M. Markels, Jr

General Electric Company
General Engineering Lab.
Schenectady, 5, New York
(1) Attn: Mr. F. F. Buckland
(1) Dr. R. H. Norris
Thermal Systems Engrg
(1) D.H. Brown
Thermal Systems Engrg.

General Electric Company
Design Section, Engrg. Dept.
Richland, Washington
(1) Attn: Mr. Gardner L. Locke

General Electric Company
Small Aircraft Engine Dept.
1000 Western Avenue
West Lynn 3, Mass
(1) Attn: Paul C. Setze

(1) General Metals Corp.
Enterprise Division
18th and Florida Sts.
San Francisco, California

General Motors Corp.
Allison Division
Indianapolis, 6, Indiana
(1) Attn: Mr. R.N. Hazen
Dir. of Engrg.

General Motors Corp.
Research Laboratories
12 Mile and Mound Roads
Warren, Michigan
(2) Attn: Mr. W. A. Turunen, Gas
Turbine Dept.
(1) Dr. V. C. Smith

General Motors Corp.
Harrison Radiator Div.
Lockport, New York
(2) Attn: Mr. John W. Godfrey

General Nuclear Engineering
Corporation
Dunedin, Florida
(1) Attn: Ray L. Lyerly, Staff
Engineer
(1) Librarian

The Oriscom-Russell Company
285 Madison Avenue
New York, 17, New York
(1) Attn: Mr. George Root
Chief Engineer

Mine Safety Appliances Co.
Callery Plant
Callery, Pennsylvania
(1) Attn: Dr. C. B. Jackson

Modine Manufacuting Co.
1500 DeKoven Avenue
Racine, Wisconsin
(1) Attn: Mr. C. T. Perkins, Pres.

Morgantown Research Center
Bureau of Mines
Morgantown, West Virginia
(1) Attn: Mr. J. P. McGee

North American Aviation, Inc.
International Airport
Los Angeles, 45, Calif.
(1) Attn: Mr. M. A. Sulkin

Perfex Corporation
500 West Oklahoma Avenue
Milwaukee, 7, Wisconsin
(1) Attn: Mr. W. W. Schwid
(1) Mr. G. Hazaloop
Res. Dev. Engineer

Westinghouse Electric Corp.
Lester Branch P.O.
Philadelphia 13, Pa.
(1) Attn: Mr. F. K. Fischer, Mgr.
Dev. Engrg.

Westinghouse Electric Corp.
Atomic Power Division
P. O. Box 1468
Pittsburgh, 30, Pa.
(1) Attn: Technical Library

Westinghouse Electric Corp.
Research Laboratory
East Pittsburgh, Pa.
(1) Attn: Dr. Stewart Way

Wolverine Tube Division
1411 Central Avenue
Detroit, 9, Michigan
(1) Attn: Mr. F. C. Eddens

Sanderson and Porter
72 Wall Street
New York 5, New York
(1) Attn: Mr. S. T. Robinson

Shell Development Company
Emeryville, California
(1) Attn: Dr. C. R. Garbett

A. O. Smith Corp.
3533 North 27th Street
Milwaukee 1, Wisconsin
(1) Attn: Mr. M. B. Ziering

Solar Aircraft Company
San Diego, 12, California
(2) Attn: Mr. P. A. Pitt, Chief
Engineer
(1) Mr. E. A. Drury
Project Engineer

Stalker Development Company
903 Woodside Avenue
Essexville, Michigan
(1) Attn: Mr. E. A. Stalker

Stanford Research Institute
Menlo Park, California
(1) Attn: Dr. Kevin K. Hiester
(1) Mr. S. H. Clark
(1) Mr. W. A. Casler

Worthington Corp.
Harrison Division
Harrison, New Jersey
(1) Attn: Mr. Norman L.
Myerson, Dir. of
Research
(1) Mr. David Aronson

Young Radiator Company
709 S. Marquette St.
Racine, Wisconsin
(1) Attn. Mr. H. F. Brinen
Res. Engineer

(1) Mr. Hector H. Aiken
404 Willow Road
Menlo Park, Calif.

(1) Dr. W. Bollay
Hope Ranch
Santa Barbara, Calif.

(1) Mr. F. A. Brooks
Dept. of Agr. Engrg.
Univ. of Calif. Agr.
Experiment Station
Davis, California

(1) Prof. Alberto Coimbra
Escola Nacional de Quimica
Av. Pasteru 404
Rio De Janeiro, BRASIL

(1) Mr. W. H. Comtois
129 Thornberry Drive
Pittsburgh, 25, Pa.

(1) Mr. Paul Dawson
8320 East Galbristh
Cincinnati, 43, Ohio

(1) Mr. A. J. Ede
Heat Division
Mech. Eng. Research Lab.
D.S I.R., East Kilbride
near Glasgow, SCOTLAND
SEND TO:
Office of the Asst. Naval
Attache for Research
Naval Attache, American
Embassy
Navy No. 100, Fleet P.O.
New York, New York

(1) Prof. R. W. Stuart Mitchell
Laboratorium Voor Verbrandingsmotoren
en Gasturbines
Technische Hogeschool
Prof. Mekelweg 2
Delft, HOLLAND

(1) Dr. Carl A. Moore, Jr.
3307 Sunnywood Drive
Fullerton 1, California

(1) Mr. A. W. Morris
University of Texas
Austin, Texas

(1) Mr. A. J. Oberg
Minneapolis-Honeywell
Regulator Company
Research Center
500 Washington Avenue, S.
Hopkins, Minnesota

(1) Mr. R. C. Perpall
5453 Whitefox Drive
Palos Verdes Estates
California

(1) Major Walter E. Rafert
Asst. Prof. - Armament
Department of Ordnance
U.S. Military Academy
West Point, New York

(1) Mr. D. W. Retzinger
Perfex Corporation
Heat Transfer Products
500 West Oklahoma Avenue
Milwaukee 7, Wisconsin

(1) Mr. L.P. Saunders
P.O. Box L
Carmel, California

(1) Mr. Wolfgang Schaechter
Thiokol Chemical Corporation
Rocket Operations Center
P.O. Box 1640
Ogden, Utah

(1) Mr. David M. Schoenfeld
Mariomi Road
New Canaan, Connecticutt

The Trane Company
2nd and Cameron Avenues
La Crosse, Wisconsin
(2) Attn: Mr. H. C. Rooks
(1) Mr. J. T. Wetzel
(1) Mr. W. C. Leckie

(2) Union Carbide Nuclear Co.
Oak Ridge Gaseous Diffusion
Plant
Plant Records Department
P. O. Box P
Oak Ridge, Tennessee

United Aircraft Corp.
400 Main Street
East Hartford 8, Conn.
(1) Attn: Mr. Robert C. Sale
Chief Librarian
(1) Mr. Ned C. Rice, Jr.
Research Dept.

Vidya Inc.
2626 Hanover Street
Palo Alto, Calif.
(1) Attn: M. W. Rubesin
(1) D. E. Abbott
(1) D. C. Briggs

Western Supply Co.
P. O. Box 1888
Tulsa, 1, Oklahoma
(1) Attn: E. D. Anderson,

(1) Dr. Robert W. Fox
Dept. of Mach. Engrg.
Purdue University
Lafayette, Indiana

(1) Mr. Ralph M. Heintz
P. O. Box. 546
Los Gatos, Calif.

(1) Mr. Albert L. Holiday
550 Lakewood Circle
Walnut Creek, Calif.

(1) Mr. Robert V. Kleinschmidt
20 East Street
Stoneham, 80, Mass.

(1) Dr. Milton B. Larson
Dept. of Mech. Engrg.
Oregon State College
Corvallis, Oregon

(1) Rear Adm. Paul F. Lee,
USN Ret.
14975 Manuella Avenue
Los Altos, California

(1) Mr. E. J. Le Fevre
Dept. of Mechanical Engineering
Queen Mary College
London E. 1., ENGLAND

(1) Mr. Alex London
Space Systems Thermal Analysis
General Electric Company
3198 Chestnut Street
Philadelphia 1, Pa.

(1) Mr. R. E. Lundberg
Stanford Research Institute
Menlo Park, California

(1) Dr. J. J. McMullen
1114 Clinton Street
Hoboken, New Jersey

(1) Mr. Frank L. Maker
156 Moraga Highway
Orinda 1, California

(1) Prof. J. W. Mitchell
University of Wisconsin
Dept. of Mechanical Engineering
Madison 6, Wisconsin

(1) Mr. Edward Simons
355 Taraval Street
San Francisco 16, California

(1) Mr. S. B. Spangler, Jr.
4315 Miranda Avenue
Palo Alto, California

(1) Mr. Richard L. Stone
William Wallace Company
Belmont, California

(1) Mr. John Cook Wyllie
Alderman Library
University of Virginia
Charlottesville, Virginia

(1) Mr. Stanley Wong
1128 West 126th Street
Los Angeles 44, California

(1) Dr. J. G. Woodroof, Chairman
Food Processing Division
Georgia Experimental Station
Experiment, Georgia

(1) Prof. F. L. Schwartz
Dept. of Mechanical Engineering
University of Florida
Gainsville, Florida

ARL (AFRO)
(1) Attn: RRLA-Library
Wright-Patterson AFB
Ohio

AFIT (AU)
(1) Attn: MCLI Library
Wright-Patterson AFB
Ohio

AMC
(1) Attn: Library
Wright-Patterson AFB
Ohio

(1) David Taylor Model Basin
Aerodynamics Laboratory
Attn: Library
Washington 7, D.C.

TECHNICAL REPORTS DISTRIBUTION LIST, CONTRACT Nonr 225(23)

Atomics International
P.O. Box 309
Canoga Park, Calif.
(1) Attn: Library

Atomic Power Dev.Associates, Inc.
1911 First Street
Detroit, 26, Michigan
(1) Attn: Mr. A. Amorosi
(1) Dr. Wayne H. Jens

Avco Research Lab.
2385 Revere Beach Parkway
Everett, 49, Mass.
(1) Attn: Technical Library

(1) The Babcock and Wilcox Co.
Research and Dev. Center
P.O. Box 835
Alliance, Ohio

Bettelle Memorial Institute
505 King Avenue
Columbus, 1, Ohio
(1) Attn: Dr. H. W. Russell

C F. Braun and Co.
1000 S. Fremont St.
Alhambra, Calif.
(1) Attn: Mr Earl Phillips

Brookhaven National Laboratory
Technical Information Division
Upton, Long Island, New York
(1) Attn: Research Library

Brown Boveri Corp.
19 Rector St.
New York, 6, New York
(1) Attn: Mr. P. R. Sidler, Pres.

Brown Flintube Co.
300 Huron Street
Elyria, Ohio
(1) Attn: Mr. John W Brown, Jr.

California Research Corp.
Richmond, Calif.
(1) Attn: Dr J. H. Macphereon

Carrier Corporation
South Geddes St.
Syracuse, 1, New York
(1) Attn: Engineering Lib.

Chief, Bureau of Ships
Department of the Navy
Washington 25, D.C.
(2) Attn: Code 312
(2) 430
(2) 550
(1) 590
(1) 513
(1) 551
(1) Director of Research

Chief, Bureau of Aeronautics
Department of the Navy
Washington 25, D.C.
(1) Attn: Aer-AE-651
(2) PP-22
(2) PP-33

Director
Naval Research Laboratory
Washington 25, D.C.
(6) Attn: Code 2028

Director
U.S. Army Engineer Research
and Development Laboratories
Fort Belvoir, Virginia
Attn: Technical Documents Center

Naval Engineering Exp. Station
Annapolis, Maryland
(6) Attn: Arthur H. Senner

U. S. Naval Postgraduate School
Monterey, California
(1) Attn: Library
(1) Prof. Paul Pucci
(1) Prof. C. P. Howard

(1) Office of the Asst. Chief of Staff,
G-4
Research and Development Division
Department of the Army
Washington 25, D.C.

Armed Services Technical Information
Agency
Arlington Hall Station
Arlington 12, Virginia
(10) Attn: DSC

U. S. Army Ordnance Missile Command
Army Ballistic Missile Agency
Redstone Arsenal, Alabama
(1) Attn: ORDAB-RRT

Gulf Oil Corp.
Gulf Building
Pittsburgh, 30, Pennsylvania
(1) Attn: Mr. Charles F. Kottcamp

The Heat-X-Changer Co., Inc
Brewster, New York
(1) Attn: Mr W. J Donovan,
Vice President

Hughes Aircraft Company
Florence and Teale Sts.
Culver City, California
(1) Attn: Dana H. Johnson, Dir
Technical Library

Ingersoll-Rand Company
11 Broadway
New York, New York
(1) Attn: Mr. M. C. Davison

International Harvester Co.
Engineering Research Dept.
5225 S. Western Blvd
Chicago, 9, Illinois
(1) Attn: Dr. Simon K. Chen

I-T-E Circuit Breaker Co.
601 E. Erie Avenue
Philadelphia, 34, Pa
(1) Attn: Mr. Ashton T. Scott

Caterpillar Tractor Co.
Peoria, 8, Illinois
(1) Attn: Mr S.S. Eberhard, Pres
(1) Mrs.M.M. Landuyt, Res.Library
(1) Mr. Floyd E. Johnson

Chrysler Corporation
Automotive Research,
Dept, 981
12483 Greenfield Ave.
Detroit, 27, Michigan
(1) Attn: Mr. A. Charismb, Res.Eng.

Continental Aviation and Energy Corp.
12700 Kercheval
Detroit, Michigan
(1) Attn: Mr. A.Toprizian

Cooper Bessemer Corp.
Mt. Vernon, Ohio
(1) Attn: Mr. R. L. Boyer, V.P.

Cornell Aeronautical Lab.
4455 Genesee St.
Buffalo, 21, New York
(1) Attn: Slme T. Evans, Librarian

(1) Detroit Edison Co,
Nuclear Power Division
Detroit, Michigan

Cosmodyne Corporation
5300 West 104th Street
Los Angeles, 45, CalifornLa
(1) Attn: Albert B. Seed,
Project Manager, Applications

Drayer-Hanson, Inc.
Box 2215 Terminal Annex
Los Angeles, 54, Calif.
(1) Attn: Mr. Gordon M. Jackson, V.P.

Electric Boat Company
Groton, Connecticut
(1) Attn: Mr.E.S. Dennison

Elliott Company
Jeannette, Pennsylvania
(1) Attn: Dr. J.Rodger Shields,
Dev.Engrg.Dept.

Eitel-McCullough, Inc.
798 San Mateo Ave.
San Bruno, California
(2) Attn: Mr. J.S.McCullough, Mgr.Res.

Chief of Naval Research
Department of the Navy
Washington 25, D.C,
(2) Attn: Code 429
(1) Code 438

(2) Commanding Officer
Office of Naval Research
Branch Office
1000 Geary Street
San Francisco 9, Calif.

(1) Commanding Officer
Office of Naval Research
Branch Office
1030 East Green Street
Pasadena 1, Calif.

(1) Commanding Officer
Office of Naval Research
Branch Office
John Crerar Library Bldg.
86 East Randolph Street
Chicago 1, Illinois

(25) Commanding Officer
Office of Naval Research
Branch Office
Keysign House
429 Oxford Street
London, W.1., ENGLAND
<u>SEND TO:</u>
Commanding Officer
Office of Naval Research
Branch Office
Navy No. 100
Fleet Post Office
New York, New York

(1) Office of Naval Research
346 Broadway
New York 13, New York
Attn: Dr. Saul Berman

(1) Office of Naval Research
Attn: Mechanics Branch
Washington 25, D.C.

(1) Office of Naval Research
Attn: Air Branch
Washington 25, D.C.

Lockheed Aircraft Corp.
Missile Systems Division
Aerodynamics Dept.
Sunnyvale, California
(1) Attn: Mr O. A. Etemad

Lummus Company
146 Haynes Avenue
Newark, New Jersey
(1) Attn: Stanley Grossel,
Process Engineer

McCulloch Motors Corp.
6101 West Century Blvd.
Los Angeles, 45, Calif.
(1) Attn: W. K. Deacon, Chief
Eng., Aircraft
Engines

The Marquardt Corp.
Controls and Accessories Div.
16655 Saticoy Street
Van Nuys, California
(1) Attn: Robert T. Loncet

Micro-Precision Inc.
Engineering Department
2205 Lee Street
Evanston, Illinois
(1) Attn: Mr Louis G. Kaplan

(5) Administrator
National Aeronautics and
Space Administration
1520 H Street, N.W.
Washington 25, D.C.

Oak Ridge National Laboratory
9204-1; Y-12
P.O. Box P
Oak Ridge, Tennessee
(1) Attn: Mr. Richard M. Lyon
(1) Technical Library

(1) American Society of Heating,
Refrigerating and Air-Conditioning
Engineers, Inc,
United Engineering Center
345 East 47th Street
New York 17, New York

American Society of Mechanical
Engineers
United Engineering Center
345 East 47th Street
New York 17, New York
(1) Attn: Mrs. D.M. Sheckelford,
Standards Administrator

(1) Detroit Public Library
Technology Department
96 Putnam Avenue
Detroit 2, Michigan

(1) Engineering Societies Library
United Engineering Center
345 East 47th Street
New York 17, New York

Mr.Graw-Hill Publishing Company
330 West 42nd Street
New York 36, New York
(1) Attn: Mr. L.M. Rowley, Exec. Ed.,
POWER

Auburn University
Department of Mechanical Engineering
Auburn, Alabama
(1) Attn: Prof. Donald Vestel, Chairman

Brooklyn Polytechnic Institute
99 Livingston Street
Brooklyn 1, New York
(1) Attn: Engineering Library

California Institute of
Technology
Mechanical Engineering Dept.
1201 East California Street
Pasadena 4, California
(1) Attn: Mechanical Engrg. Library

University of CalifornLa
College of Engineering
Berkeley 4, California
(1) Attn: Dean E.D. Howe
(1) Prof. R.A.Seban, M.E.
(1) Prof. H.A. Johnson, M.E.
(1) Prof. A.E. Oppenheim, M.E.

University of California at
Los Angeles
Engineering Department
Los Angeles 24, California
(1) Attn: Dean L.M.K. Boelter
(1) Prof. W.J. King
(1) Prof. Myron Tribus
(1) Mr. H, Buchberg

Case Institute of Technology
Department of Mechanical Engrg.
University Circle
Cleveland 6, Ohio
(1) Attn: Prof. J.N. Mosayneki

The Catholic University of America
Department of Mechanical Engineering
Washington 17, D.C.
(1) Attn: Mr. E.D. Jordan

Columbia University
Heat Transfer Research Facility
P.O. Box 245, Station J
New York 27, New York
(1) Attn: AEC Contract Custodian

Cornell University
College of Engineering
Department of Heat Power Engrg.
Ithaca, New York
(1) Attn: Prof. David Dropkin

University of Houston
Mechanical Engineering Department
Houston, Texas
(1) Attn: Prof. D.G. Williams

Illinois Institute of Technology
Department of Mechanical Engineering
Technology Center
Chicago 16, Illinois
(1) Attn: Heat Transfer Laboratory

University of Santa Clara
Santa Clara, California
(1) Attn: Prof. R.K, Pefley

Stanford University
Stanford, California
(1) Attn: Dean J.M. Pettit,
School of Engrg.
Engineering Library

Syracuse University
Syracuse, New York
(1) Attn: Ralph M. Watson
Dean of Engrg.

Tufts University
Mechanical Engineering Dept.
Medford, 5,, Mass.
(1) Attn: Dr. L. M. Trefethen,
Chairman

Virginia Polytechnic Inst.
Blacksburg, Virginia
(1) Attention: Carol M. Newman Lib.

University of Washington
College of Engineering
Seattle, 5, Washington
(1) Attn: Dean R. E Wessman

University of Wisconsin
Dept. of Mechanical Engrg.
Madison, Wisconsin
(1) Attn: Prof. Edward Obert

U. S. Atomic Energy Commission
Plans and Analysis Branch
Washington 25, D.C.
(1) Attn: Major J.B. Radcliff, USAF

U. S. Atomic Energy Commission
Division of Reactor Development
Washington 25, D.C.
(5) Attn: Chief, Reactor Component
Development Branch
(1) Mr. Nordlinger

(1) U. S. Atomic Energy Commission
Technical Information Service
P.O. Box 62
Oak Ridge, Tennessee

Director
Engineering Research and
Development Laboratory
Fort Belvoir, Virginia
(1) Attn: Head, Nuclear Power Branc

U. S. Coast Guard Headquarters
Testing and Development Division
1300 E Street
Washington, D.C.
(1) Attn: W.S. Vaughn, Cdr., USCG

Wright Air Development Center
Wright-Patterson AFB, Ohio
(1) Attn: WCNEO-2
(1) Mr. M.E. Davis, WCLOS

National Aeronautics and
Space Administration
Ames Research Center
Moffett Field, California
(2) Attn: Library

National Aeronautics and
Space Administration
Langley Research Center
Langley Field
Hampton, Virginia
(1) Attn: Library

National Aeronautics and
Space Administration
Lewis Research Center
21000 Brookpark Road
Cleveland 35, Ohio
(1) Attn: Library

University of Illinois
Mechanical Engineering Dept.
Urbana, Illinois
(1) Attn: Prof. S.L. Soo

Massachusetts Institute of
Technology
Cambridge 39, Massachusetts
(1) Attn: Prof. Joseph Kaye,
Mech. Engrg.
(1) Prof. Harold S. Mickle
Chem. Engrg.
(1) Prof. Edward S. Taylor
Gas Turbine Lab.
(1) Prof. William H. McAdams
Chem. Engrg.
(1) Prof. Warren M. Rohsenow
Mech. Engrg.

University of Michigan
228 West Engineering Bldg.
Ann Arbor, Michigan
(1) Attn: Prof. J.A. Clark
(1) Prof. F.L. Schwartz

University of Minnesota
Mechanical Engineering Dept.
Minneapolis, Minnesota
(1) Attn: Dr. E.R.G. Eckert

University of New Mexico
Department of Mechanical Engineerin
Albuquerque, New Mexico
(1) Attn: Prof. V.S. Skogland

New York University
College of Engineering
Dept. of Mechanical Engineering
University Heights
New York 53, New York
(1) Attn: Prof. Fred Landis

Princeton University
Princeton, New Jersey
(1) Attn: Prof. R.M. Drake, Jr.
Engineering
(1) Library, James Forrestal
Research Center
(1) Mr. F.L, Arnold, Periodicals
Section, Library

Purdue University
School of Mechanical Engrg.
Lafayette, Indiana
(1) Attn: Prof. D.S. Clark

AiResearch Manufacturing Co.
402 South 36th Street
Phoenix, Arizona
(1) Mr S. B. Spangler, Jr.
(1) Elmer Wheeler
Dept. 93-32

Struthers Wells Corp.
Struthers Wells Division
Warren, Pennsylvania
(1) Attn: Mr. S. Kopp

Allis-Chalmers Mfg. Co.
General Machinery Div.
Milwaukee, 1, Wisconsin
(1) Attn: Mr. R. C. Allen, Dir.Mech.Engrg.

American-Standard Advanced Technology Labs.
369 Whisman Road
Mountain View, Calif.
(1) Attn: Mr. Neal F. Lansing

American-Standard Corp.
Industrial Division
8111 Tireman Avenue
North Lansing, Michigan
(1) Attn: Mr. T. Tinker, V.P.
Technical Development

American Standard Corp.
Industrial Division
P.O. Box 2081
Buffalo, 5, New York
(1) Attn: Mr. J A. Jost, Dir.Res.
(1) Mr. I. N. Friedman, Mgr.Res.Engrg.